Observational Cosmology

The Cosmic Microwave Background
Part III: CMB Polarization & map making

Kaustuv Basu

Course website:
https://www.astro.uni-bonn.de/~kbasu/ObsCosmo

Part 2B: Polarization of the CMB

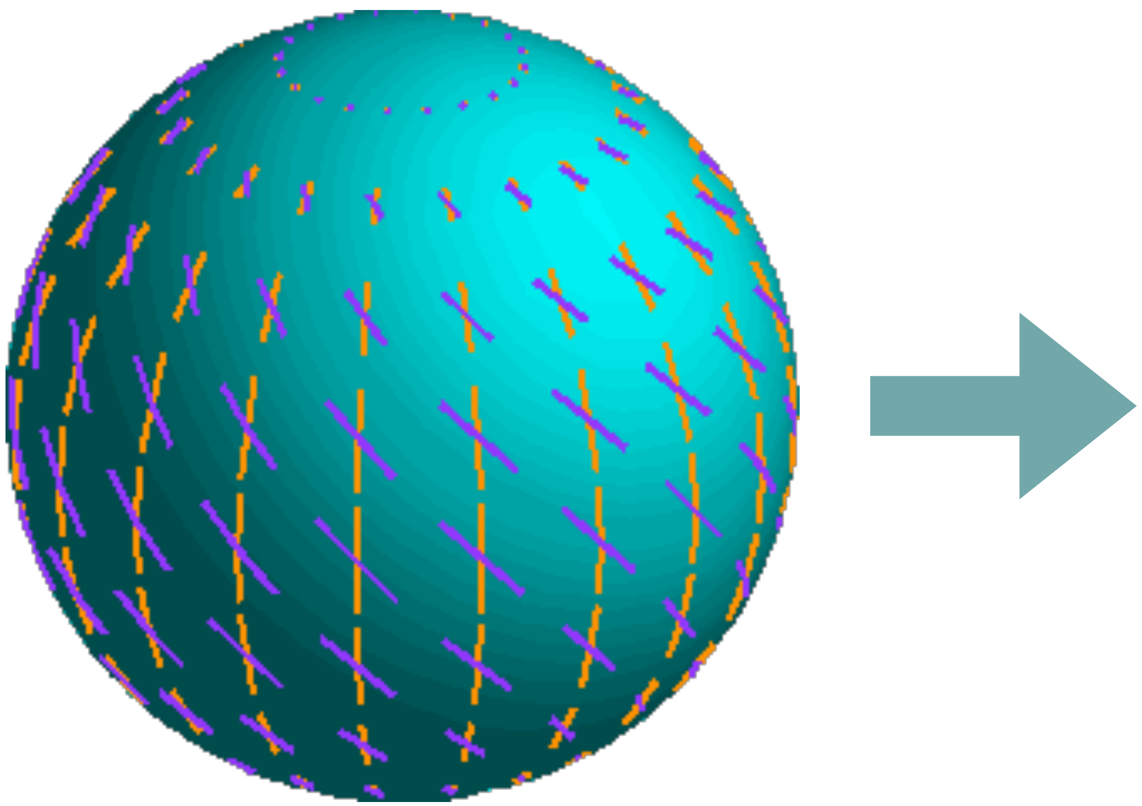

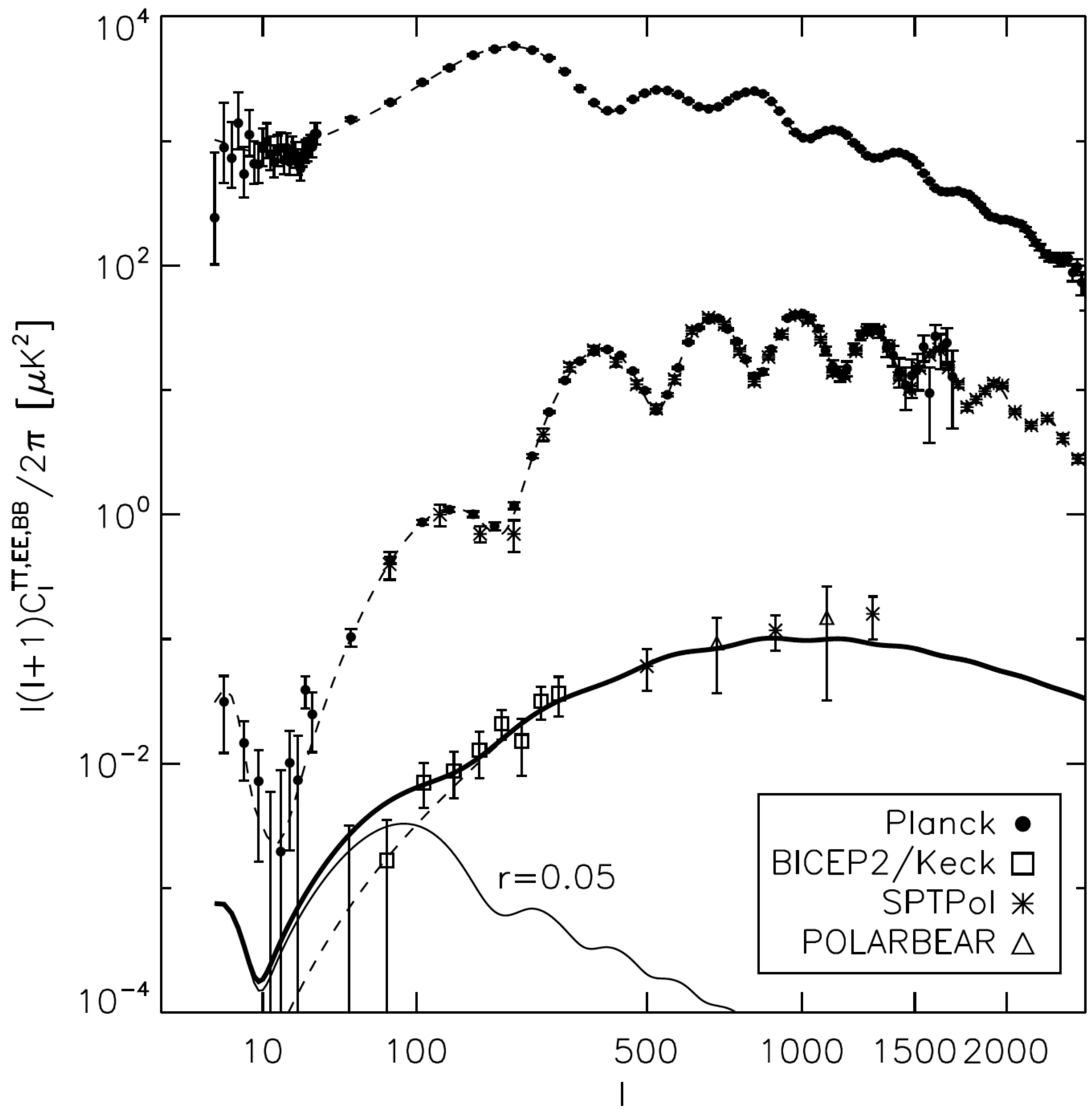

Polarization of the CMB

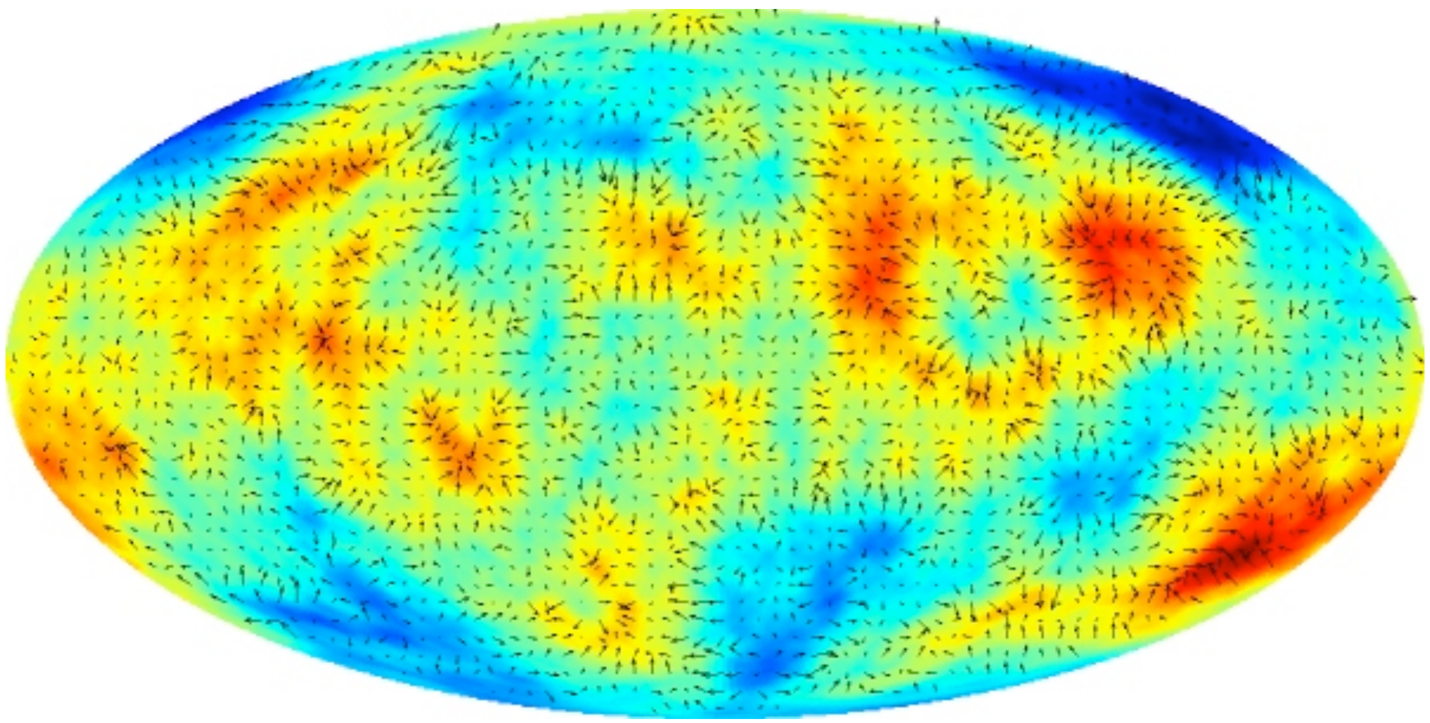

CMB radiation is linearly polarized, which means that at each point on the sky we have a vector orthogonal to the direction of CMB propagation.

One could describe the polarization by means of standard Stokes Q and U parameters, but that will make their value dependent of the choice of X- and Y-axes.

STOKES PARAMETERS FORMALISM

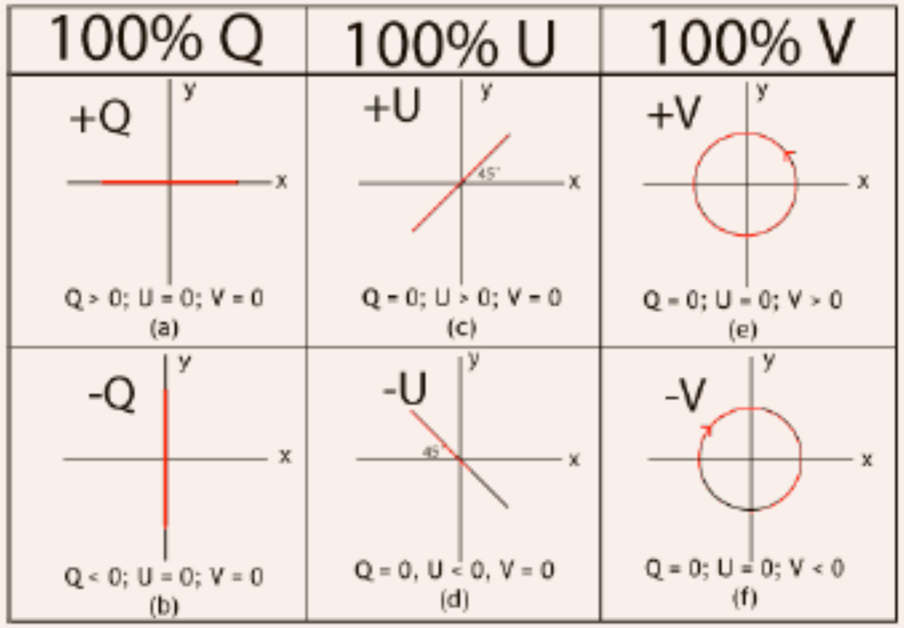

$$\left\{ \begin{array}{c} I \\ Q \\ U \\ V \end{array} \right\}$$

- ★ $\boldsymbol{I}$, *intensity*
- ★ $\boldsymbol{Q}$, $\boldsymbol{U}$, *linear polarization*
- ★ $\boldsymbol{V}$, *circular polarization*

★*in the case of the CMB,* $V = 0$

Deriving E and B modes

Stokes Q,U parameters are not rotationally invariant: under rotation of ψ degrees we get

$$I' = I \qquad V' = V$$

$$Q' = Q\cos(2\psi) - U\sin(2\psi) \qquad U' = U\cos(2\psi) + Q\sin(2\psi)$$

or in a compact form $Q' \pm iU' = e^{\pm 2i\psi}(Q \pm iU)$

i.e., (Q ± iU) transforms like a spin-2 variable under rotation.

So we use spin-weighted spherical harmonics. In general, a spin-s spherical harmonics function transform under rotation as

$${}_sY_{\ell m} \to e^{\pm si\psi}\, {}_sY_{\ell m}(\hat{n})$$

For all-sky decomposition

$$(Q \pm iU)(\hat{n}) = \sum_{\ell=2}^{\infty}\sum_{m=-\ell}^{+\ell} a_{\ell m}^{\pm 2}\, {}_{\pm 2}Y_{\ell m}(\hat{n}) = \sum_{\ell=2}^{\infty}\sum_{m=-\ell}^{+\ell} (a_{E,\ell m} \pm i a_{B,\ell m})\, {}_{\pm 2}Y_{\ell m}(\hat{n})$$

Here $a_{lm}^{\pm 2}$ are decomposition into positive and negative helicity, which are used to define the E- and B-modes

$$a_{E,\ell m} = \frac{1}{2}(a_{\ell m}^{+2} + a_{\ell m}^{-2}) \qquad a_{B,\ell m} = \frac{-i}{2}(a_{\ell m}^{+2} - a_{\ell m}^{-2})$$

Deriving E and B modes

Projection of the polarization
in the spinned spherical harmonics space

$$(Q \pm iU)(\vec{n}) = \sum_{l \geqslant 2,\ |m| \leqslant l} a_{\pm 2lm\ \pm 2}Y_l^m(\vec{n}).$$

Construction of the E *and* B *observables*
[Seljak & Zaldarriaga 1997]

$$a^E_{\ell m} = -\frac{a_{2\ell m} + a_{-2\ell m}}{2}$$

$$E(\mathbf{n}) \equiv \sum_{\ell,m} a^E_{\ell m} Y_{\ell m} = \int w(\mathbf{n}-\mathbf{n}')Q_r(\mathbf{n}')d\mathbf{n}'$$

$$a^B_{\ell m} = i\frac{a_{2\ell m} - a_{-2\ell m}}{2}$$

$$B(\mathbf{n}) \equiv \sum_{\ell,m} a^B_{\ell m} Y_{\ell m} = \int w(\mathbf{n}-\mathbf{n}')U_r(\mathbf{n}')d\mathbf{n}'$$

★*new observables independent of the chosen frame*
★ $E = f(Q_r)$, $B = f(U_r)$

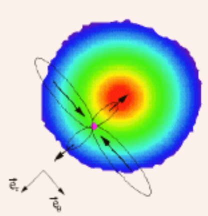

Scalar perturbations
generate Q_r *and thus* E

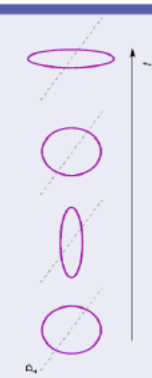

Tensor perturbations
generate Q_r *and* U_r
and thus E *and* B

Slide credit: Jonathan Aumont

E and B mode characteristics

Two flavours of CMB polarization:

Density perturbations: curl-free, "E-mode"
Gravity waves: curl, "B-mode"

E-mode
("gradient-like")

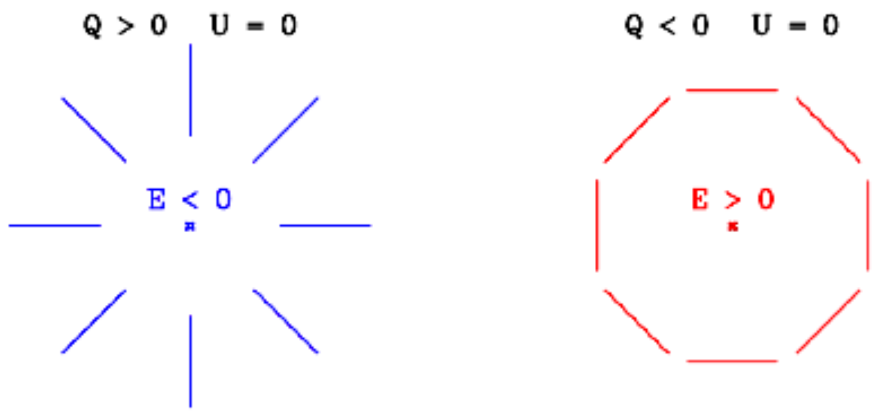

B-mode
("curl-like")

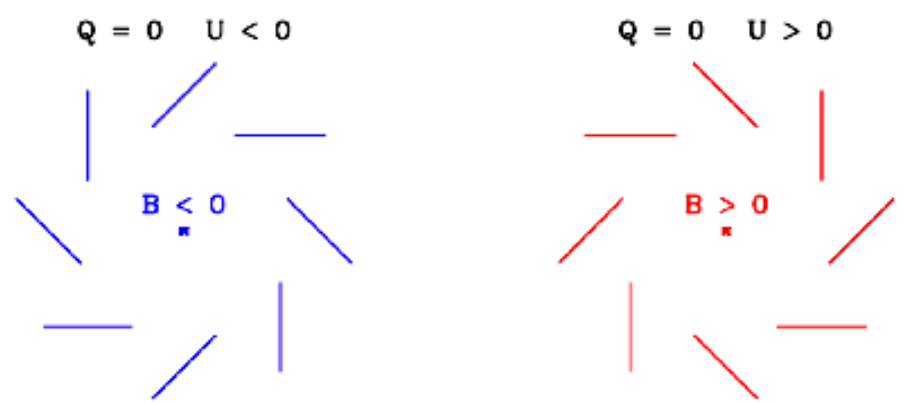

- We can break down the polarization field into two components which we call E and B modes. This is the spin-2 analog of the gradient/curl decomposition of a vector field.
- E modes are generated by density (scalar) perturbations via Thomson scattering.
- Additional vector modes are created by vortical motion of the matter at recombination – this is small
- B modes are generated by gravity waves (tensor perturbations) at last scattering or by gravitational lensing (which transforms E modes into B modes along the line of sight to us) later on.

E and B modes: 2D vector analogy

The Helmholtz's Theorem on Vector Fields

Helmholtz's theorem is also called as the fundamental theorem of vector calculus. It is stated as

"A sufficiently smooth, rapidly decreasing vector field in three dimensions can be decomposed into the sum of a solenoidal (divergence-less) vector field and an irrotational (curl-less) vector field."

The theorem is also called as Helmholtz decomposition, it breaks a vector field into two orthogonal components.

$$\mathbf{F} = -\nabla\Phi + \nabla \times \mathbf{A}$$

Instead of decomposing the vector field into E and B modes, one could also use the original Stokes Q and U parameters, but the disadvantage is that the distinction between Q and U depends on the choice of the coordinate frame. **Furthermore, E and B modes can be associated with distinct physical processes leading to the polarization!**

Quadrupole + Thomson scattering

Polarization is induced by Thomson scattering, either at decoupling or during a later epoch of reionization.

For scattering at Θ=π/2 only one component of the initially unpolarized radiation field gets scattered.

$$P(\theta, \phi) \propto 1 - \cos^2\theta$$

$$\frac{d\sigma}{d\Omega} = \left(\frac{e^2}{4\pi m c^2}\right)^2 |\hat{\epsilon} \cdot \hat{\epsilon}'|^2$$

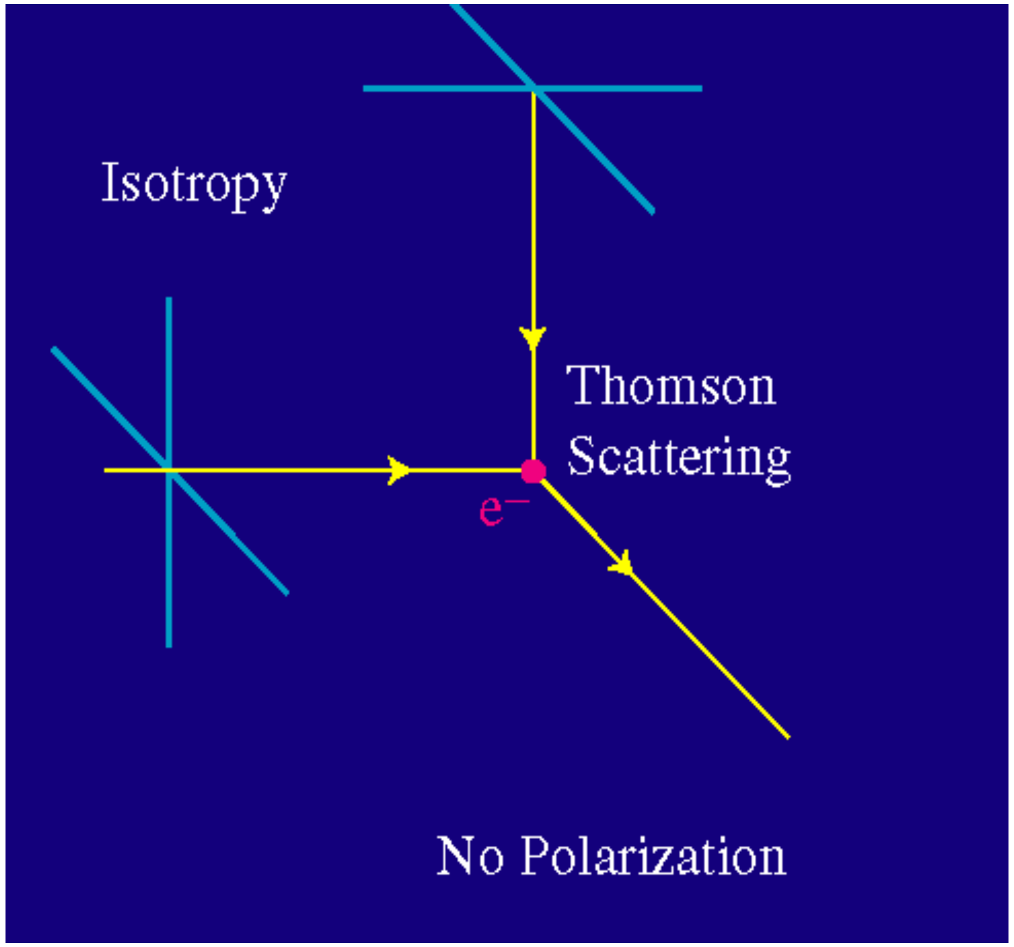

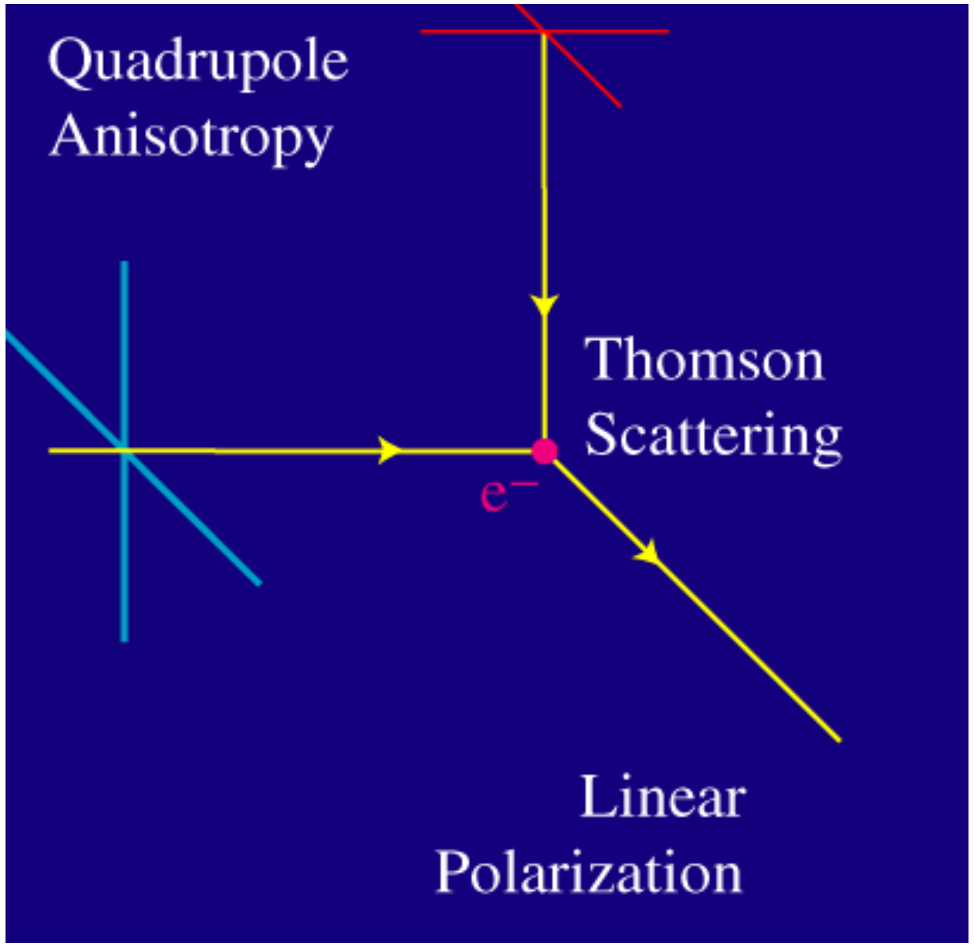


Photo Credit: TALEX


Photo Credit: TALEX
horizontally polarised


Photo Credit: TALEX

What causes the CMB quadrupole?

Two things:

"Normal" CDM: Density perturbations at $z \approx 1100$ lead to velocities that create local quadrupoles seen by scattering electrons.

=> E-mode polarization ("grad")

Gravity waves: create local quadrupoles seen by the scattering electrons.

=> B-mode polarization ("curl")

The problem of understanding the polarization pattern of the CMB thus reduces to understanding the quadrupole temperature fluctuations at the moment of last scattering.

From velocity gradients to E-mode polarization

Velocity gradients in the photon-baryon fluid lead to a quadrupole component of the intensity distribution, which, through Thomson scattering, is converted into polarization

(See Zaldarriaga, astro-ph/0305272)

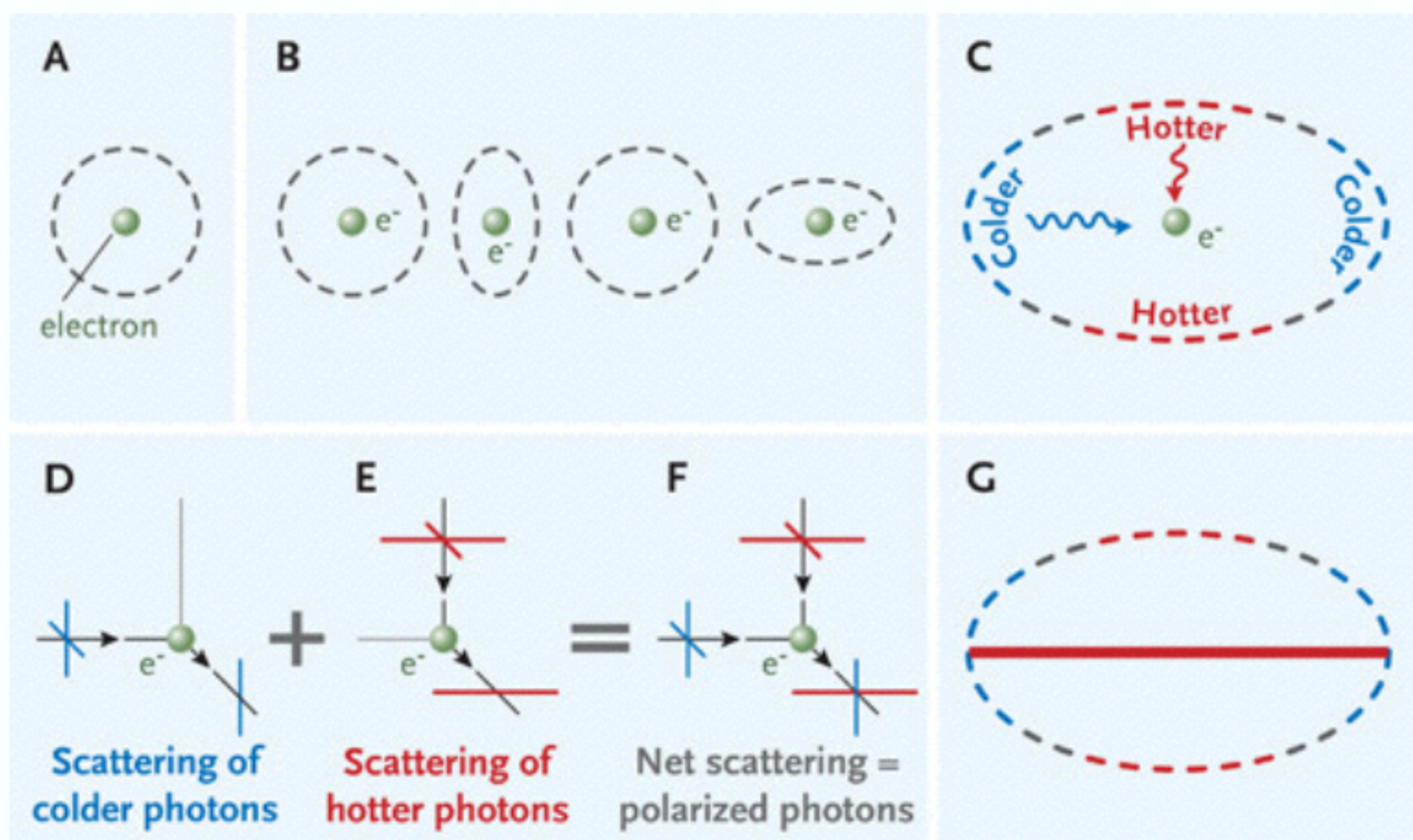

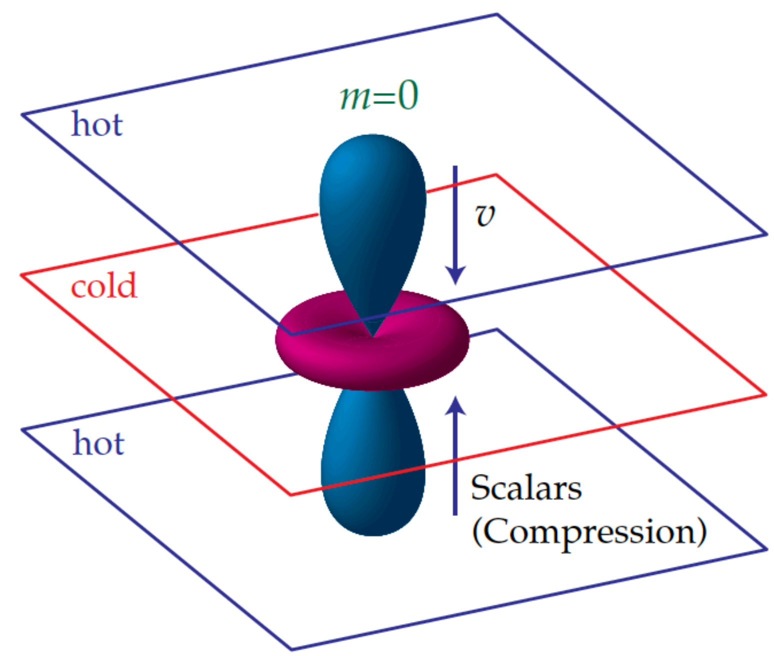

When gravity overwhelms pressure, matter flows towards the overdense regions. But these overdense regions are also colder to start with, as photons must climb out of the potential well. Hence flows are established from hot to cold regions *locally*, and these velocity gradients create the **primordial E-mode signal**.

From gravity waves to B-mode polarization

Arguably the cleanest prediction of inflation is a spectrum of primordial gravitational waves. These are tensor perturbations to the spatial metric,

$$ds^2 = a^2(\tau)\left[d\tau^2 - (\delta_{ij} + 2\hat{E}_{ij})dx^i dx^j\right] \; .$$

A plane gravitational wave causes a “quadrupolar stretching” of the space (tensor mode perturbations, as opposed to scalar modes from density).

This changes a circle of test particles into an ellipse, and the radiation acquires a *m=2* quadrupole pattern → primordial B-mode signal

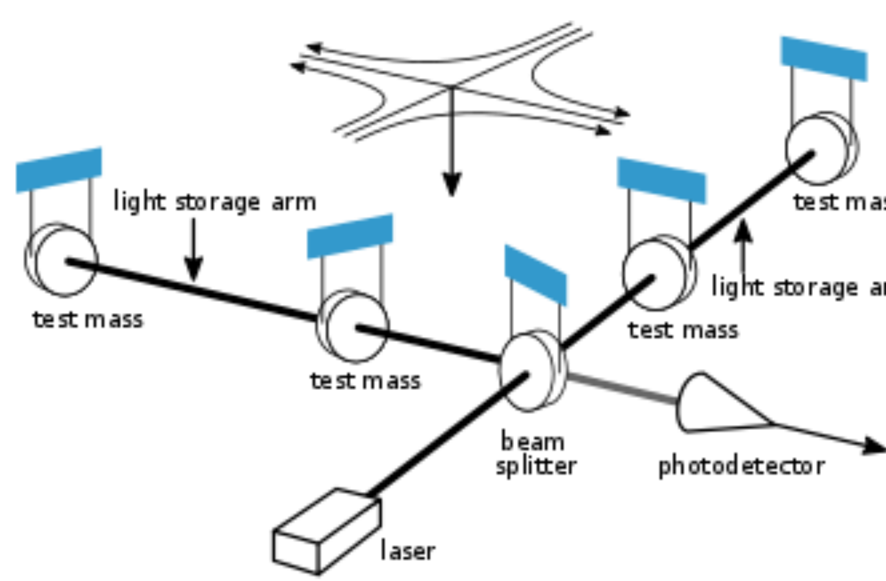

Detecting GW from CMB polarization

Isotropic electro-magnetic fields

Slide courtesy: E. Komatsu

Detecting GW from CMB polarization

GW propagating in isotropic electro-magnetic fields

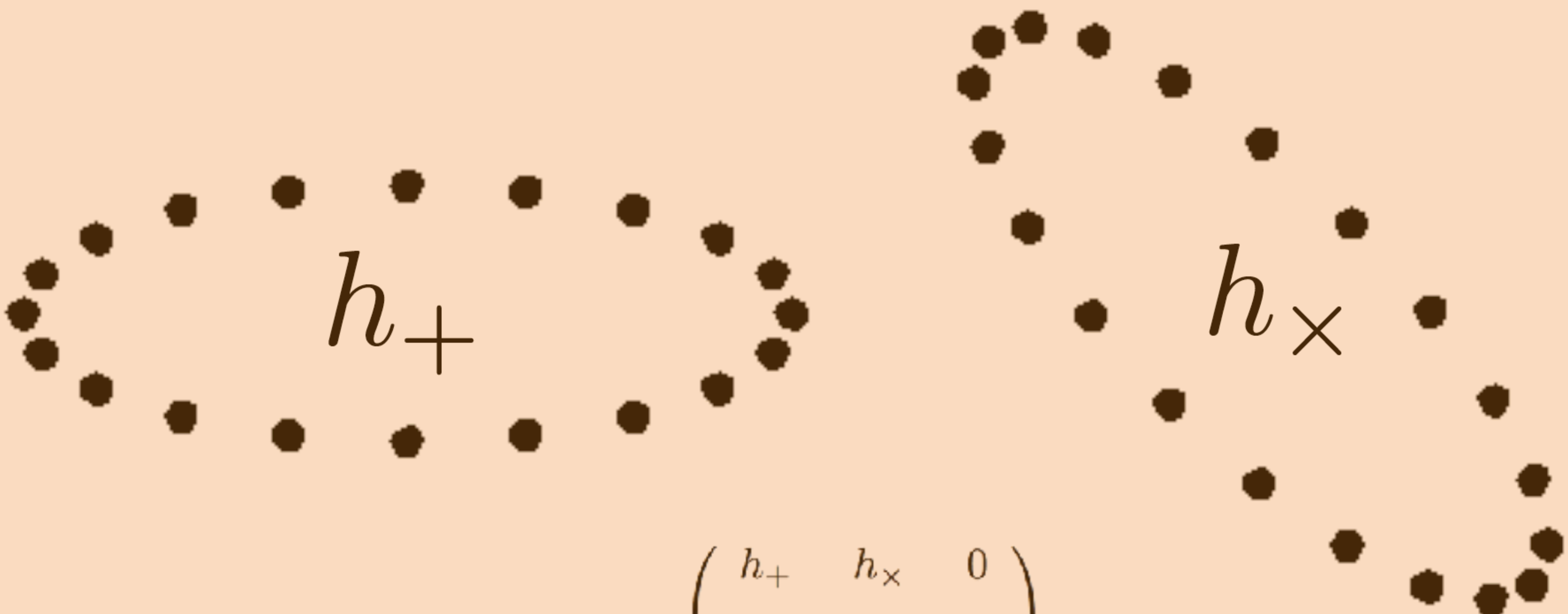

$$D_{ij} = \begin{pmatrix} h_+ & h_\times & 0 \\ h_\times & -h_+ & 0 \\ 0 & 0 & 0 \end{pmatrix}$$

D_{ij} **: Tensor metric perturbation [=gravitational waves]**

Slide courtesy: E. Komatsu

$$ds^2 = a^2 \sum_{i=1}^{3} \sum_{j=1}^{3} (\delta_{ij} + h_{ij}) dx^i dx^j$$

"metric perturbation"

Detecting GW from CMB polarization

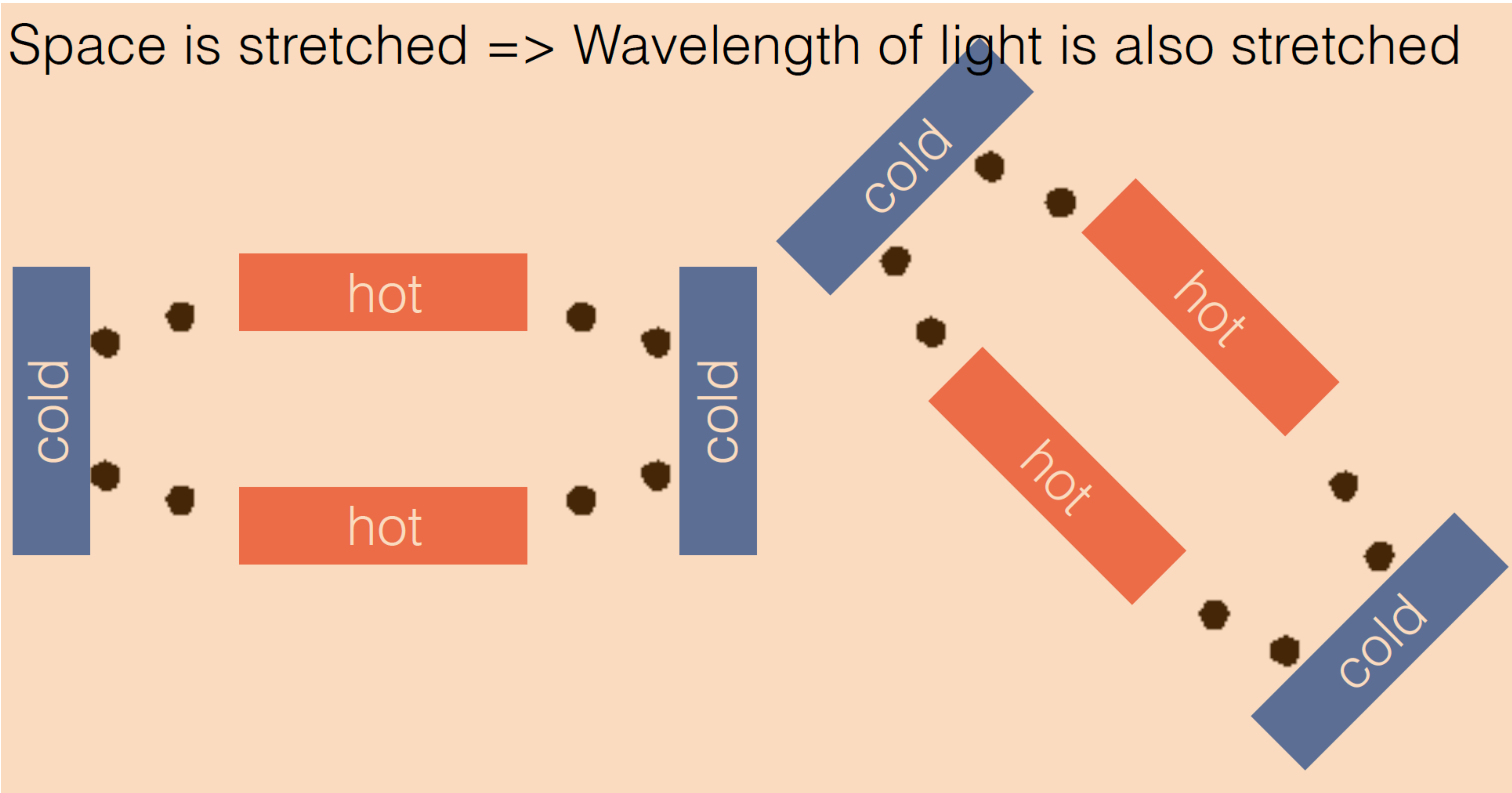

Slide courtesy: E. Komatsu

Detecting GW from CMB polarization

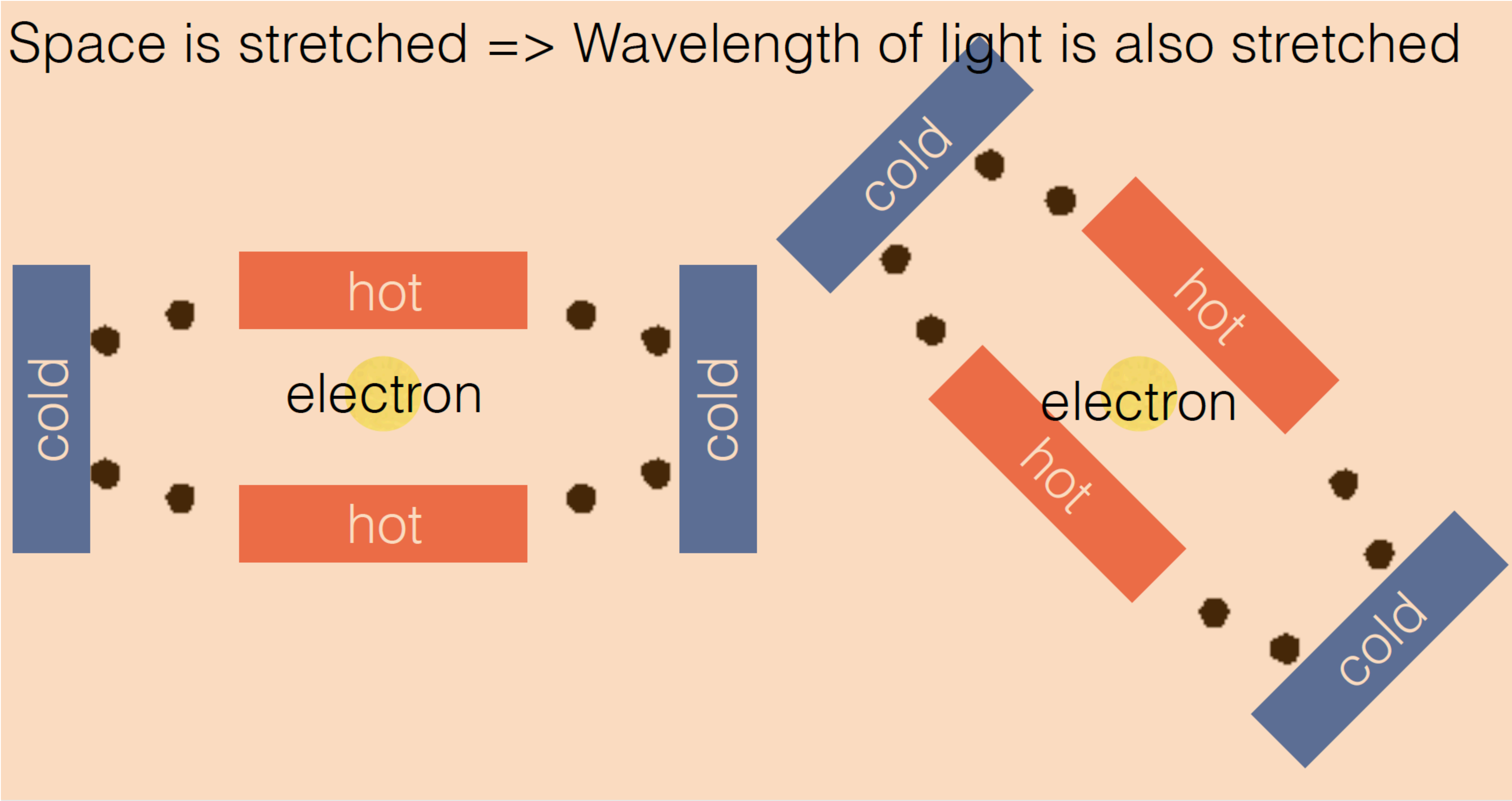

Slide courtesy: E. Komatsu

Detecting GW from CMB polarization

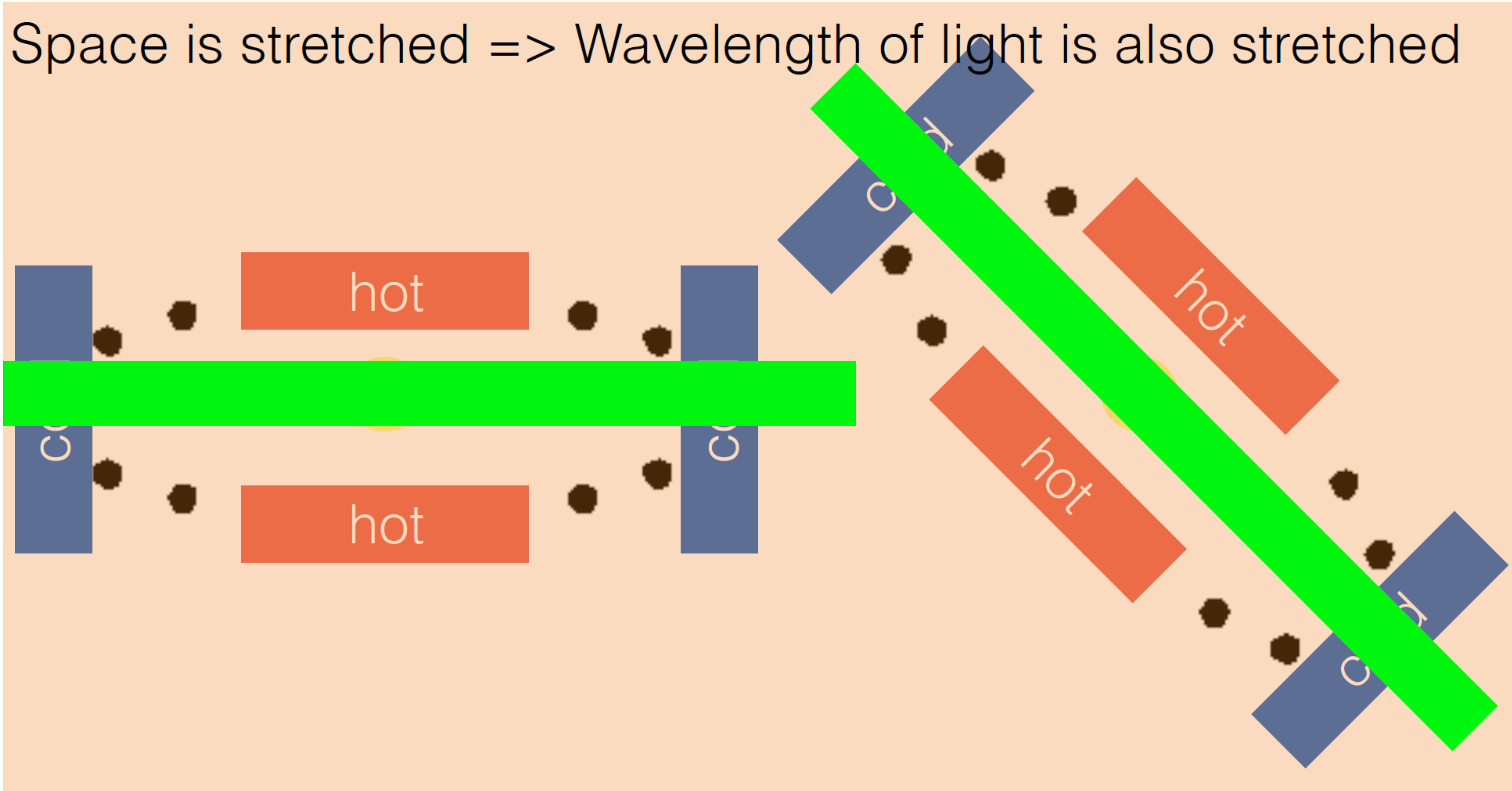

Slide courtesy: E. Komatsu

Polarization patterns on the last scattering surface

We saw that polarization pattern created at the last scattering can only come from a quadrupole temperature anisotropy present at that epoch.

In terms of multipole decomposition of a radiation field in terms of spherical harmonics, Y_{lm} (θ,ϕ), the five quadrupole moments are represented by $l = 2$; $m = 0, \pm1, \pm2$.

The orthogonality of the spherical harmonics guarantees that no other moment can generate polarization from Thomson scattering!

The problem of understanding the polarization pattern of the CMB thus reduces to understanding the quadrupolar temperature fluctuations at the epoch of last scattering.

Polarization patterns

(l,m)=(2,0)

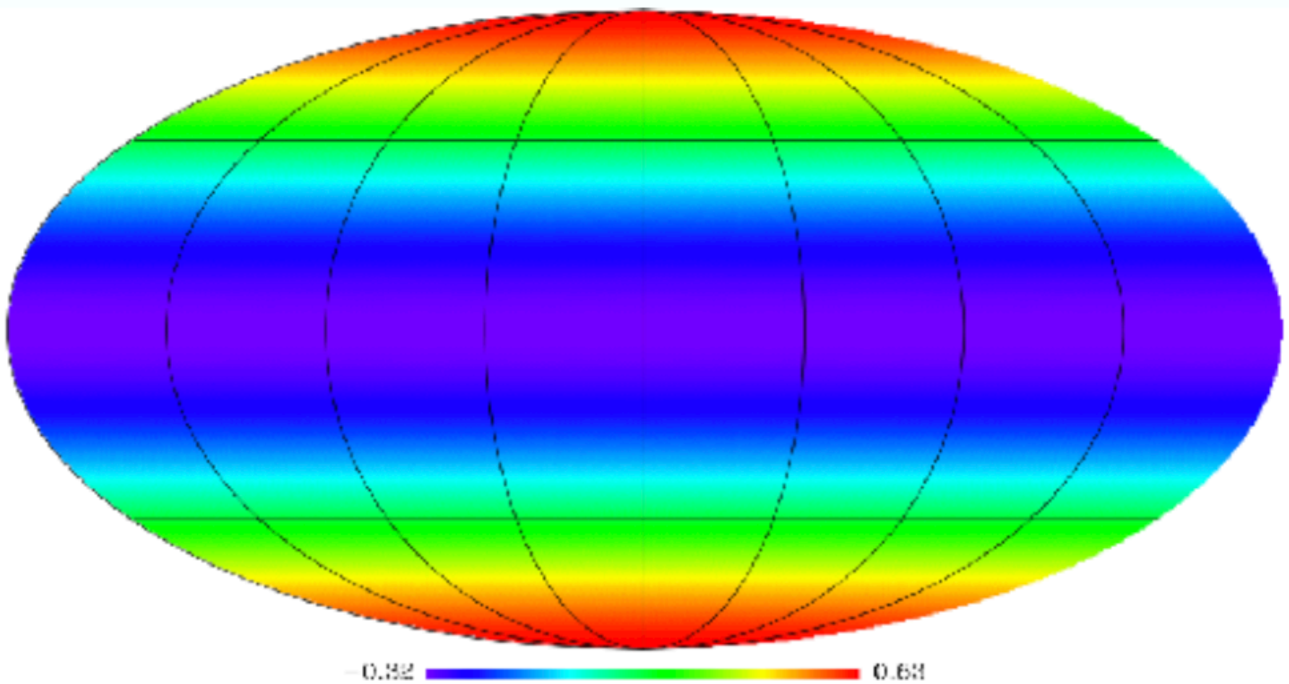

(l,m)=(2,1)

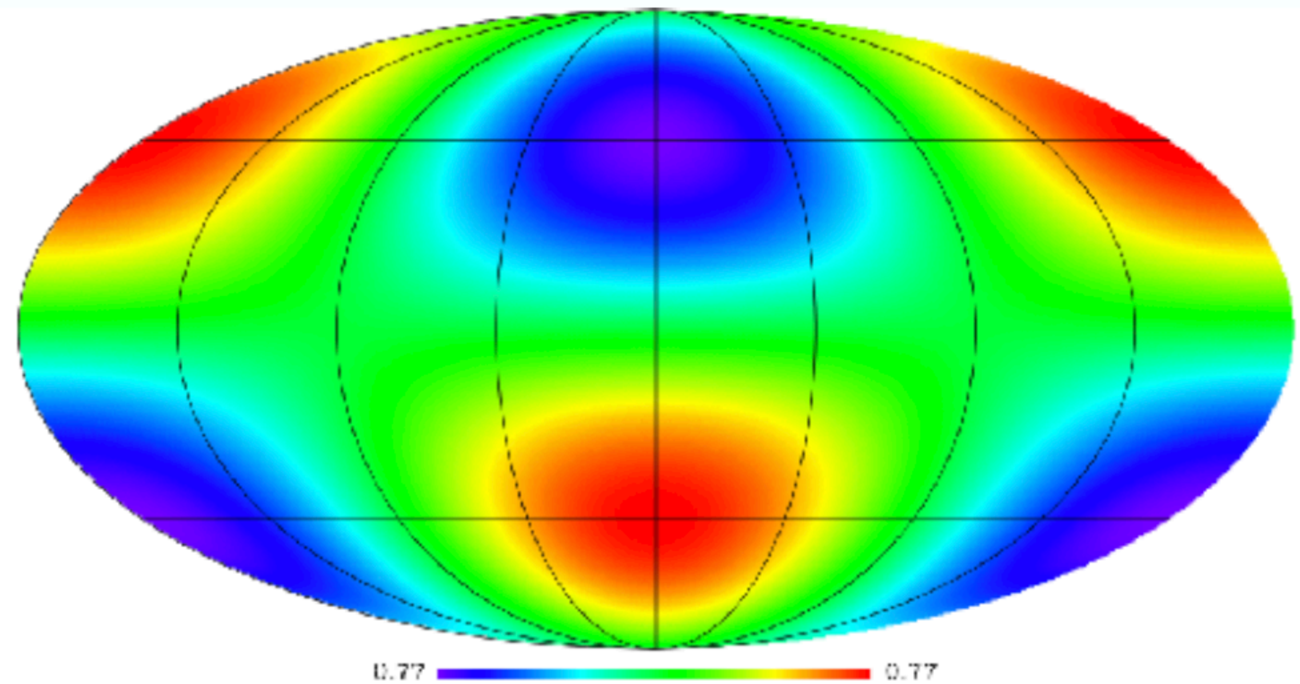

(l,m)=(2,2)

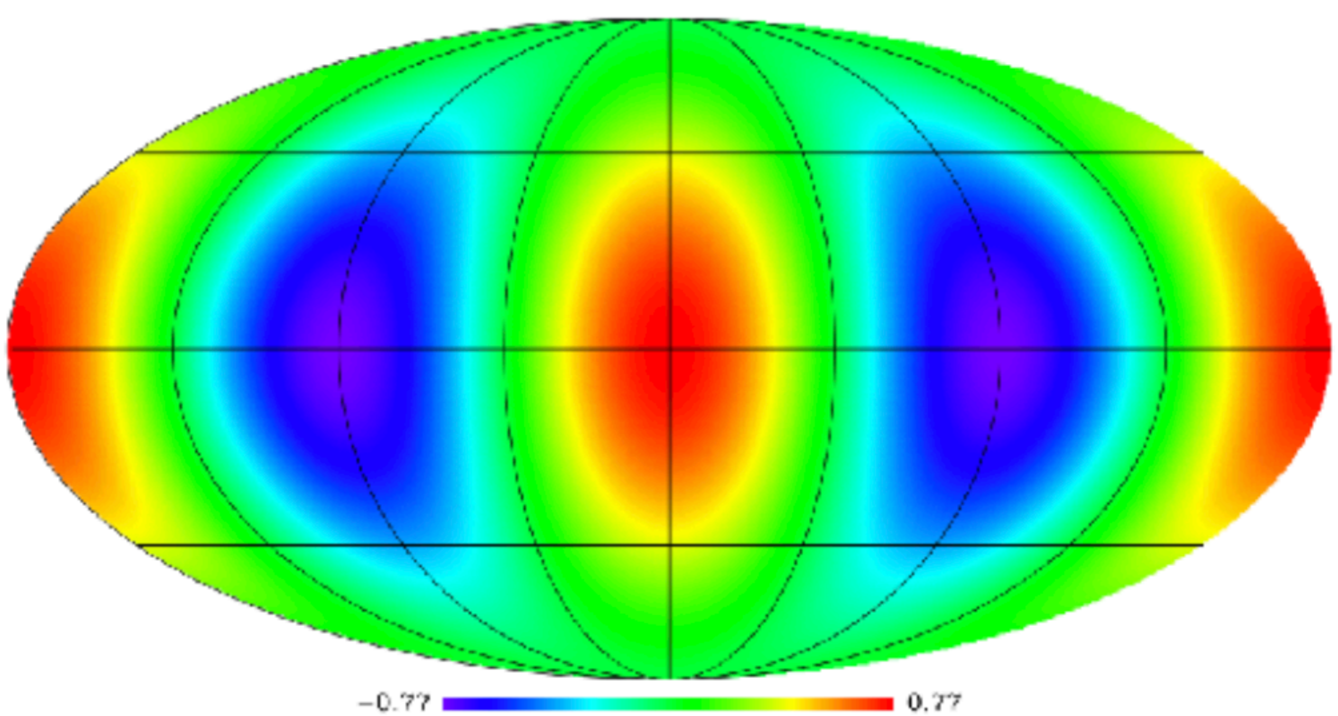

Local quadrupole temperature anisotropy seen from an electron

Polarization patterns

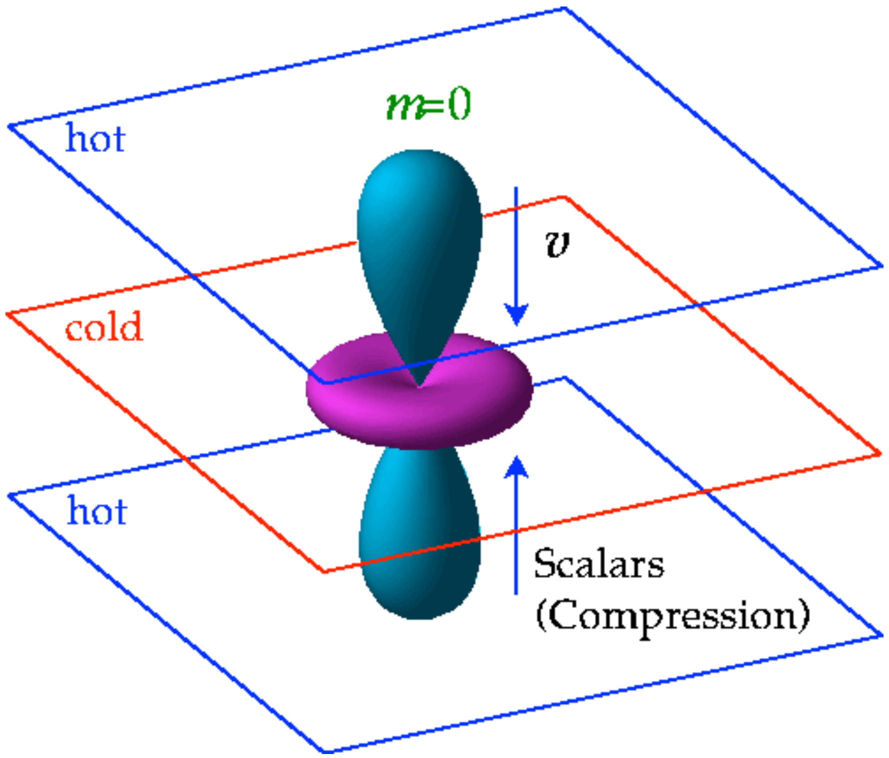

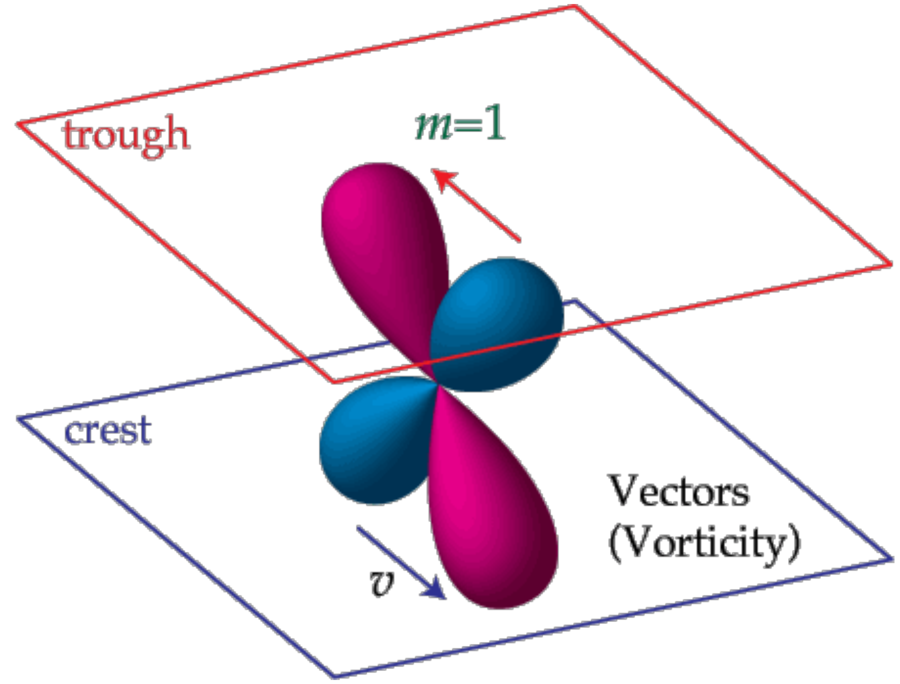

There are three sources to the quadrupole temperature anisotropy at recombination:

- scalers (m=0) for velocity perturbation
- vectors (m=1) for vorticity (negligible)
- tensors (m=2) for gravity waves

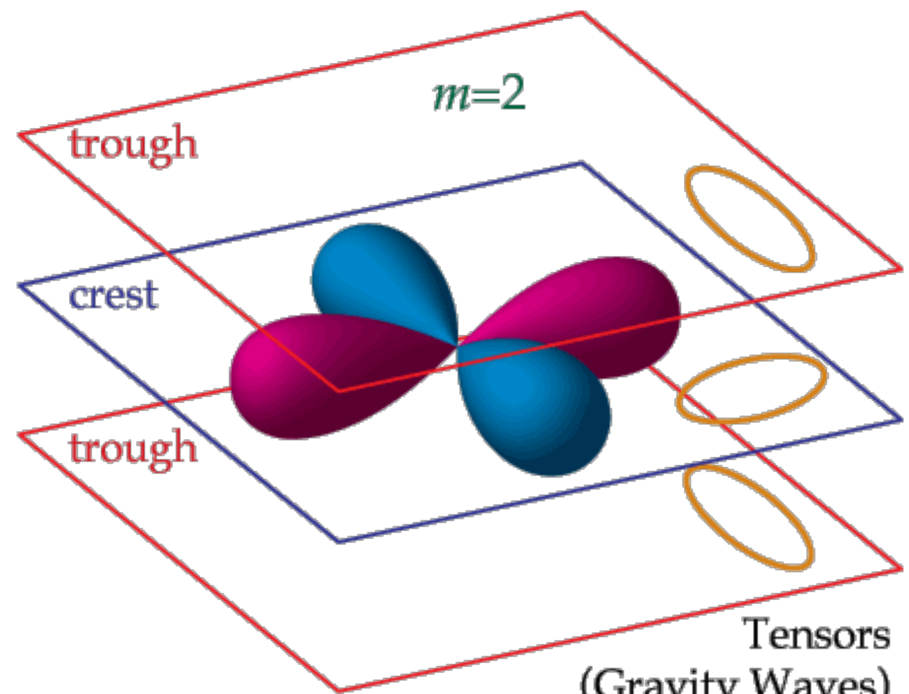

Visualization of the polarization pattern

Polarization pattern is a projection of quadropole moments

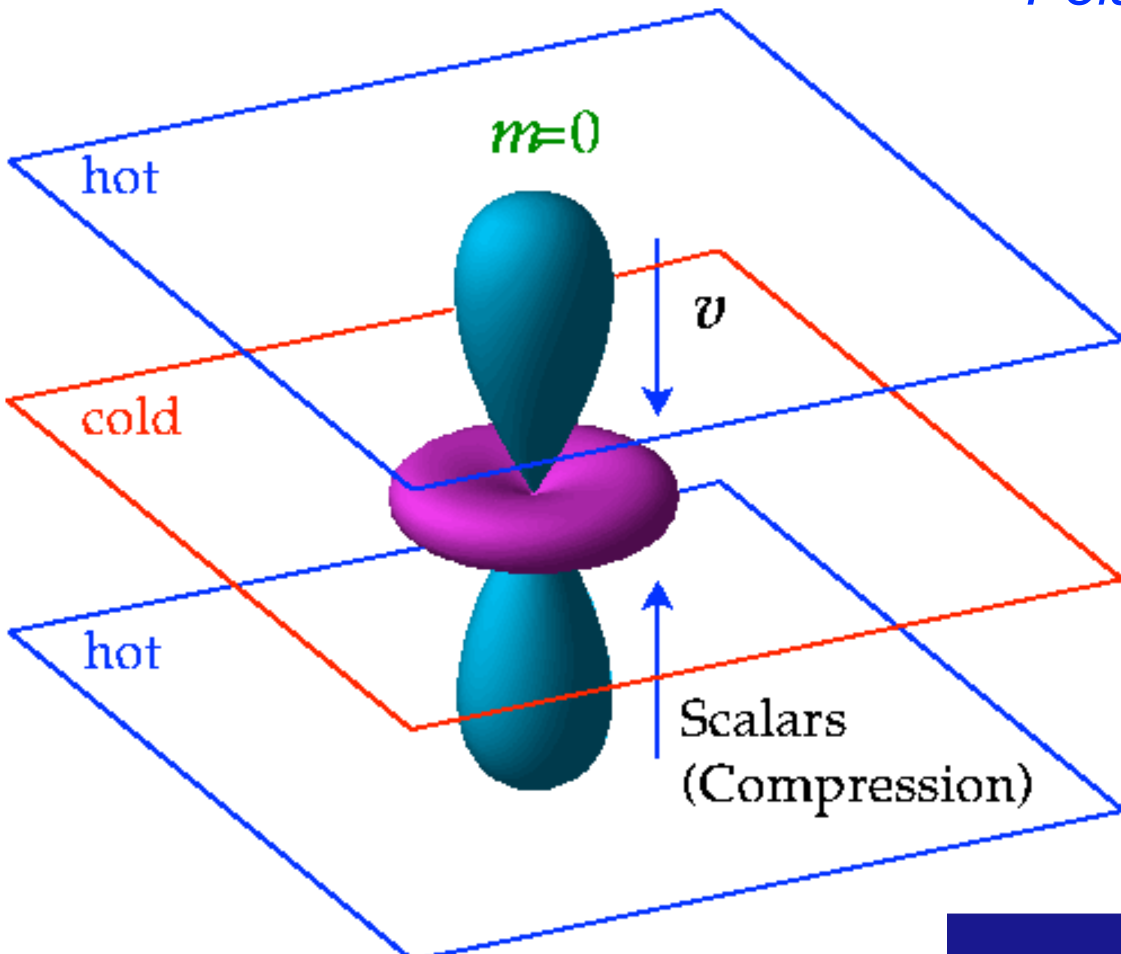

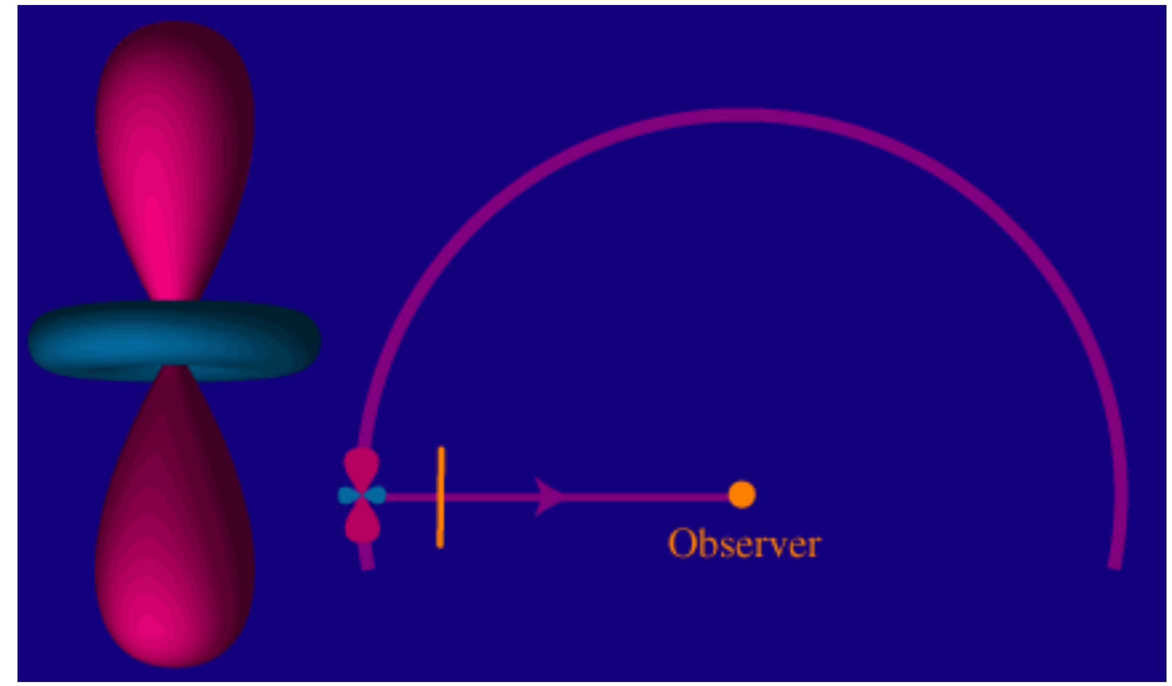

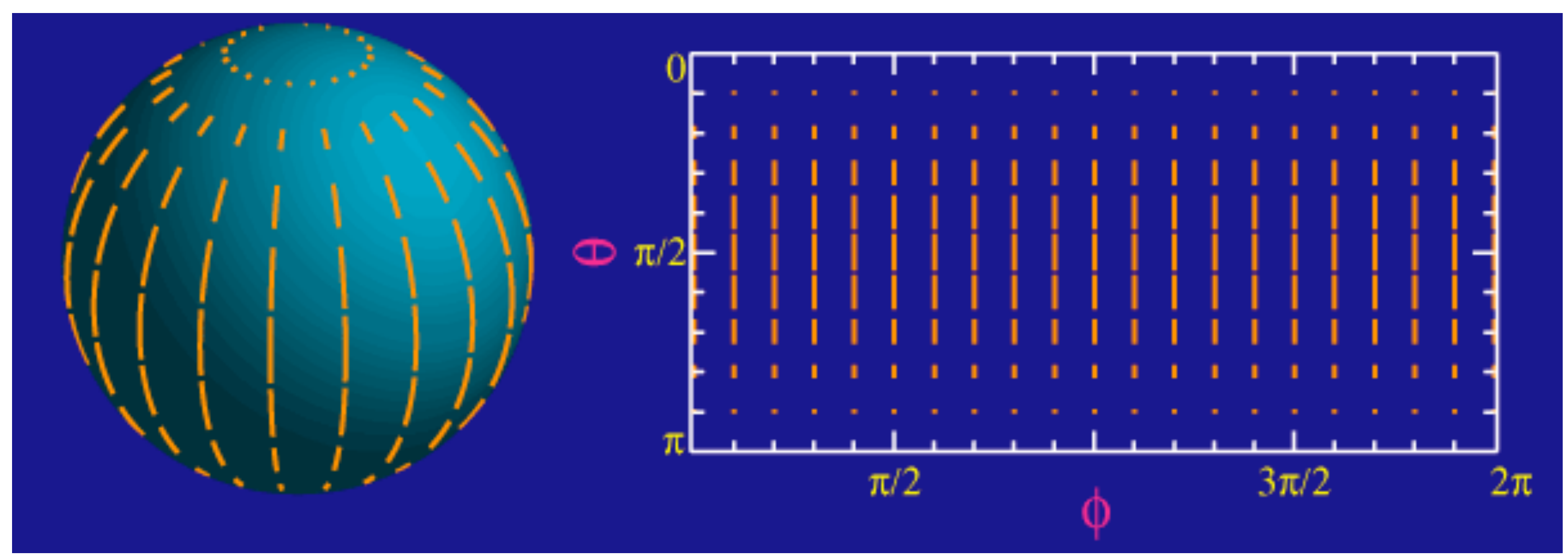

The scaler quadrupole moment, l=2, m=0. Note the azimuthal symmetry in the transformation of this quadrupole anisotropy into linear polarization.

Polarization patterns

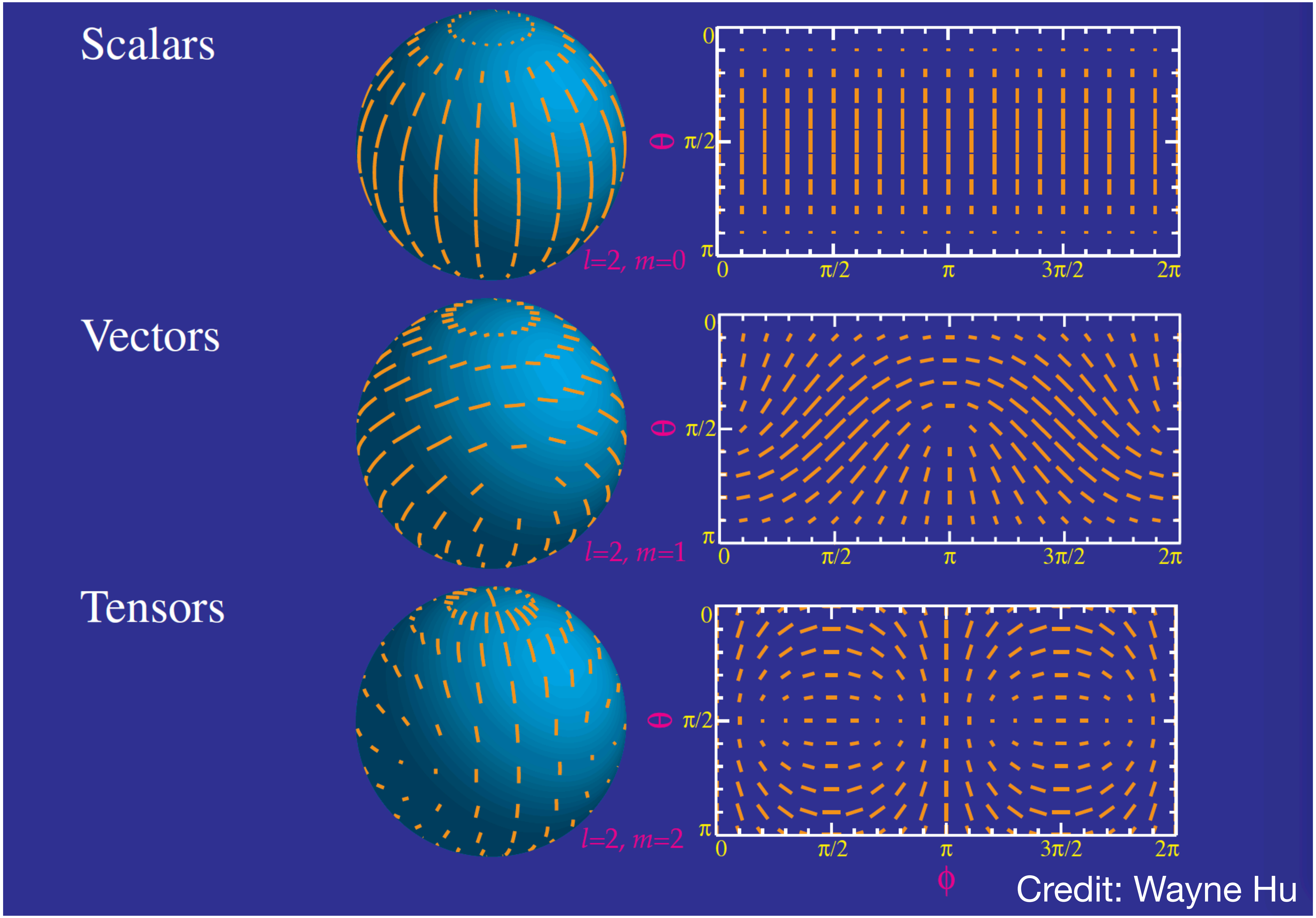

Polarization patterns

Animations by Wayne Hu. Thick and thin lines are E and B-mode patterns.

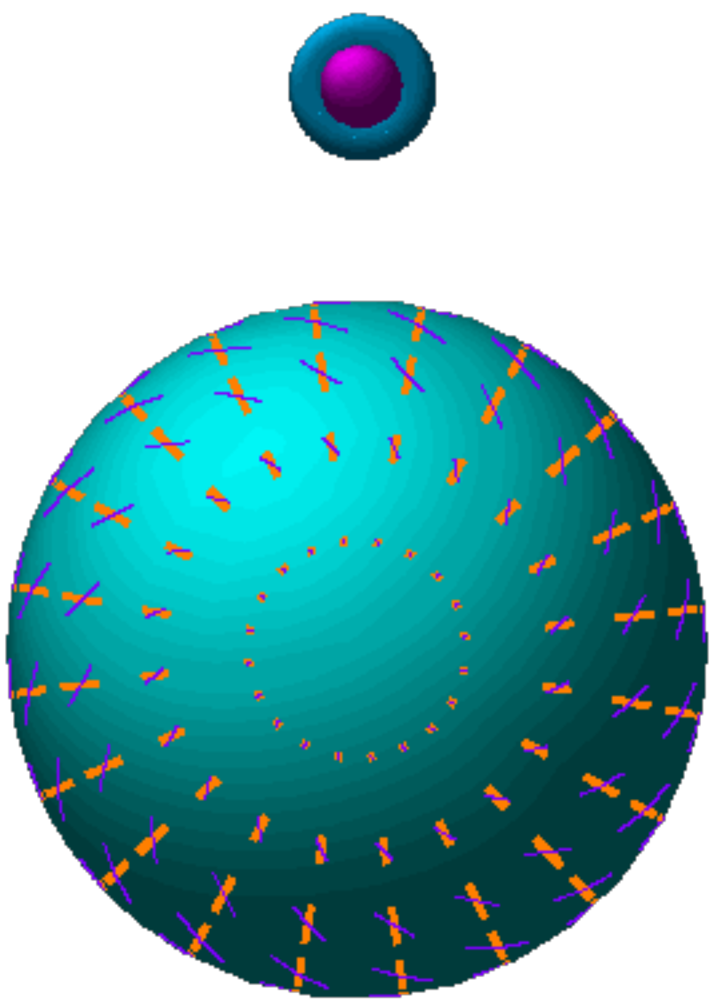

Scaler mode
(l=2, m=0)

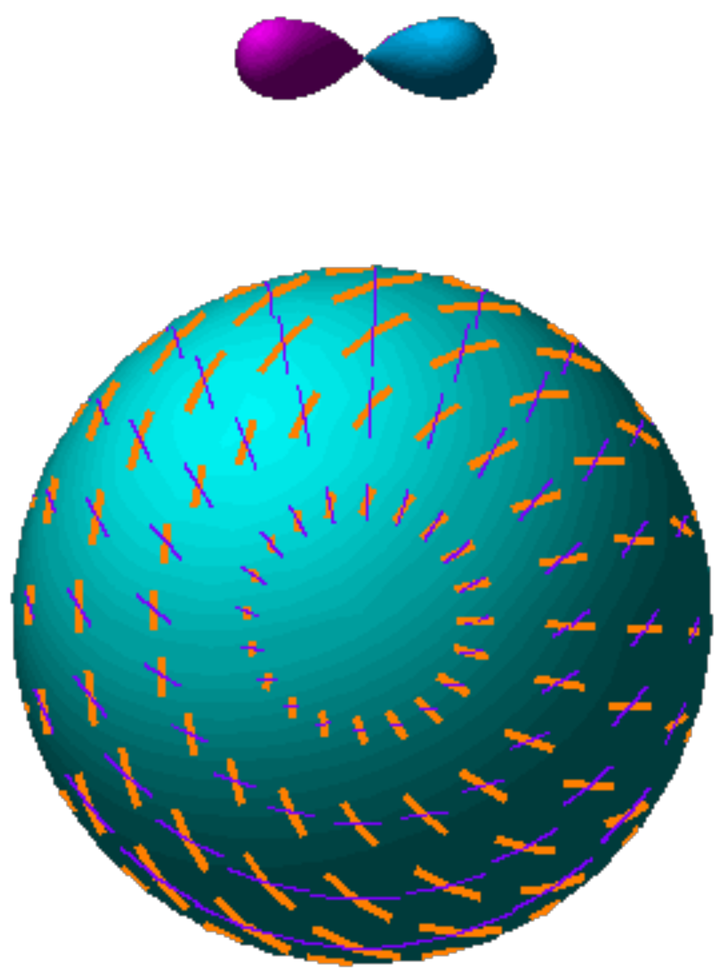

Vector mode
(l=2, m=±1)
(negligible)

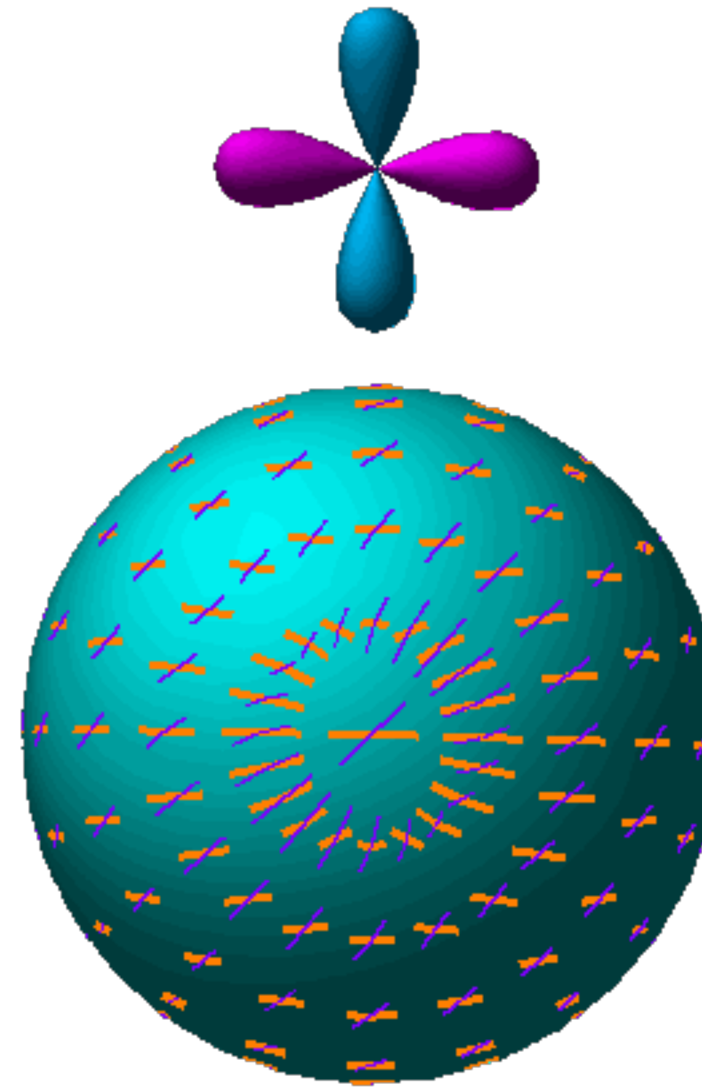

Tensor mode
(l=2, m=±2)

Parity of E & B modes

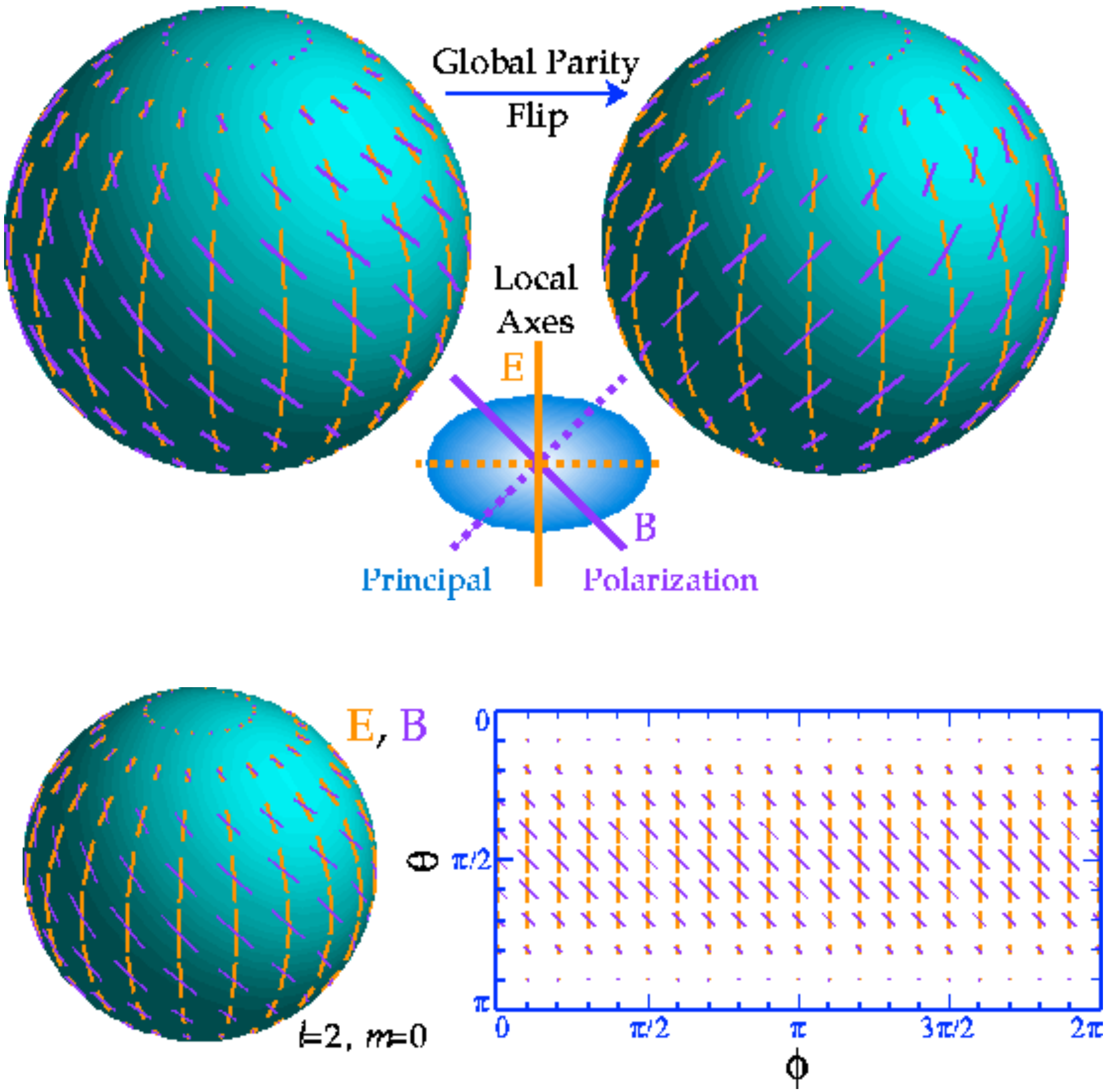

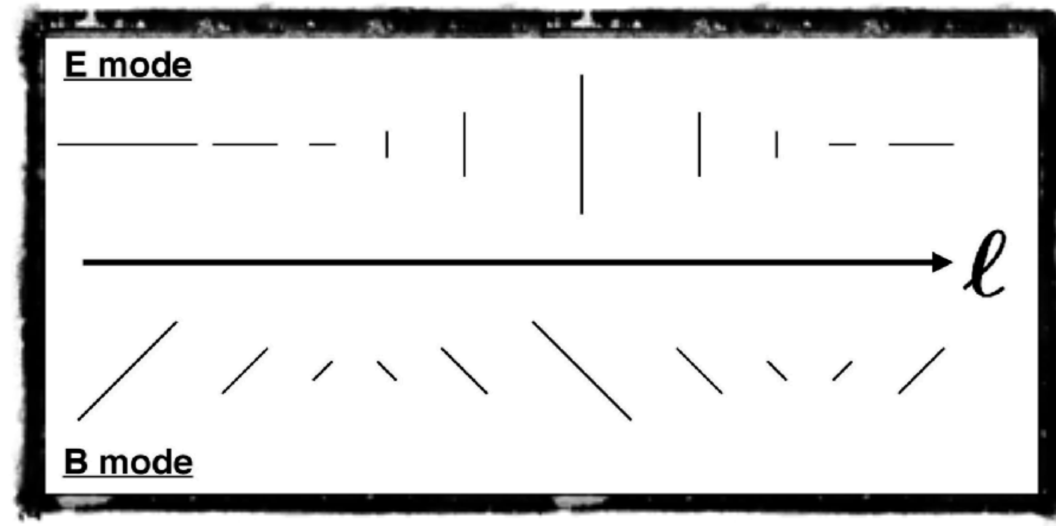

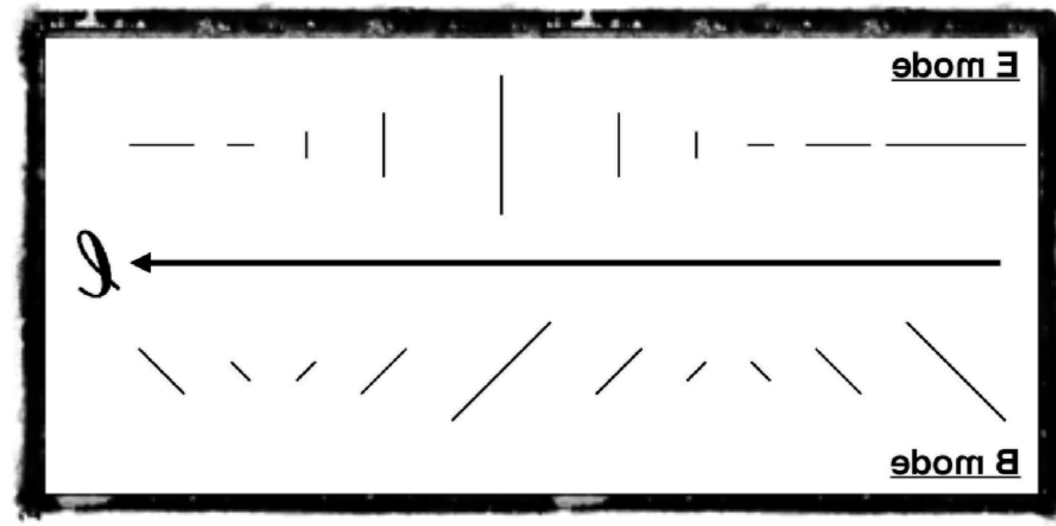

- **E mode**: Parity even
- **B mode**: Parity odd

Parity determines the number of power spectra

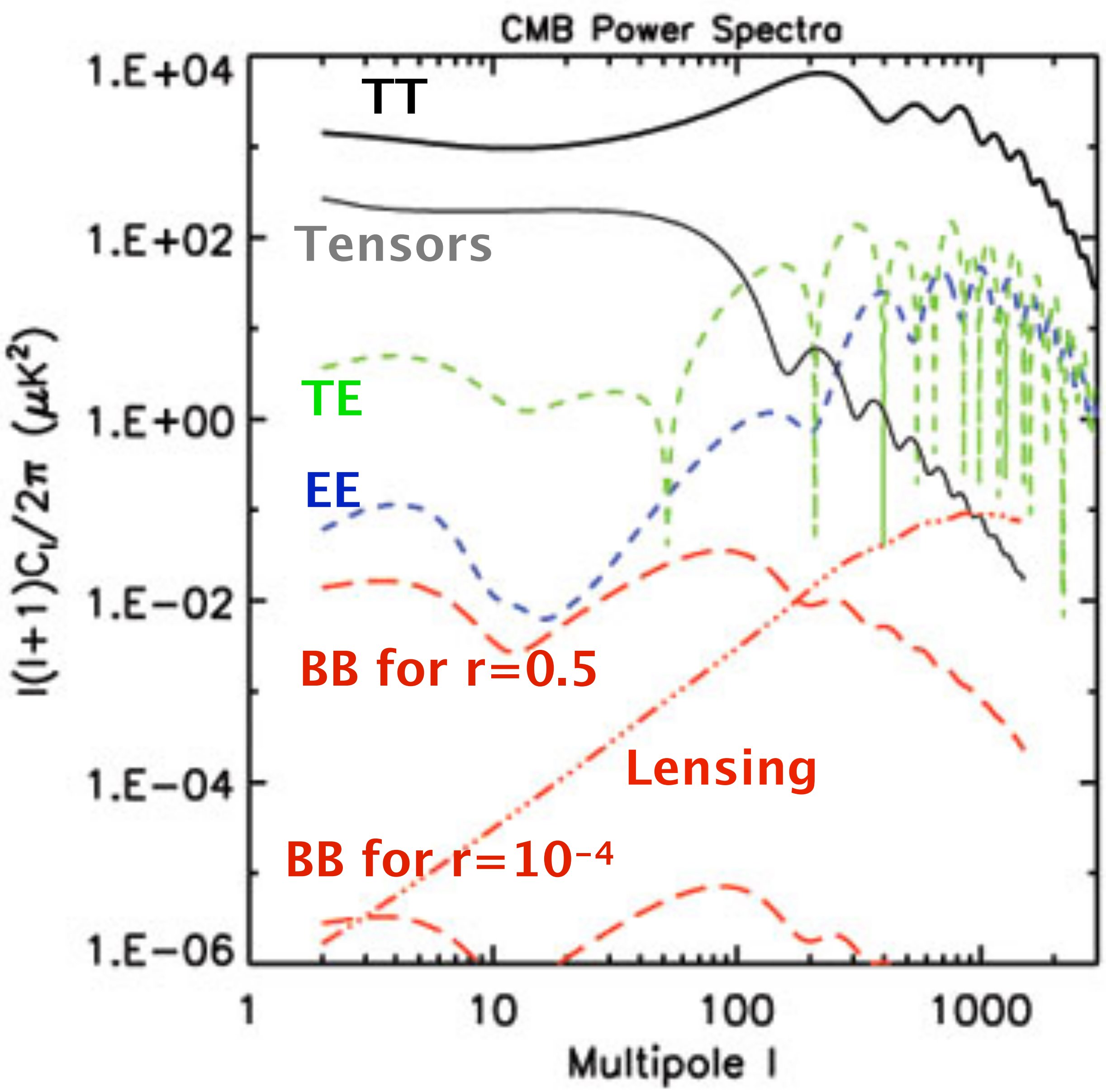

r = T/S: Tensor to scaler ratio, generated by the primordial gravity waves at last scattering

E & B modes have different reflection properties ("parities"):

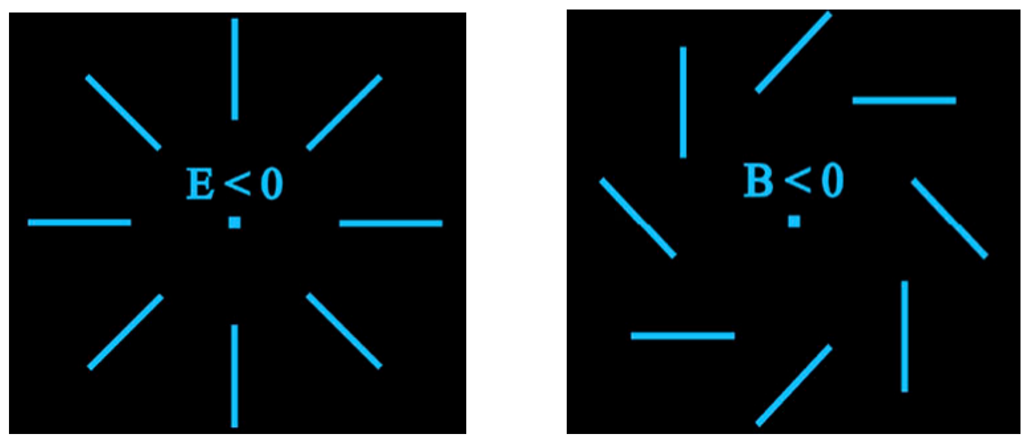

Parity: $(-1)^l$ for E and $(-1)^{l+1}$ for B (here l=2) **⇒ B has negative parity**

The cross-correlation between B and E or B and T vanishes (unless there are parity-violating interactions), because B has opposite parity to T or E.

We are therefore left with 4 fundamental observables.

Effect of gravitational lensing

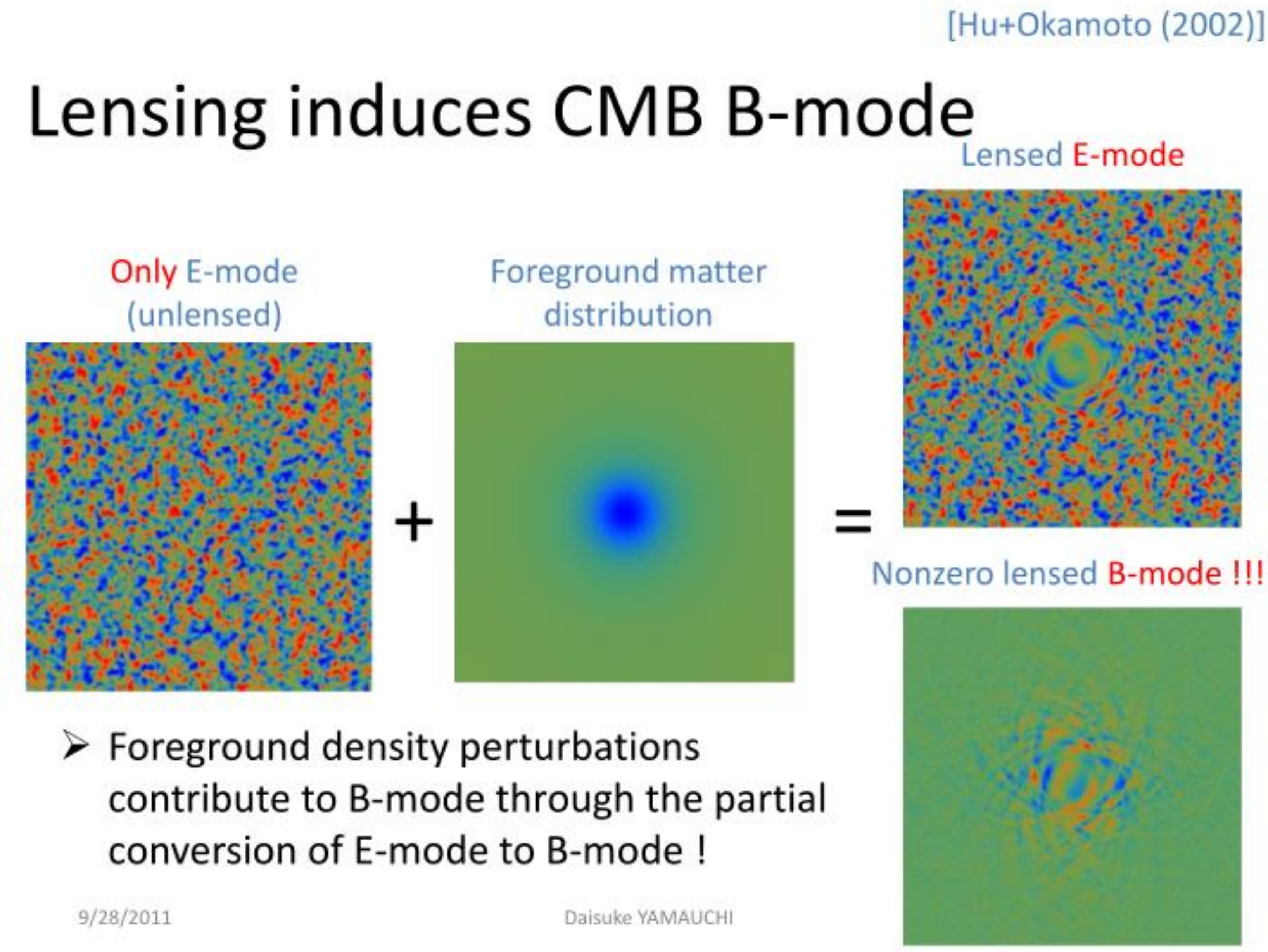

Need to de-lens to get to the primordial B-mode

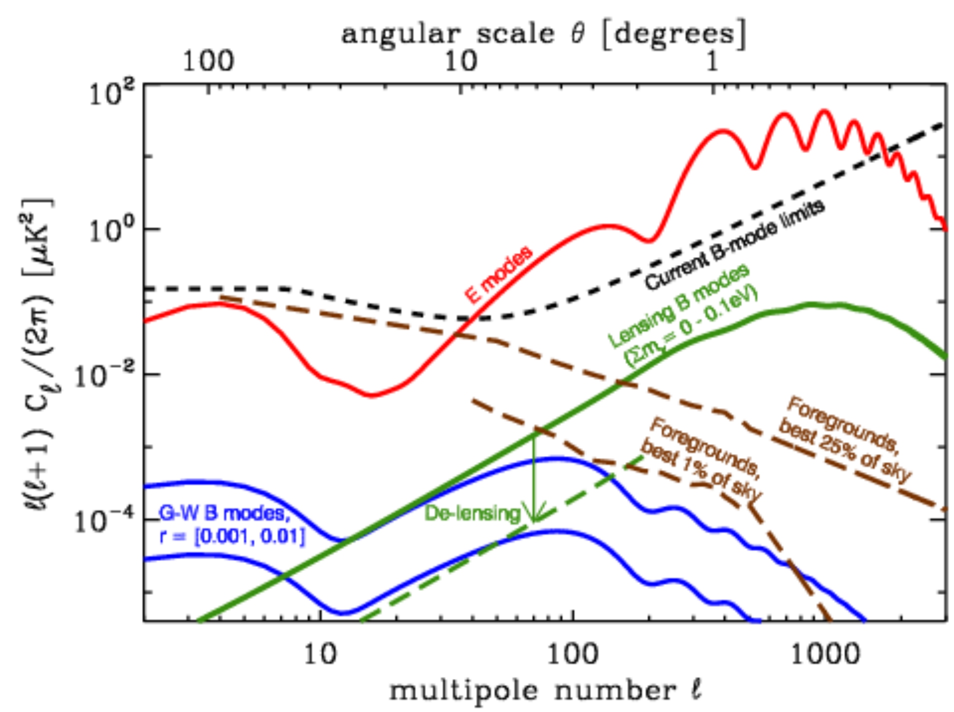

We will visit this topic in more details later!

Recap on inflation and the meaning of the tensor-to-scalar ratio, *r*

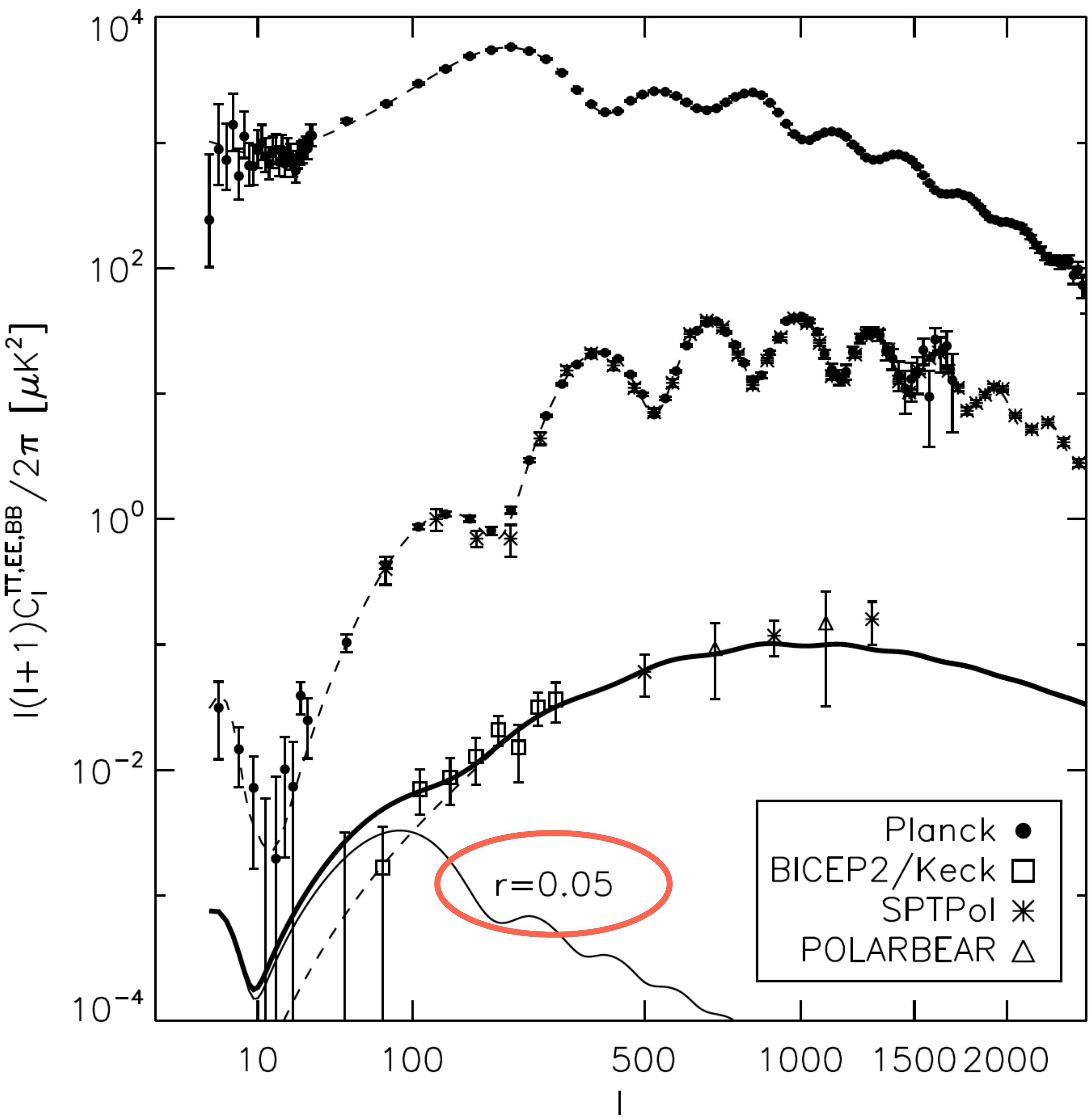

Tensor-to-scalar ratio

I. Scalar power spectrum

The scaler perturbations are Gaussian, so all information about them is contained in the two-point correlation function:

$$\langle \mathcal{R}(\mathbf{k})\mathcal{R}^*(\mathbf{k}')\rangle = \frac{P(k)}{(2\pi)^3}\delta(\mathbf{k}-\mathbf{k}'),$$

The mean square value of the initial perturbation amplitude is

$$\langle \mathcal{R}^2(\mathbf{x})\rangle = \langle \int e^{i\mathbf{kx}} R(\mathbf{k}) d^3k \int e^{-i\mathbf{k}'\mathbf{x}} R^*(\mathbf{k}') d^3k' \rangle = \int d^3k \frac{P(k)}{(2\pi)^3} = \int_0^\infty \frac{dk}{k}\mathcal{P}(k),$$

Where $\mathcal{P}(k) = k^3 P(k)/(2\pi^2)$ is also called the power spectrum, and is approximated as follows:

$$\mathcal{P}_s(k) = A_s \left(\frac{k}{k_*}\right)^{n_s-1}$$

In 1960's, Zel'dovich and Harrison independently predicted the flat spectrum of perturbations (i.e. $n_s = 1$). But we know the spectrum is *slightly red!* The WMAP5 values for a fixed $k_* = 500\ \mathrm{Mpc}^{-1}$ are:

$$A_s = (2.46 \pm 0.09)\cdot 10^{-9},$$
$$n_s = 0.960 \pm 0.014.$$

Tensor–to–scalar ratio

2. Tensor power spectrum & power ratio, *r*

Actually, the derivation of approximately flat power spectrum does not depend on whether we deal with scalar or tensor fields. **Inflation also generates tensor perturbations** (transverse traceless perturbations of spatial metric h_{ij}, i.e. gravitational waves).

We have the same picture for tensor perturbations: primordial perturbations are Gaussian random field with almost flat power spectrum. In this case we have

$$\mathcal{P}_T(k) = A_T \left(\frac{k}{k_*}\right)^{n_T} .$$

It is convenient to introduce the parameter $r = \mathcal{P}_T/\mathcal{P}_s$ which measures the ratio of tensor to scalar perturbations.

For simple inflation theories with power–law potentials (last slide), prediction is $r \sim 0.1 - 0.3$

➜ these are now practically ruled out by Planck data

Tensor–to–scalar ratio

3. Inflation and the spectral index, n_s

Inflation occurs if the universe is filled with a scalar field φ, which has non–vanishing scalar potential V(φ). The homogeneous field φ then satisfies the equation

$$\ddot{\varphi} + 3H\dot{\varphi} = -\frac{dV}{d\varphi}. \qquad a(t) \propto \exp\left(\int H dt\right), \quad H \approx \text{const.}$$

For a relatively flat potential (dV/dφ small), the acceleration term can be neglected. The Friedmann equation in this case is $H^2 = 8\pi/3G\, V(\varphi)$. So if φ varies slowly, then V(φ) and thus H also varies slowly, and the parameters of inflation are almost time independent (slow-roll inflation).

Yet, the parameters are not exactly time–independent at inflation, so the predicted value of the spectral tilt (n_s – 1) is small but non–zero. It can be positive or negative, depending on the scalar potential V(φ). In particular, it is negative for the simplest power–law potentials like

$$V(\varphi) = \frac{m^2}{2}\varphi^2 \quad \text{or} \quad V(\varphi) = \frac{\lambda}{4}\varphi^4.$$

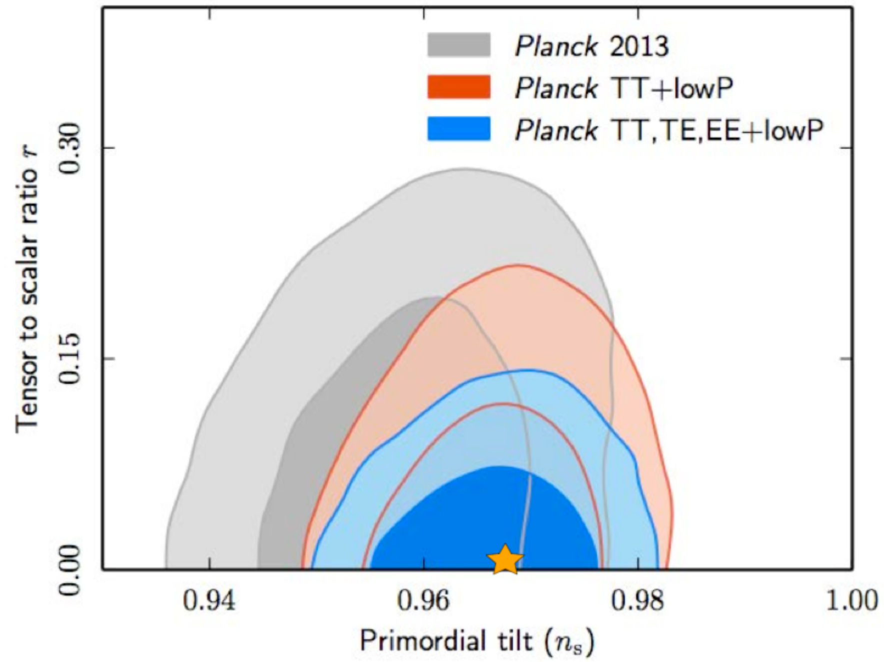

For the case of slow–roll inflation,

$$n_s - 1 = -3M_{\rm pl}^2\left(\frac{V'}{V}\right)^2 + 2M_{\rm pl}^2\frac{V''}{V}$$

with $' \equiv \frac{\partial}{\partial\phi}$.

Tensor-to-scalar ratio

4. Predictions for single-field, slow-roll inflation

Slow-Roll inflation requires the acceleration term for the potential is zero, and the shape of the potential is parametrized by the "slow-roll parameters"

$$\boxed{\ddot{\varphi} + 3H\dot{\varphi} = -V'(\varphi)}$$

$$H^2 = \frac{V(\varphi)}{3M_{\rm Pl}^2}$$
$$3H\dot{\varphi} = -V'(\varphi)$$

$$\varepsilon(\varphi) \equiv \frac{1}{2}M_{\rm Pl}^2\left(\frac{V'}{V}\right)^2$$
$$\eta(\varphi) \equiv M_{\rm Pl}^2\frac{V''}{V}$$

For scalar perturbations:

$$\Delta_{\mathcal{R}}^2(k) \equiv A_s\left(\frac{k}{k_\star}\right)^{n_s-1}$$

$$\boxed{n_s - 1 = -2\varepsilon - \eta}$$

For tensor perturbations:

$$\Delta_t^2(k) \equiv A_t\left(\frac{k}{k_\star}\right)^{n_t}$$

$$\boxed{\begin{aligned} r &= 16\varepsilon \\ n_t &= -2\varepsilon \end{aligned}}$$

The tensor amplitude is a direct measure of the expansion rate H during inflation. This is in contrast to the scalar amplitude which depends on both H and ε.

- Single-field slow-roll inflation looks remarkably good:
  - **Super-horizon fluctuation**
  - **Adiabaticity**
  - **Gaussianity**
  - **n_s<1**

But we want a direct confirmation of inflation and probe its energy scale: ***Gravitational waves!***

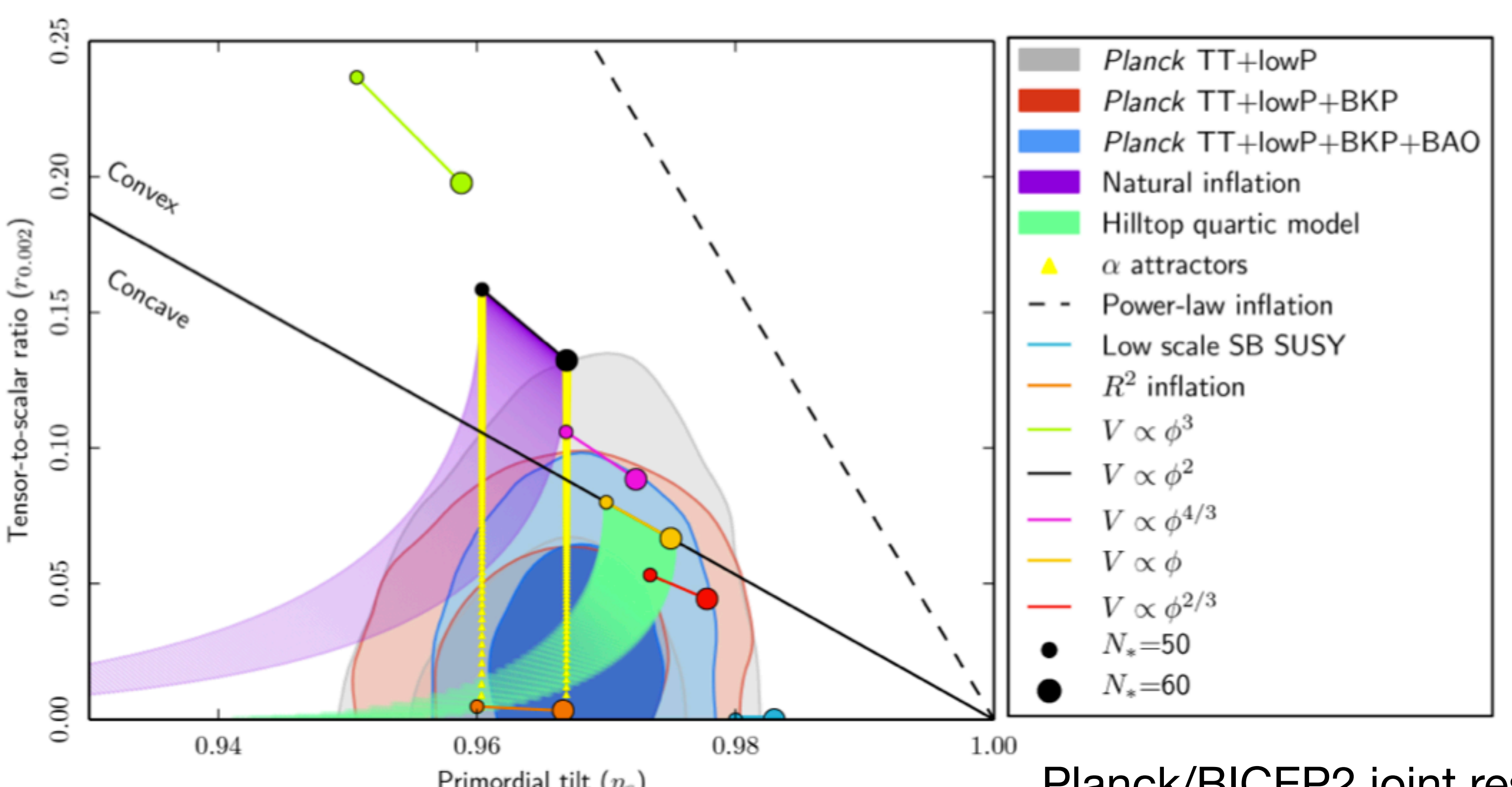

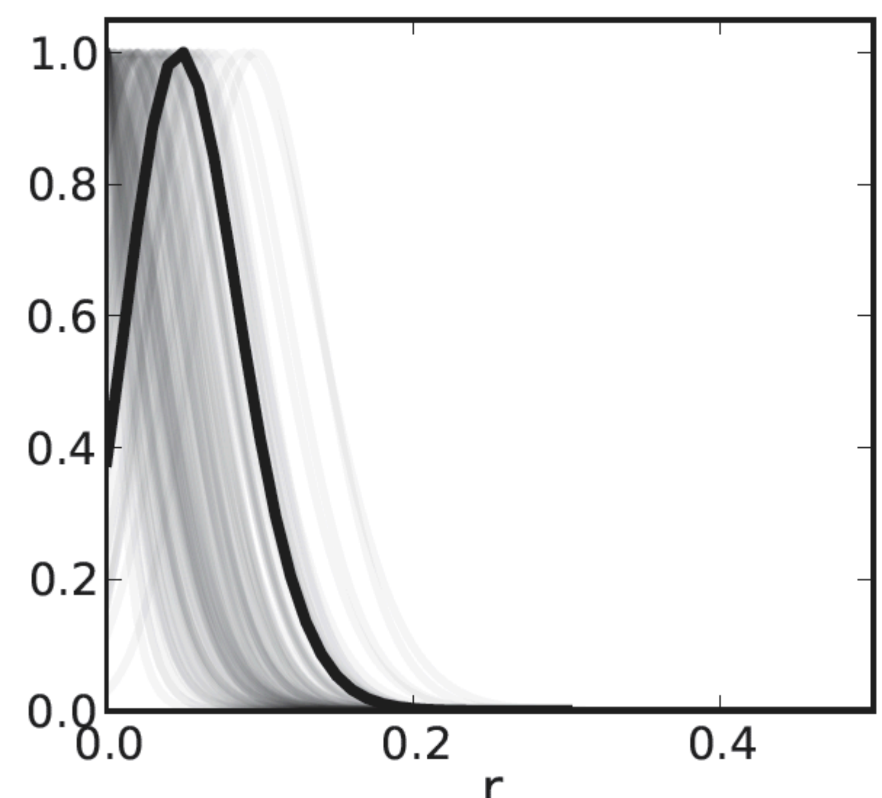

Planck/BICEP2 joint results (2015)

Detecting polarization is difficult!

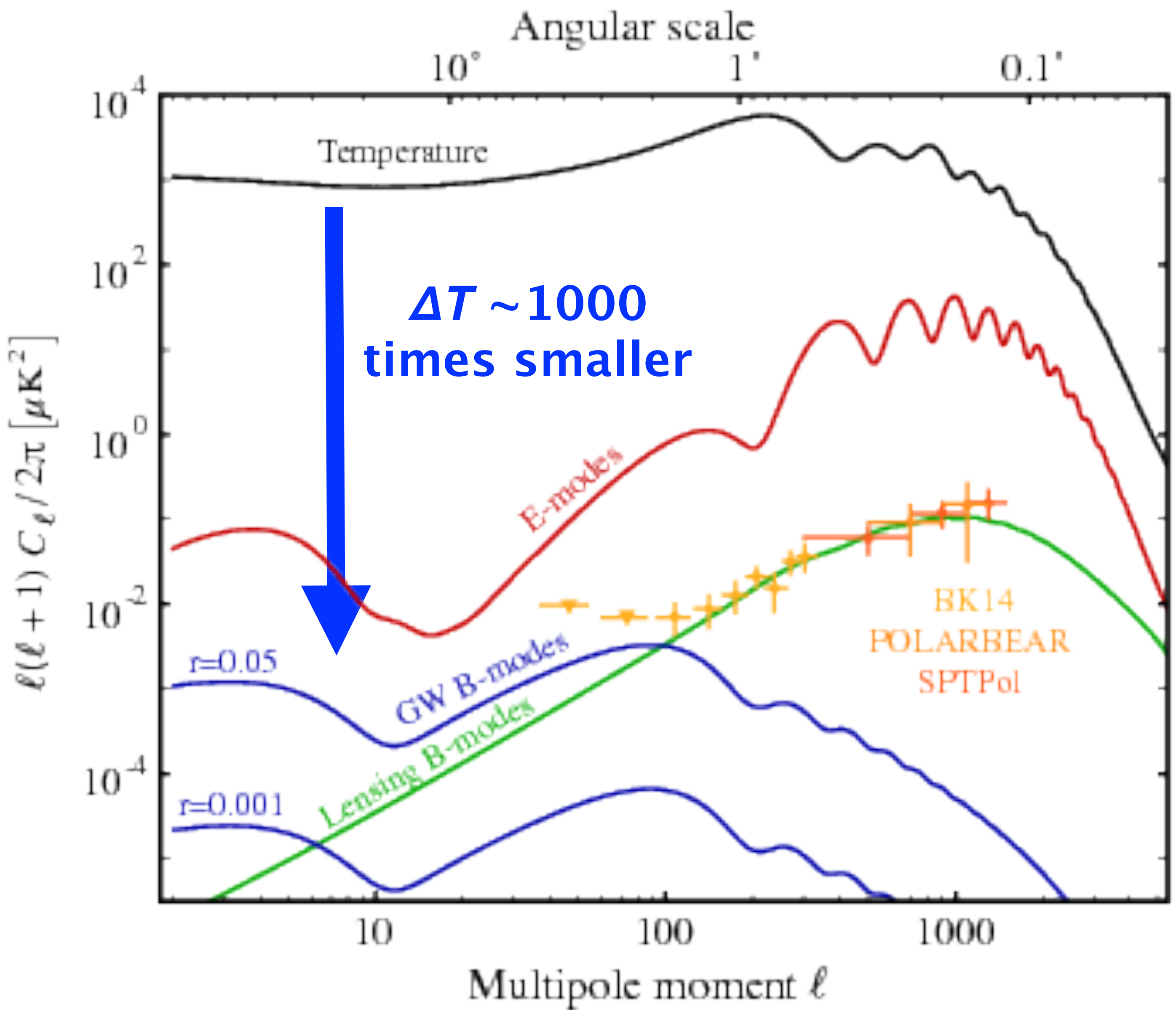

Polarization signal amplitude is much smaller than the temperature, since it requires a scattering event and hence can only be produced in optically thin condition (any subsequent scattering will cancel the polarization signature).

We are getting a snapshot of the quadrupole anisotropies from the moment of last scattering.

Power spectra of CMB temperature anisotropies (black), grad polarization (red), and curl polarization due to the GWB (blue) and due to the lensing of the grad mode (green), all assuming a standard CDM model with T/S = 0.28. The dashed curve indicates the effects of reionization on the grad mode for $\tau = 0.1$.

Shape of polarization power spectra

The polarization power also exhibits acoustic oscillations since the quadrupole anisotropies that generate it are themselves formed from the acoustic motion of the fluid.

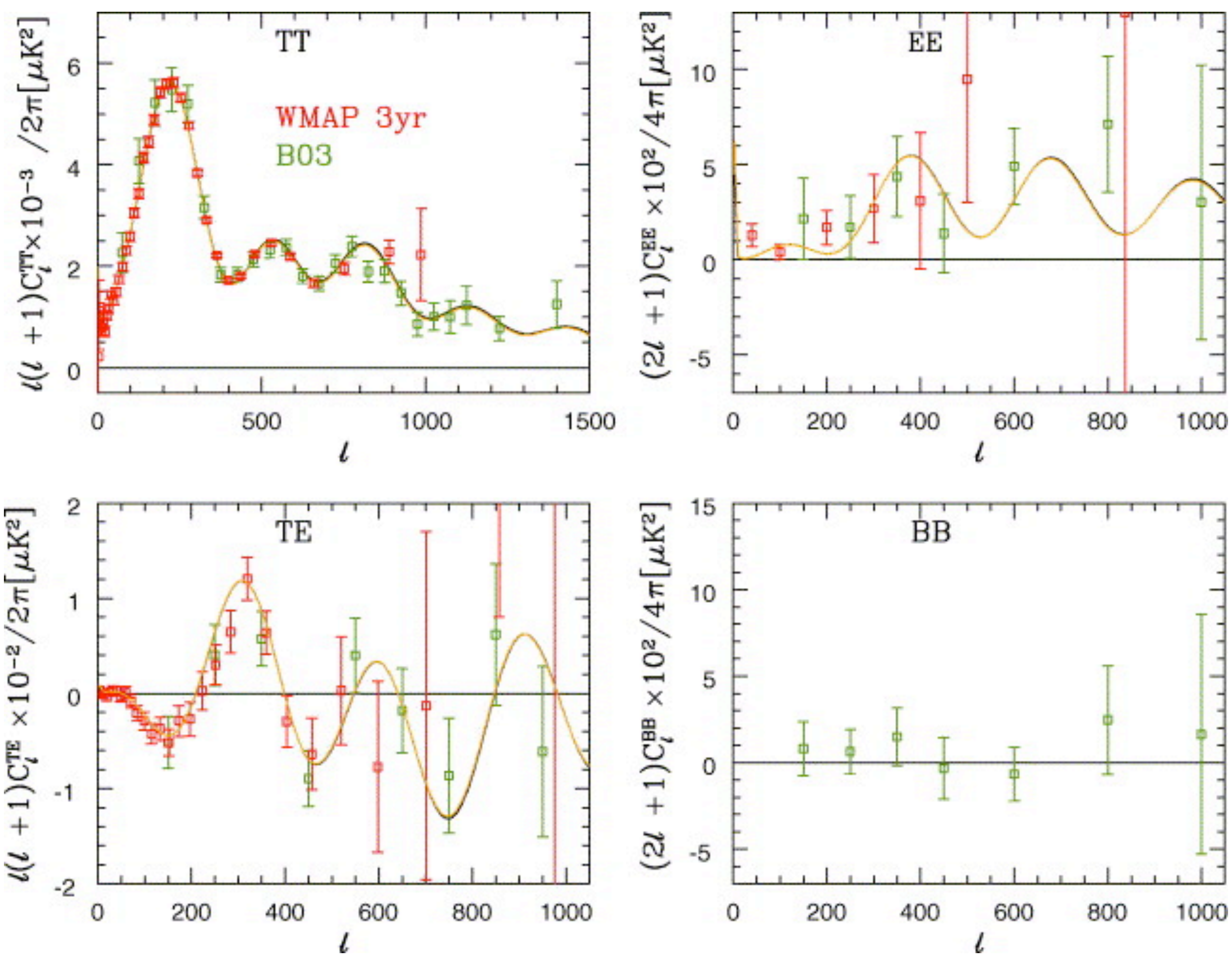

The EE peaks are out of phase with TT peaks because these E-mode primordial polarization anisotropies are sourced by the fluid velocity (hence *roughly* in-phase with velocity maxima).

Shape of polarization power spectra

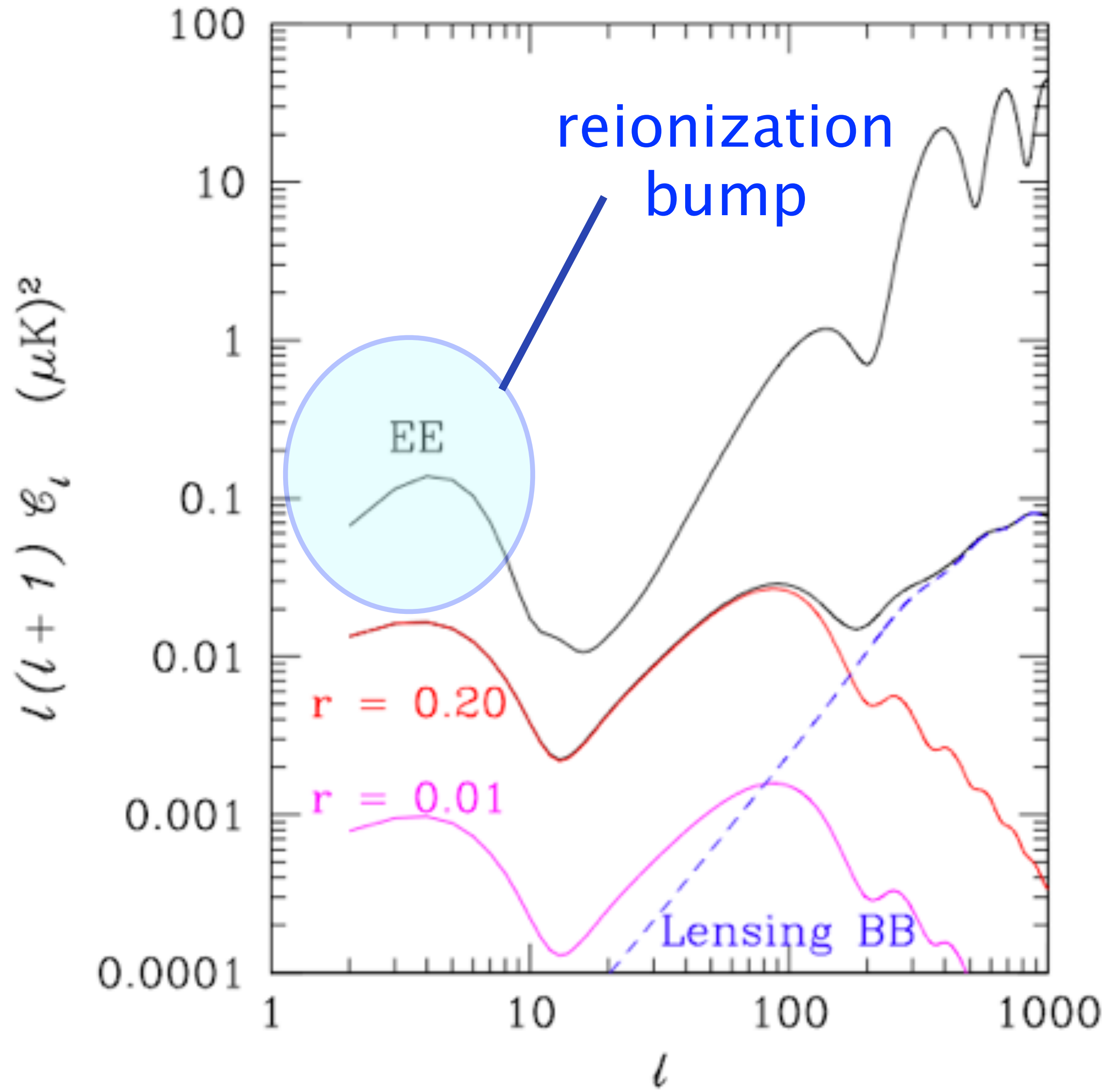

- Primordial E-mode signal peaks at small scales, corresponding to the width of the epoch of last scattering
- The primordial B-mode signal (due to a stochastic background of gravitational waves) dominates only at large angular scales
- On similarly large angular scales, the E-mode polarization signal is dominated by secondary fluctuations imprinted by reionization
- The lens-generated signal grows at smaller scales (turning E modes into B modes!)

Shape and amplitude of EE are predicted by ΛCDM.

Shape of BB is predicted "scale-invariant gravity waves".

Amplitude of BB is model dependent, and not really constrained from theory.
Measuring this amplitude would provide a direct handle of the energy scale of inflation!

EE power spectrum

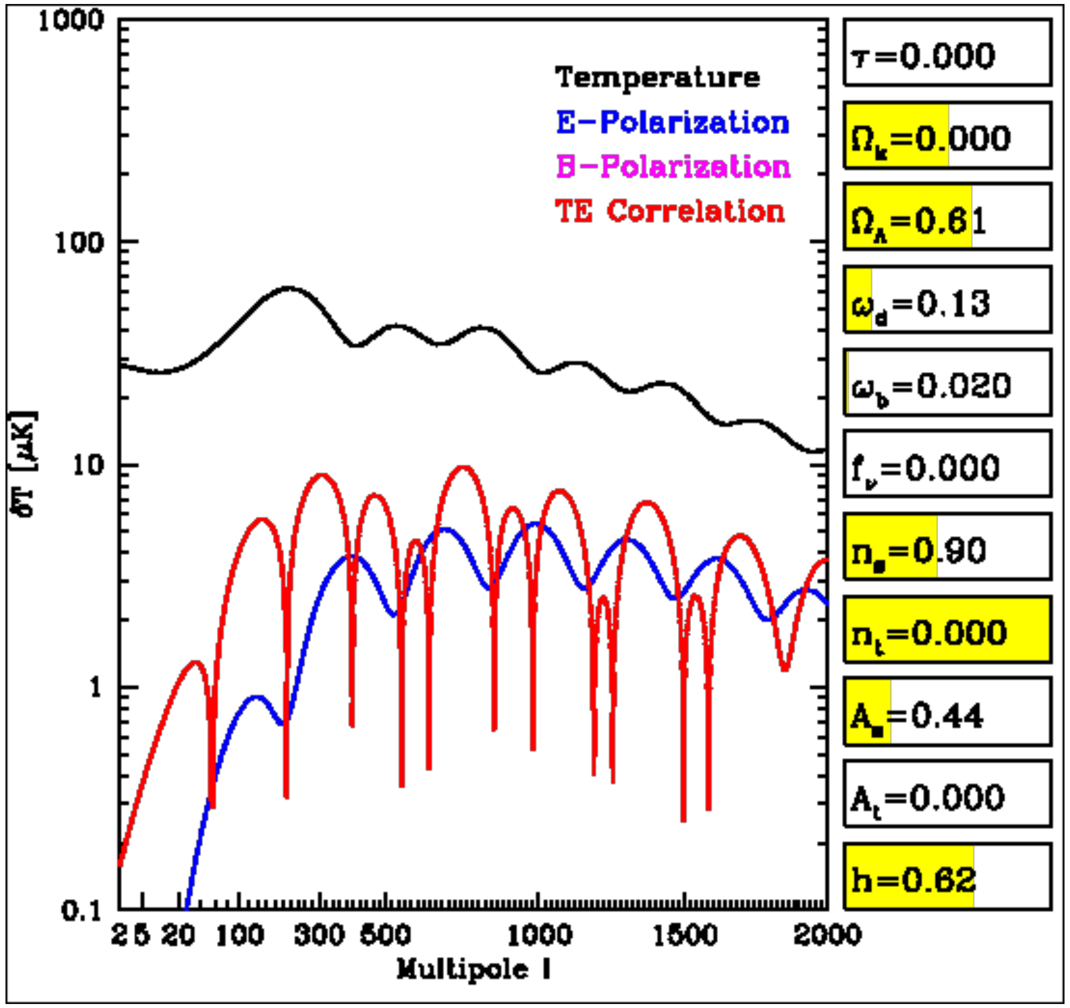

MCMC simulations from K. Vanderlinde

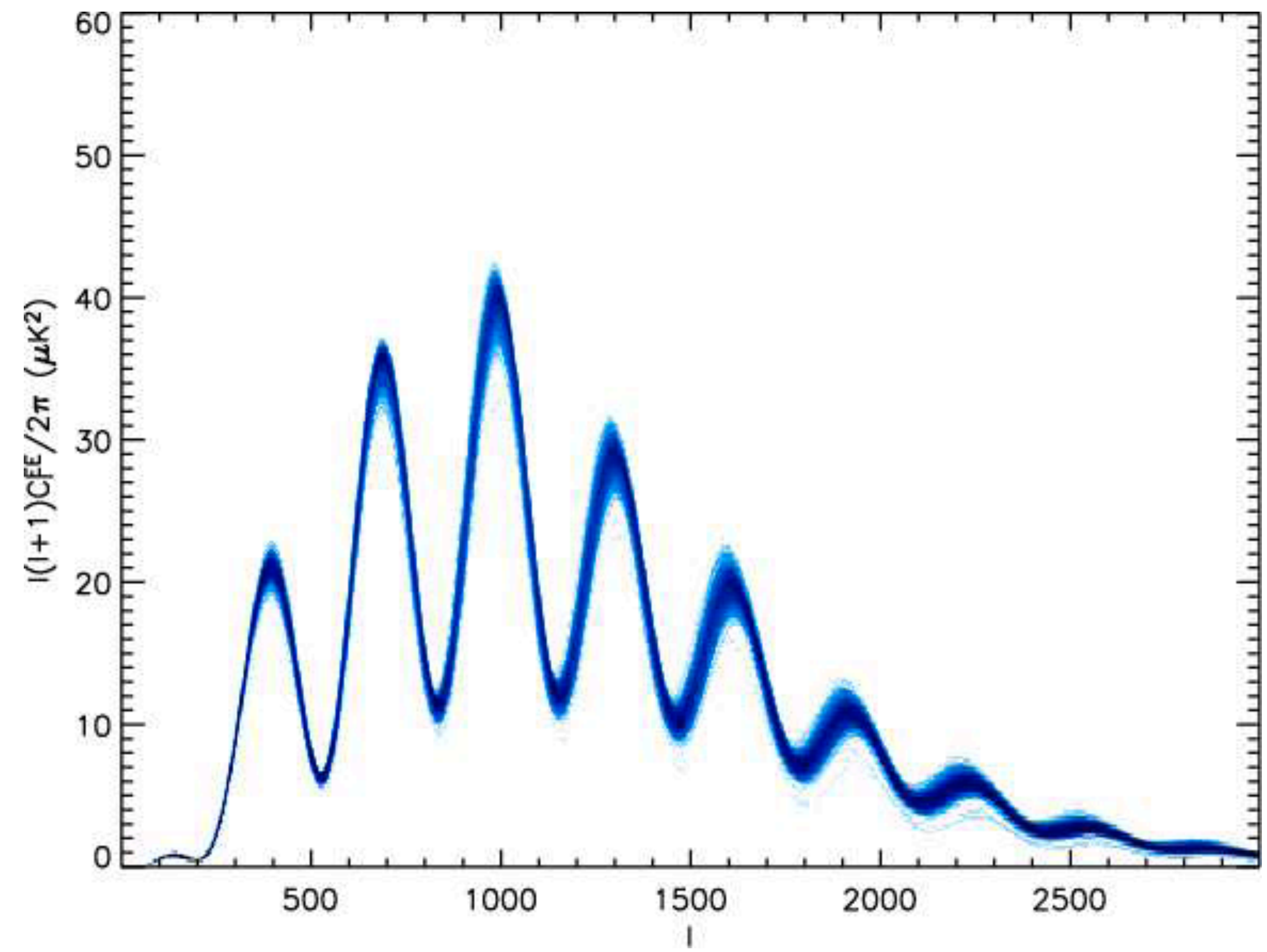

The intermediate to small scale EE polarization signal is sensitive only to the physics at the epoch of last scattering (unlike TT which can be modified).

The EE spectrum is already well constrained from the cosmological models, but it provides additional checks and helps to break some degeneracies. **Plus, it gives a more accurate measurement of the reionization optical depth.**

BB spectrum uncertainties

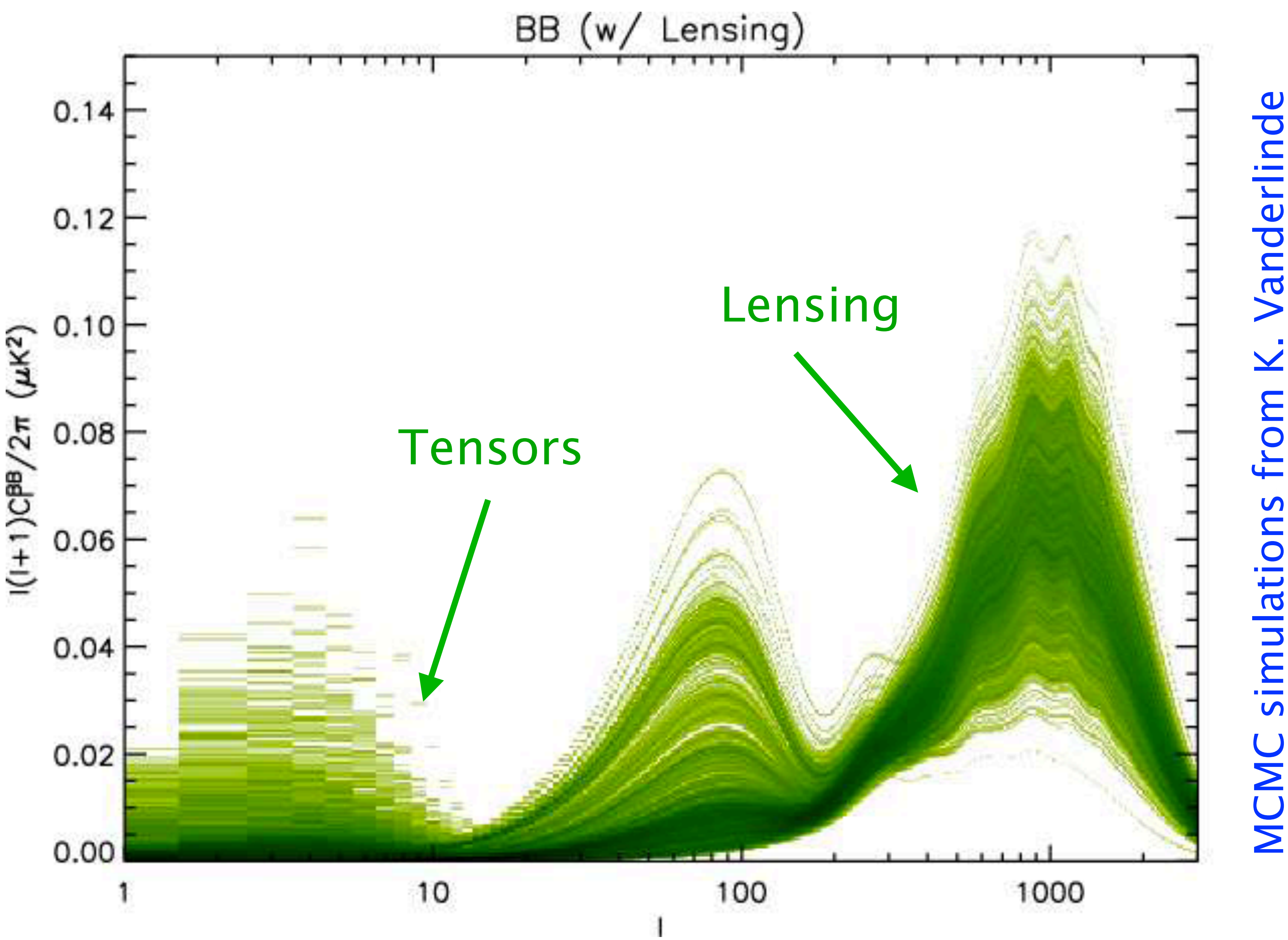

BB mode can tell us about a lot of new physics (energy scale at inflation, neutrino mass, etc.), but its prediction is still very uncertain.

Latest (2015) Planck+BICEP results put $r < 0.07$ at 95% confidence.

Detection of E-mode polarization

- The DASI experiment at the South Pole was the first to detect E-mode CMB polarization
- It was followed by WMAP's measurement of $C^{TE}(l)$ for $l<500$
- Both the BOOMERANG and the CBI experiments have reported measurements of C^{TT}, C^{TE}, C^{EE} and a non-detection of B modes
- E-mode has also been measured by CAPMAP and Maxipol
- B-mode polarization has not been detected yet (current noise level for ground-based experiment is below 1 μK in Q and U))

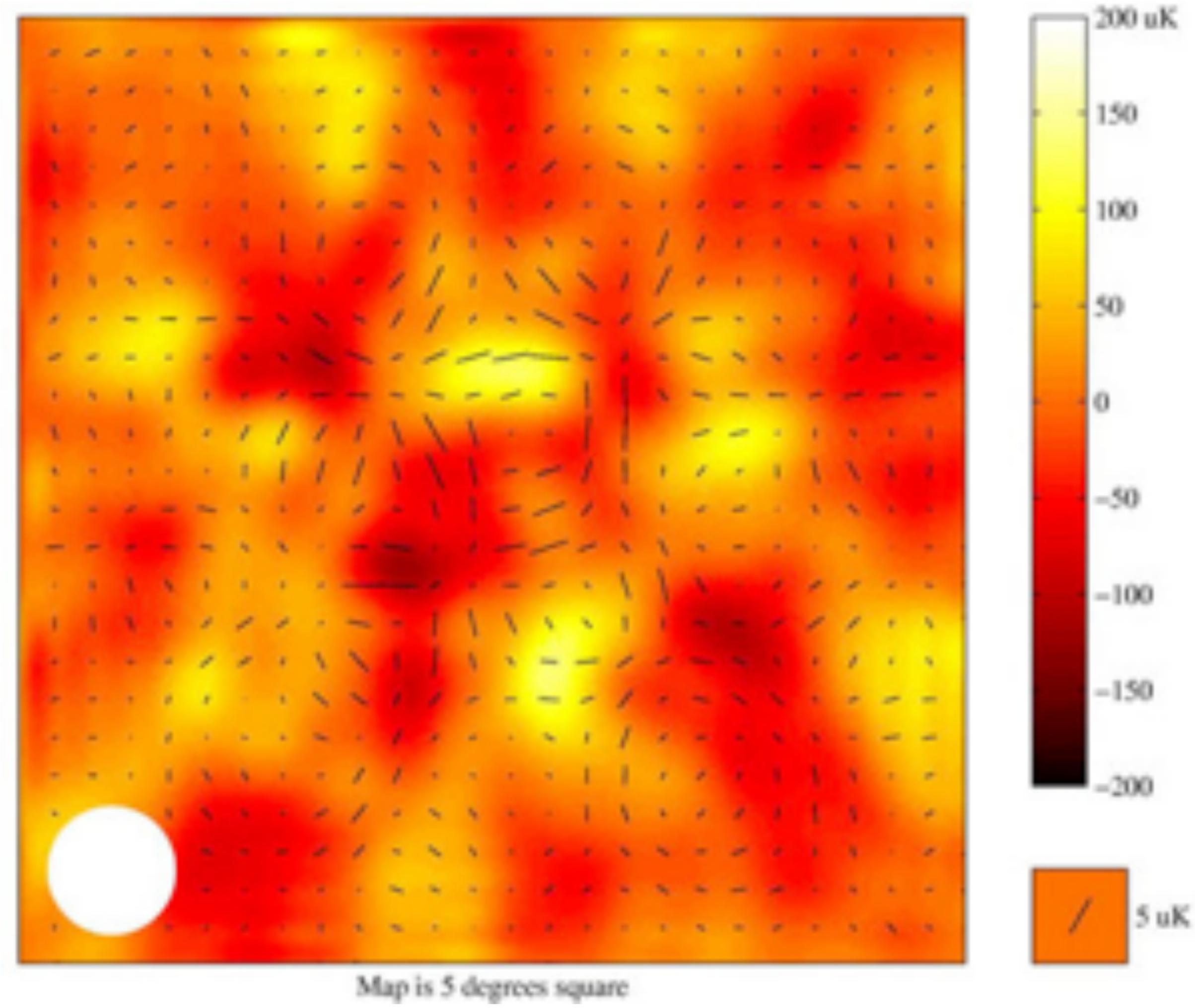

DASI collaboration, 2002

WMAP measurement of E-mode

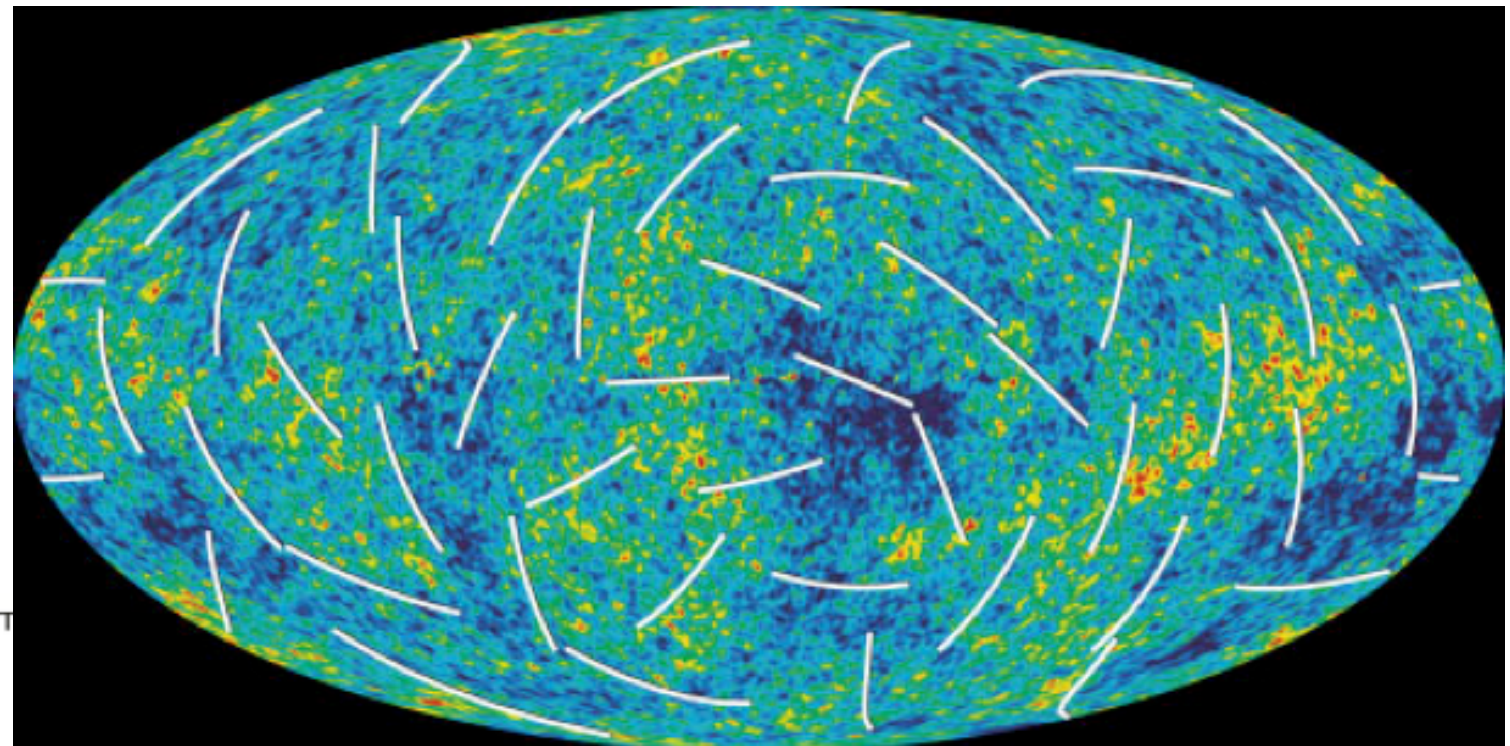

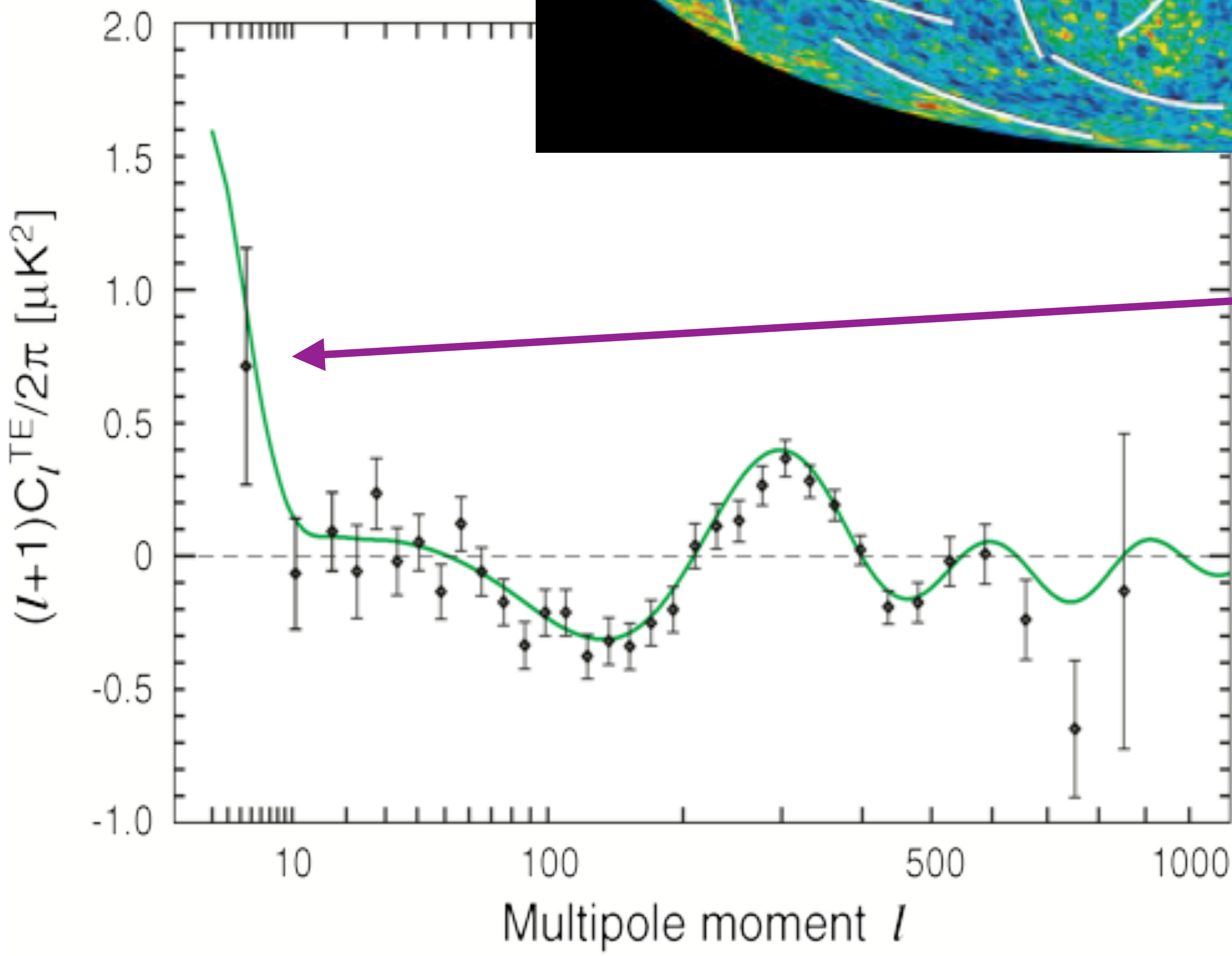

Re-scattering of the CMB photons during and after reionization added to the polarized power on large angular scales

(scale comparable to the horizon, H^{-1}, at the epoch of scattering)

Measurements of Planck TE, EE

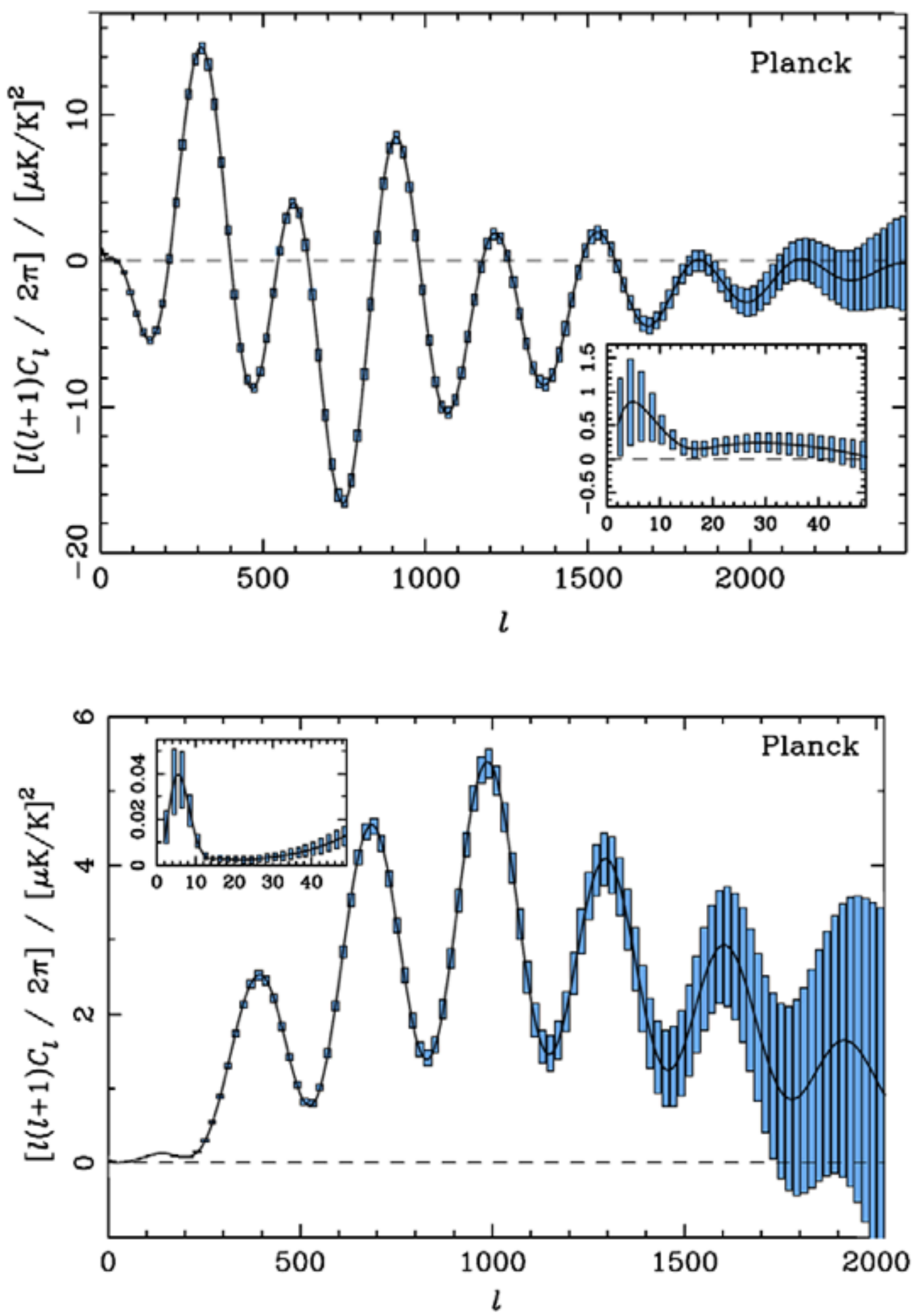

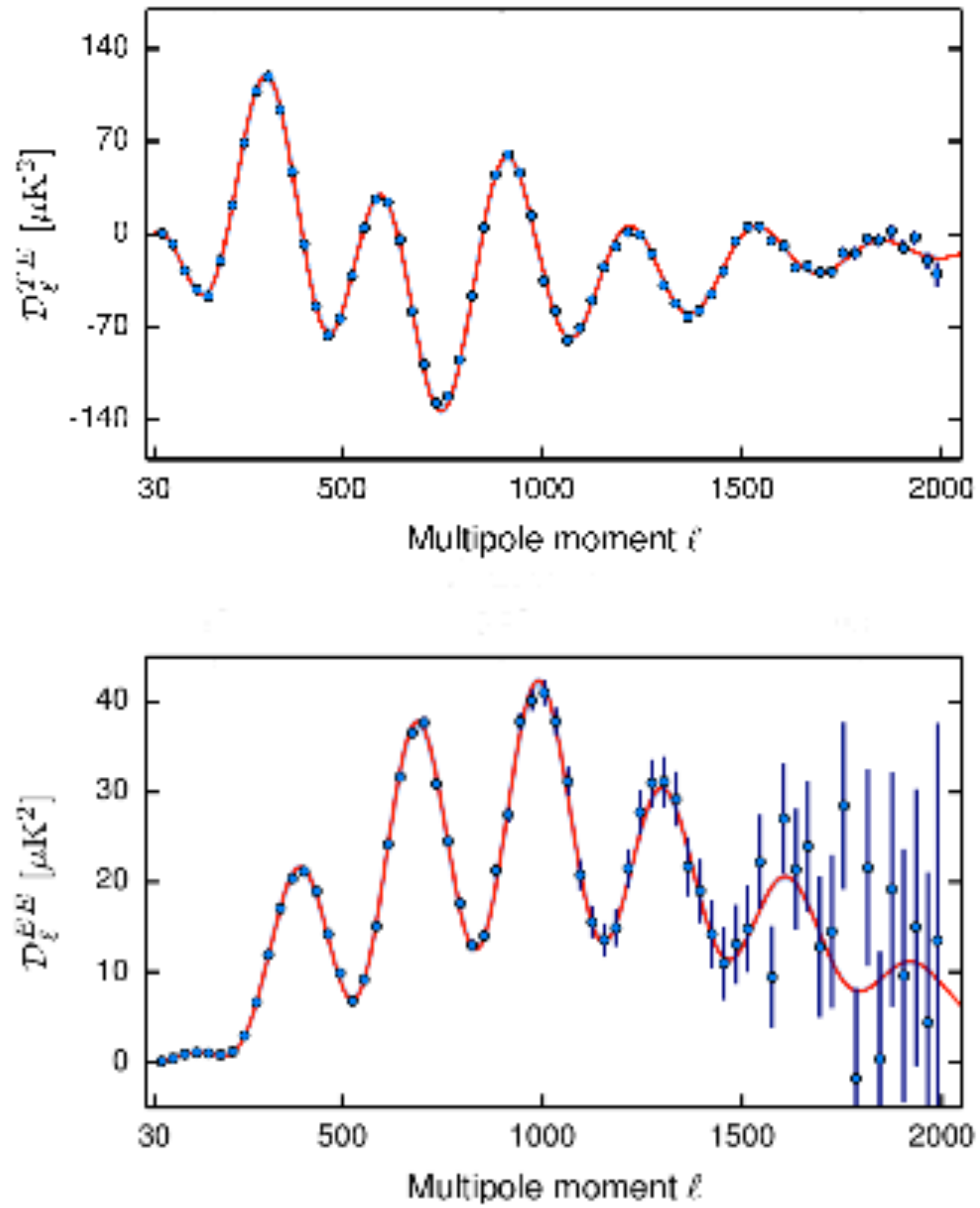

Prediction (Planck bluebook)

Measurements (Planck 2015)

Planck limits from TEMPERATURE data

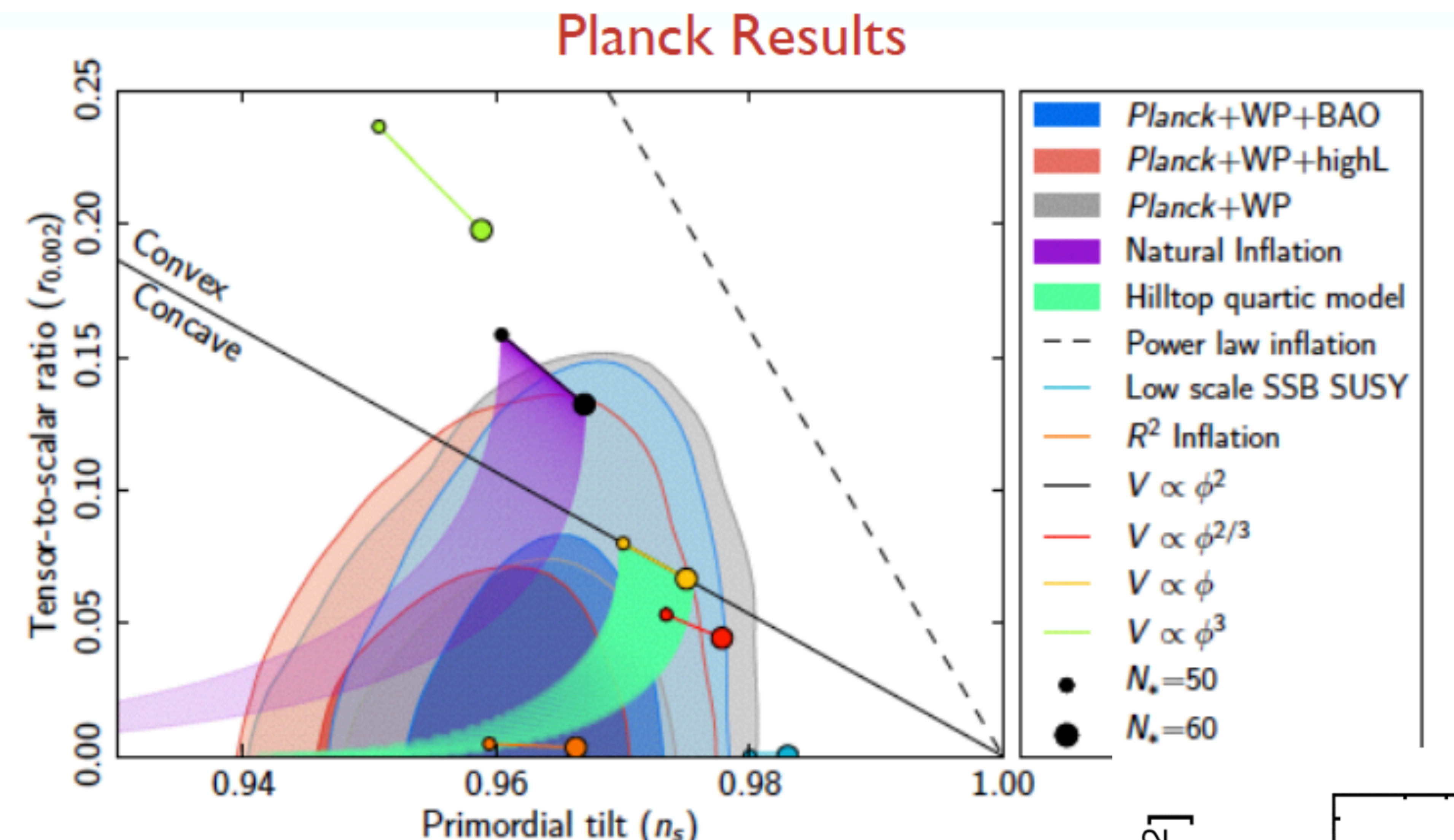

From precise TT measurements, Planck could constrain the slope of the primordial spectrum, n_s, and hence constrain inflation. This already excludes a lot of parameter space for inflationary models.

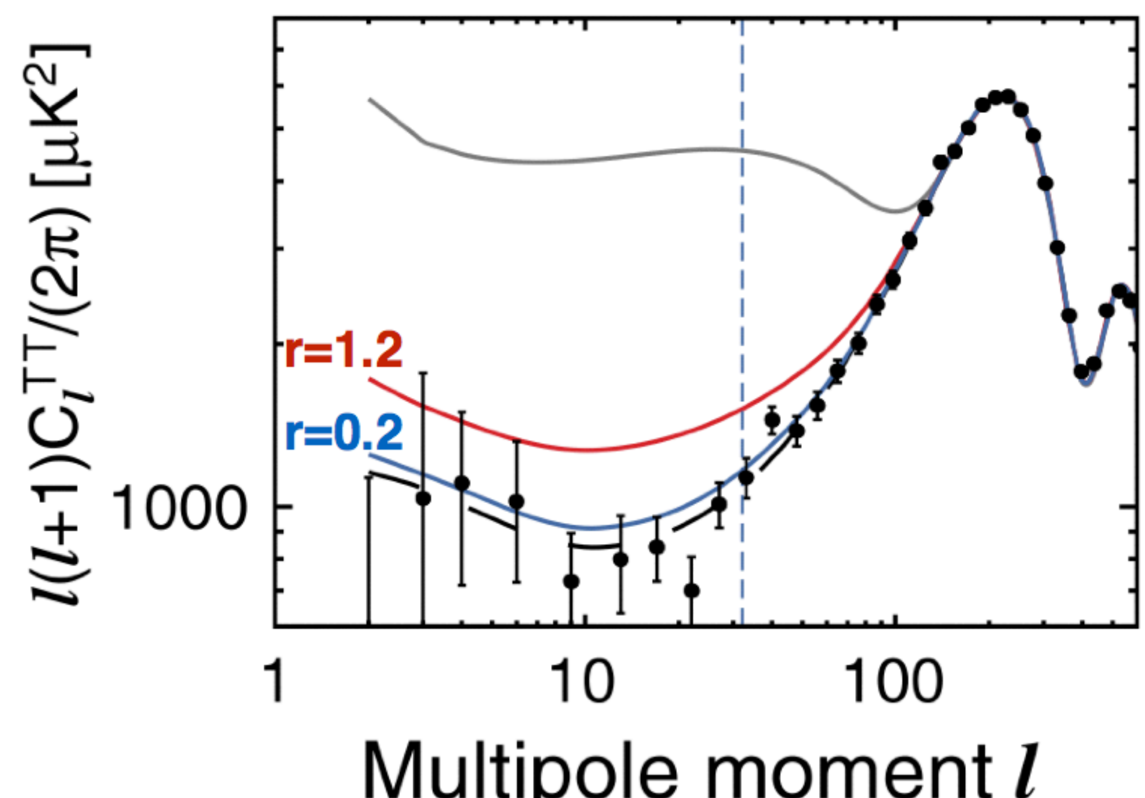

Planck limits from TEMPERATURE data

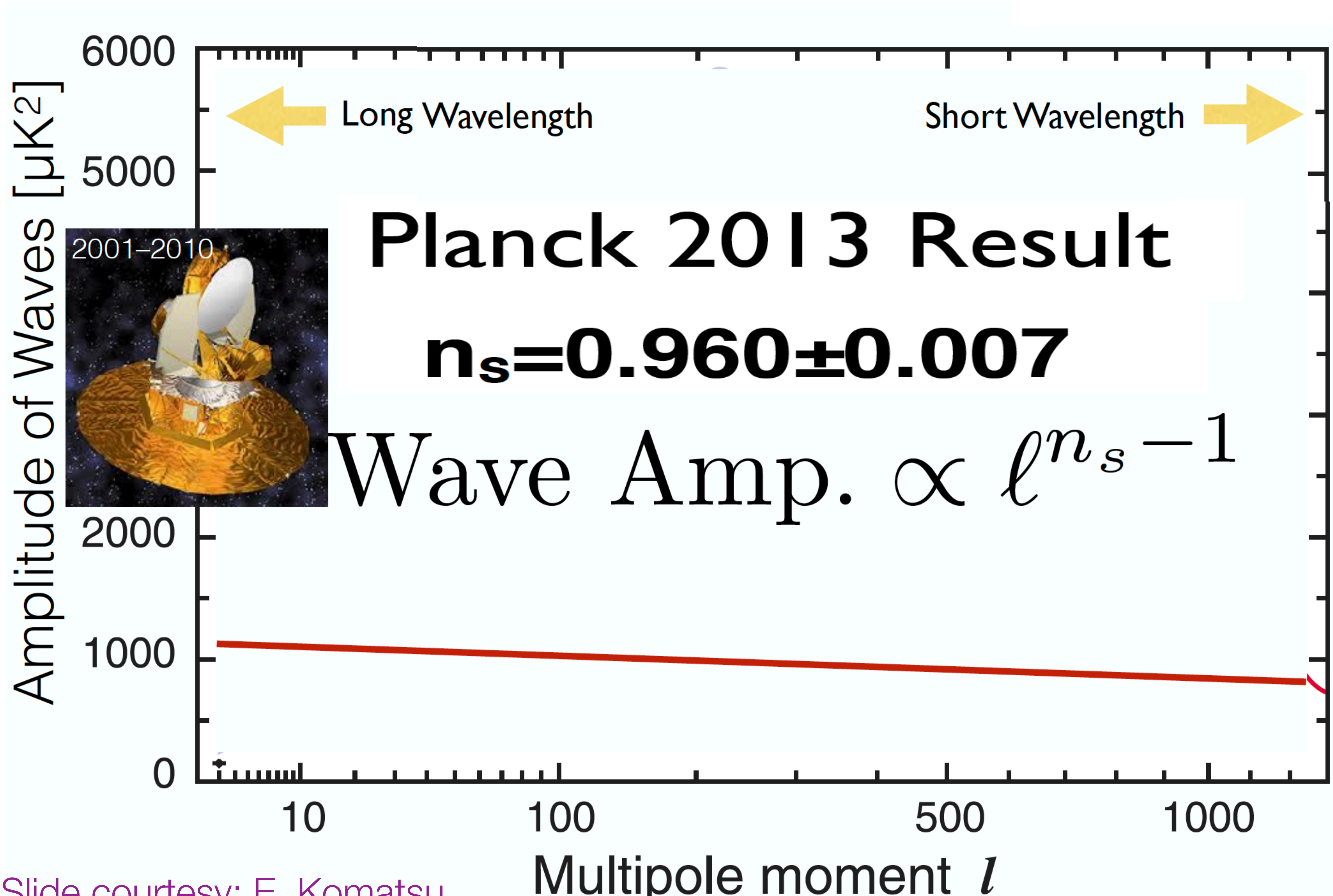

Slide courtesy: E. Komatsu

Other measurements of EE, BB

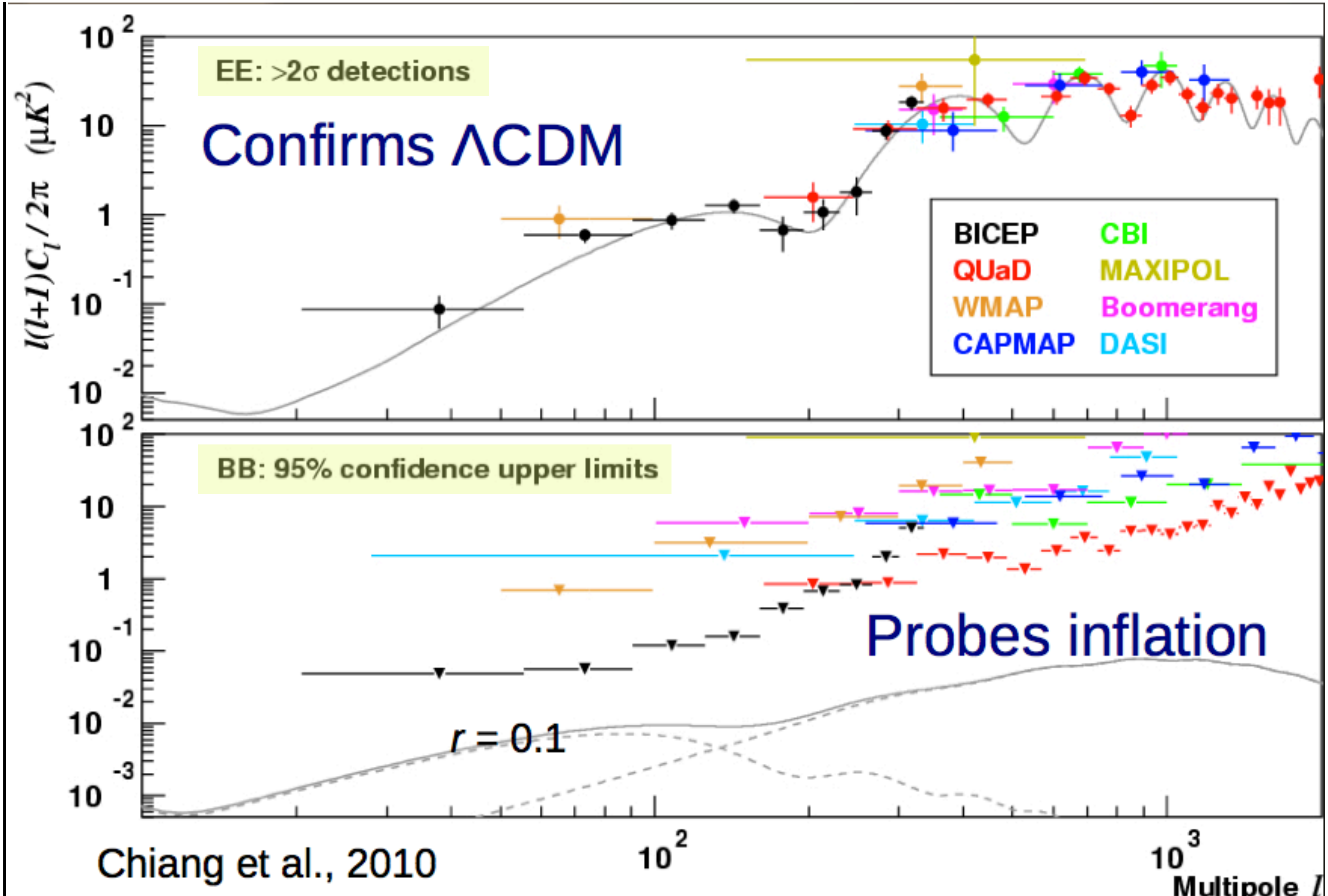

Chiang et al., 2010

BICEP-2 result in 2014

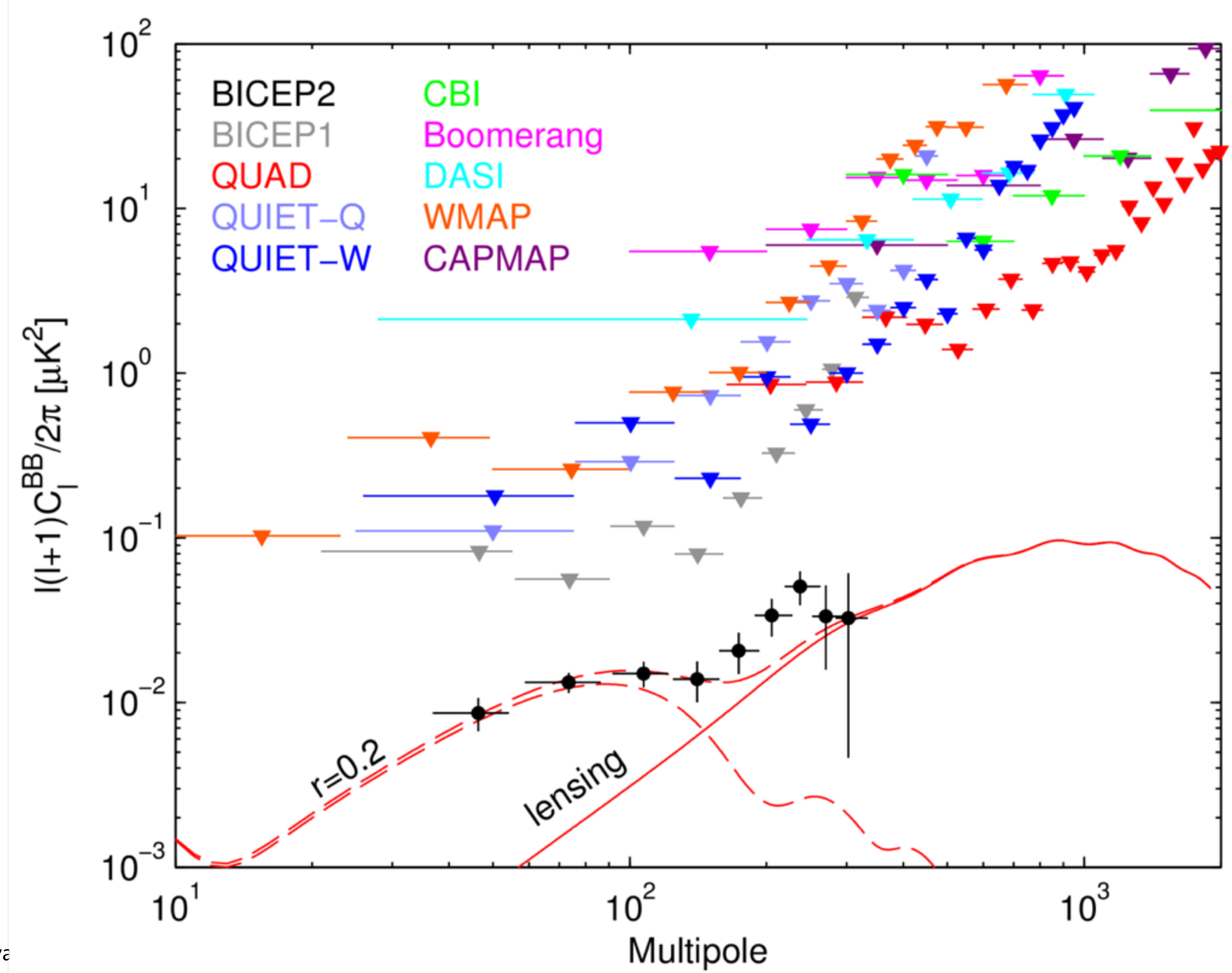

BICEP-2 observation of the CMB

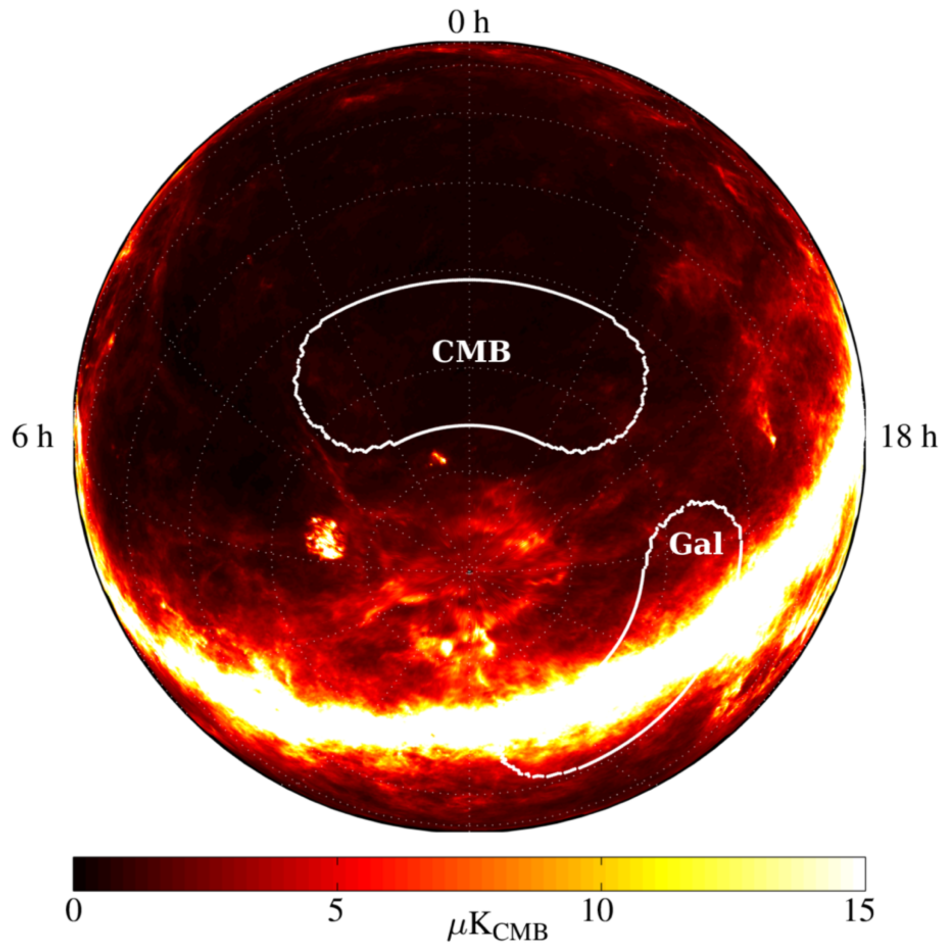

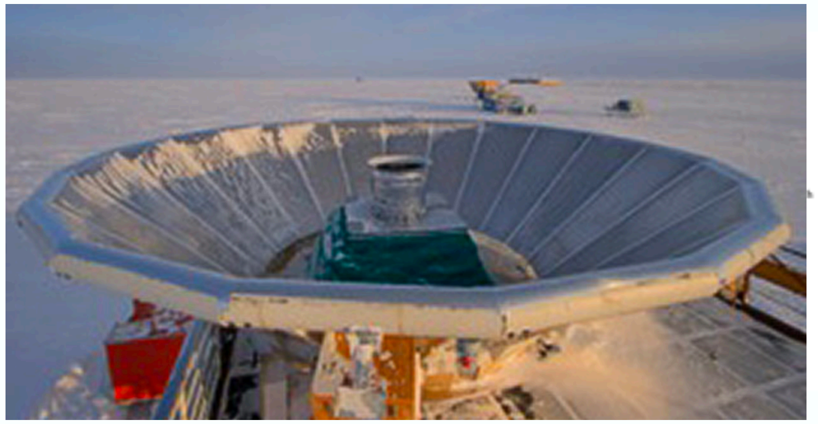

- Small telescope at South Pole
- 512 bolometers at 150 GHz
- Observed 380 square degrees for three years (2010 - 2012)
- Previous BICEP1 at 100 and 150 GHz (2006-2008)
- Current: Keck Array = 5 x BICEP2 at 150 GHz (2011 - 2013) and additional detectors at 100 and 220 GHz (2014 onwards)

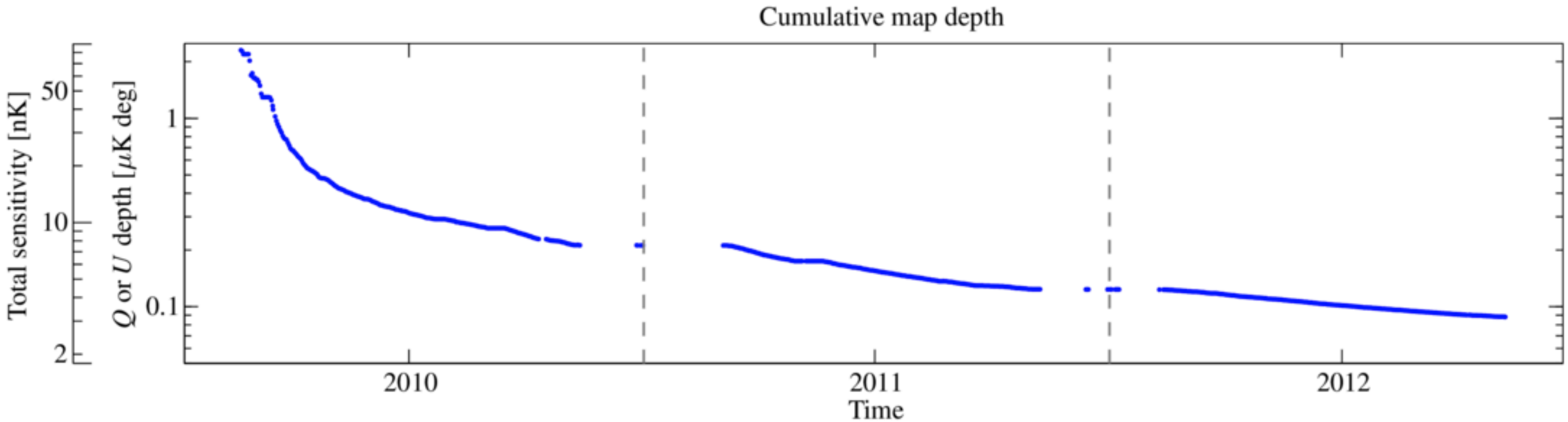

BICEP2 E- and B-mode CMB maps

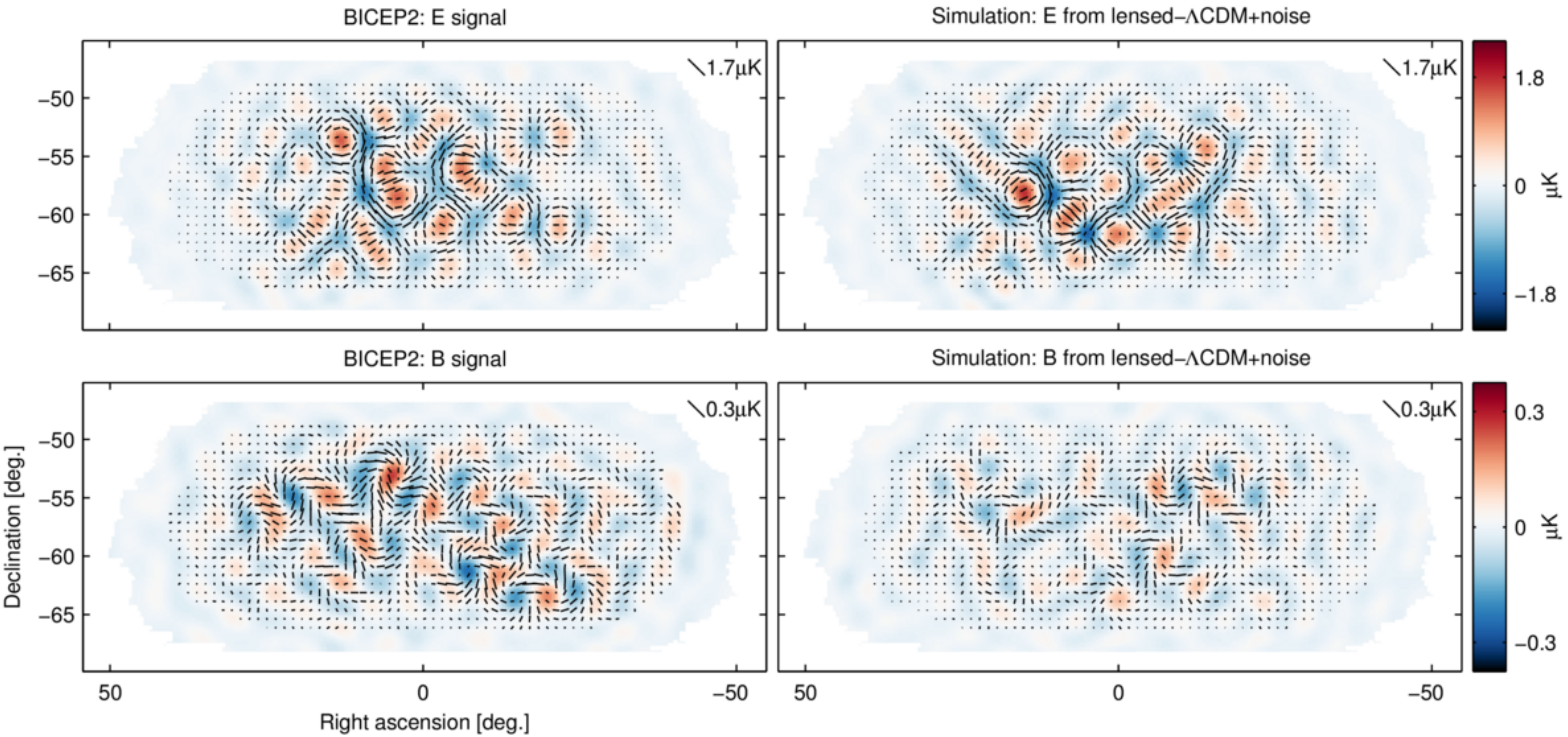

BICEP2 scaler-to-tensor ratio

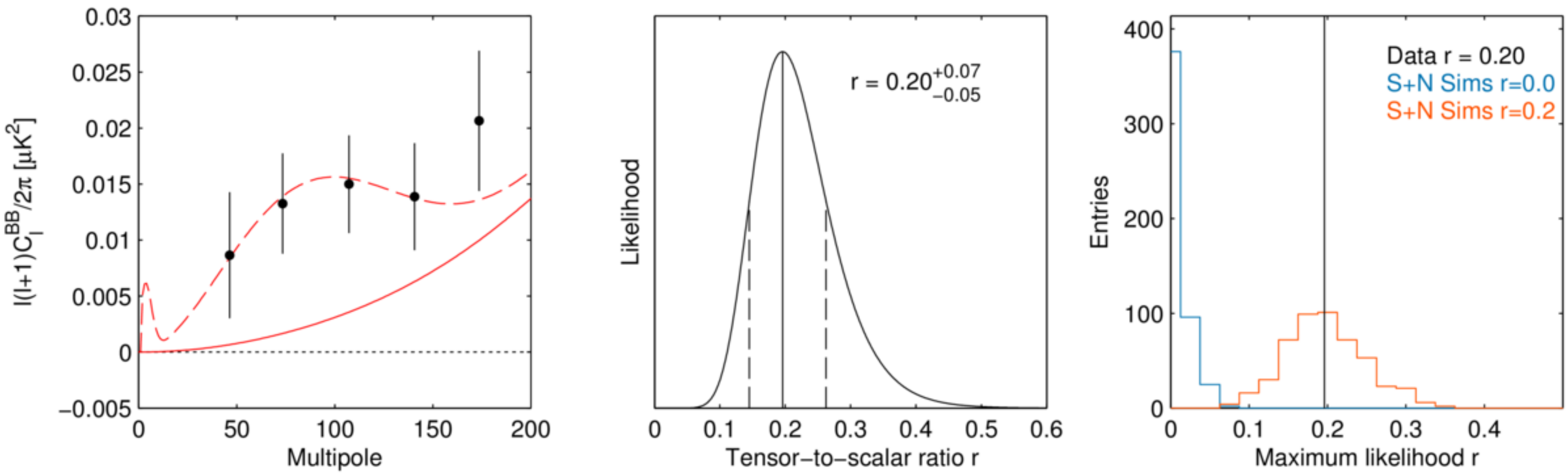

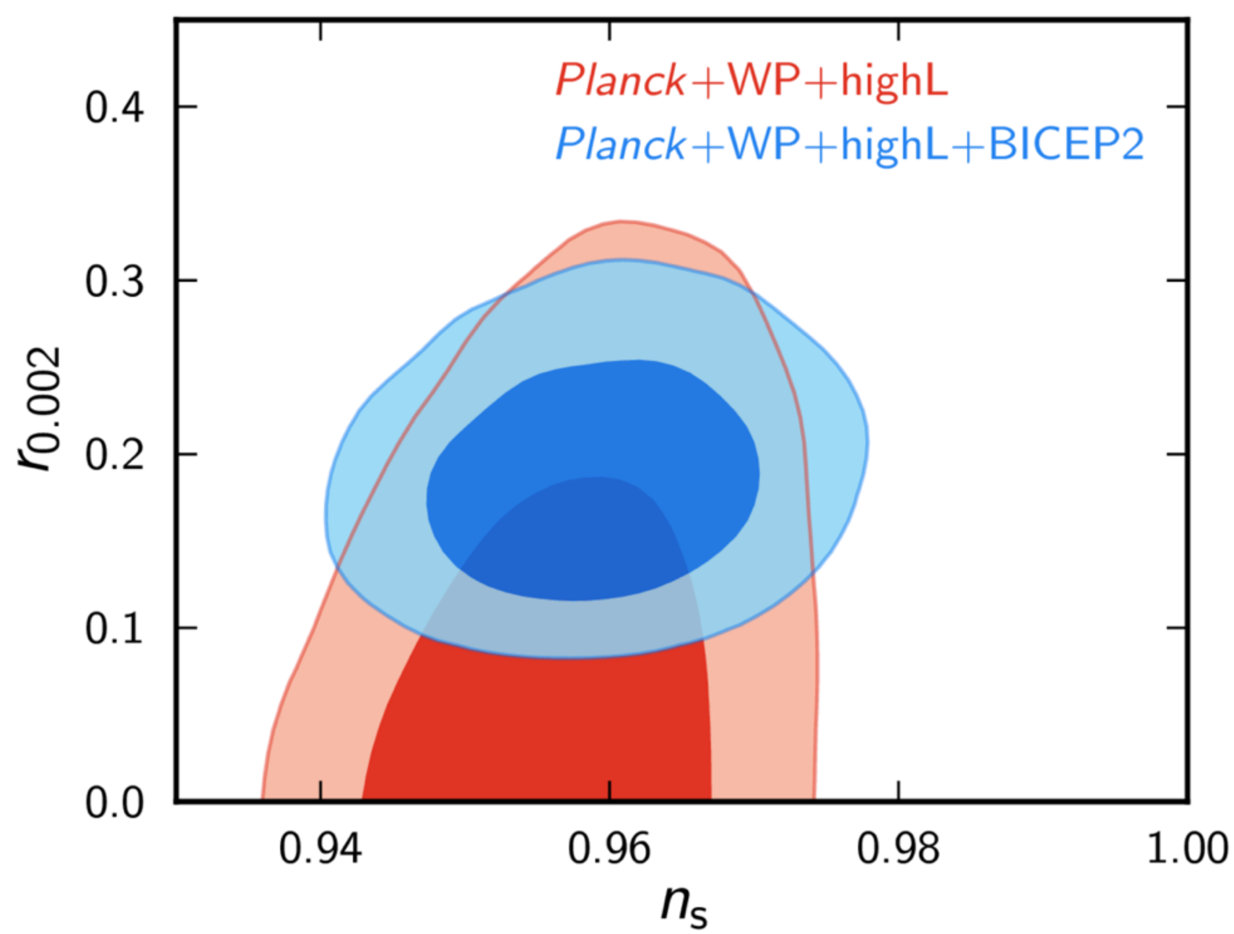

Comparison with
Planck 2013 result
→ a clear tension!

Then... proved wrong by Planck!

Planck Collaboration XXX (2014)

Dust polarization at high galactic latitudes

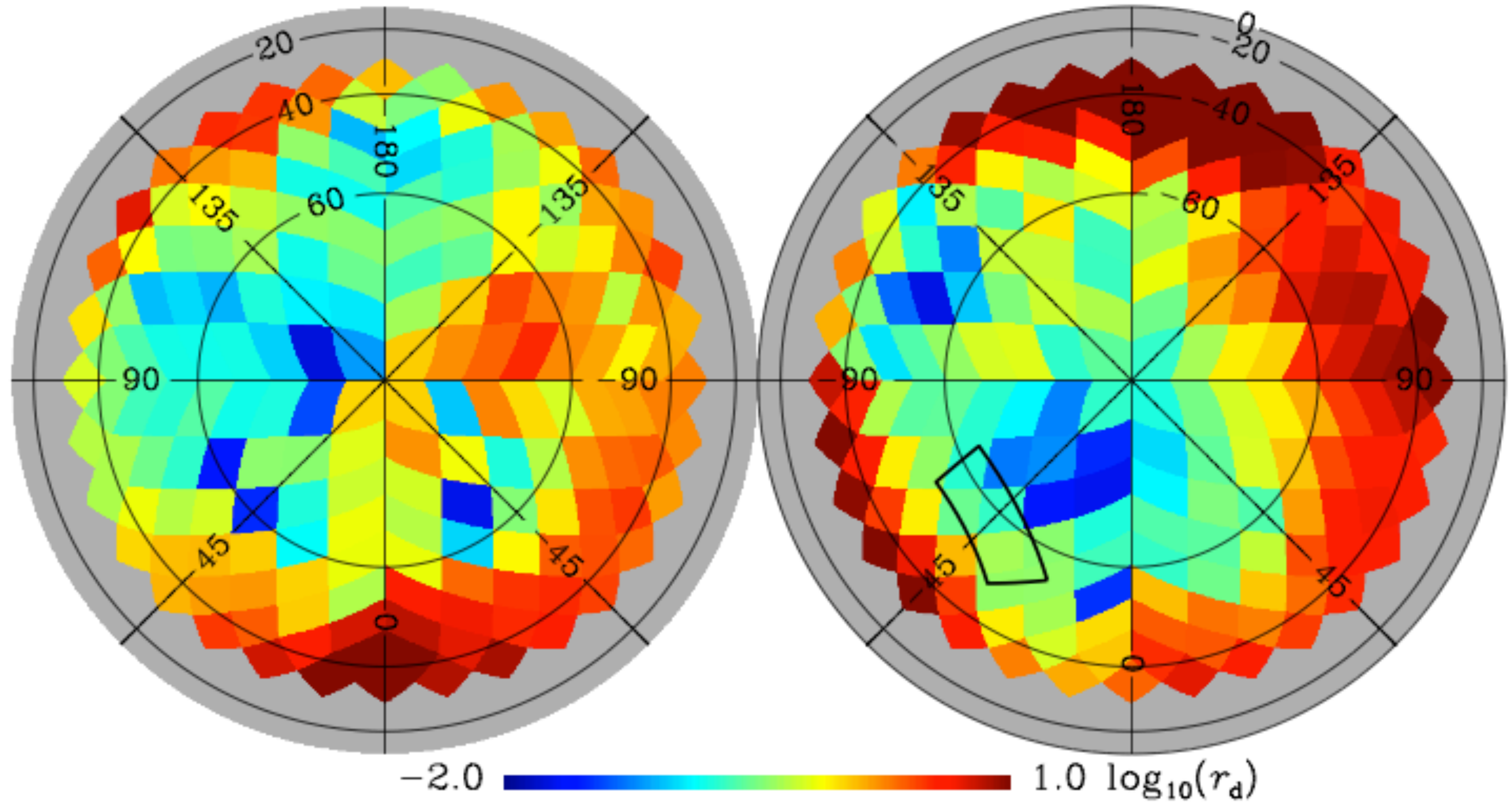

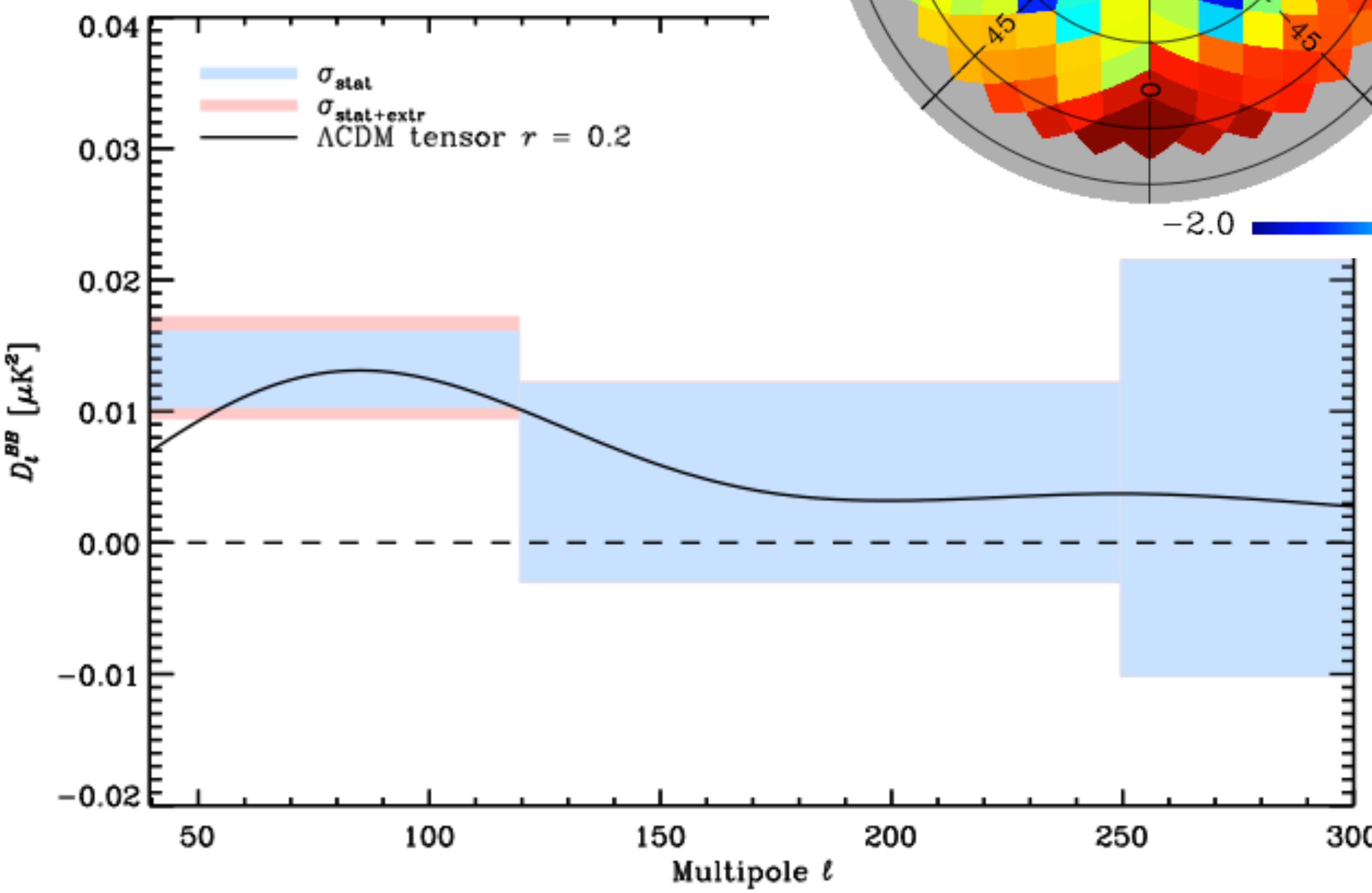

BICEP-2 severely underestimated the dust polari- -zation power at low multipoles

Planck's view of the BICEP2 field

colors → dust intensity

"engravings" → magnetic fields

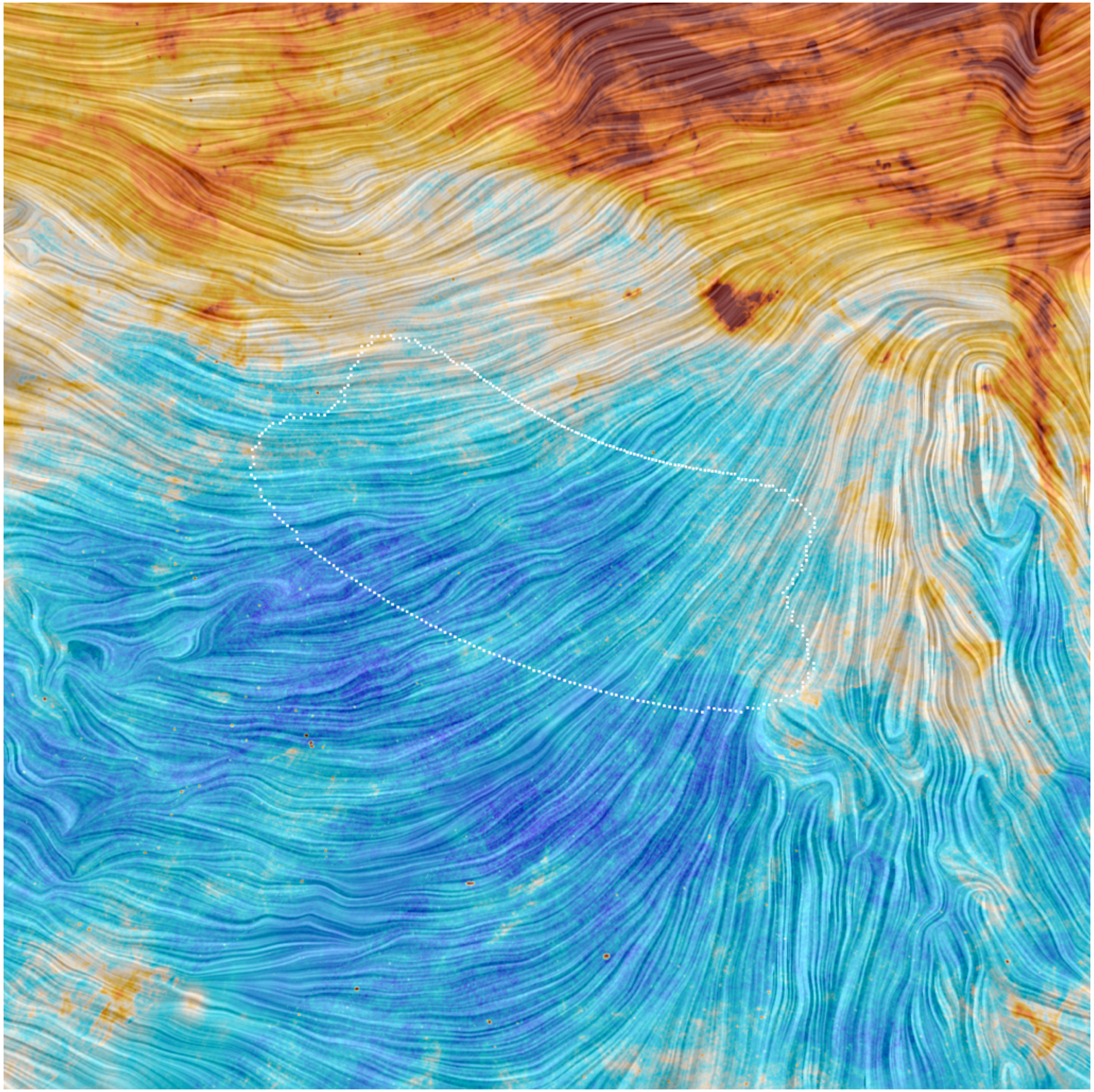

Planck results on the B-mode

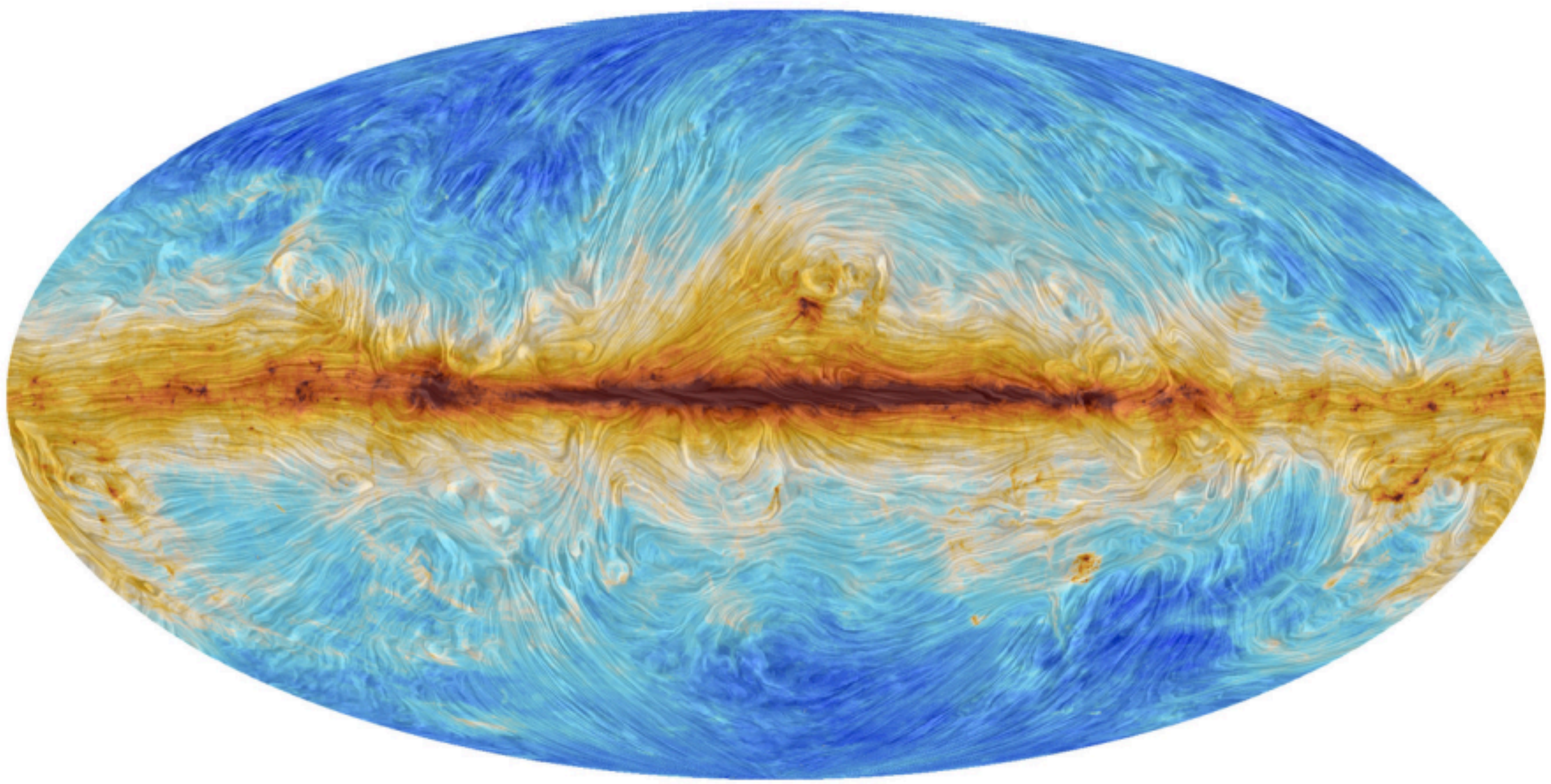

Dust polarization map
(Planck collaboration 2015)

Lensing B-mode
(Planck collaboration 2015)

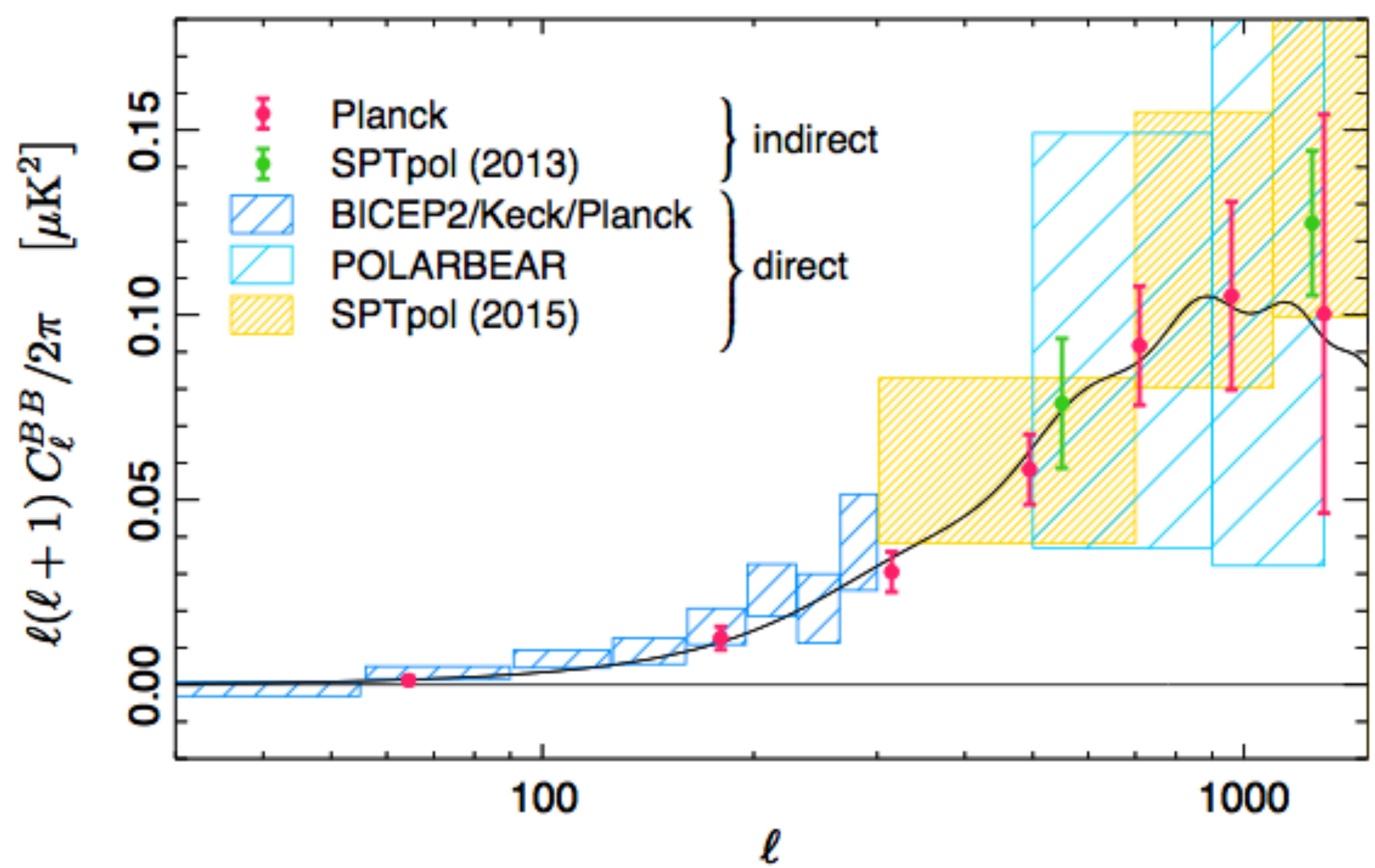

Planck 2015 + BICEP

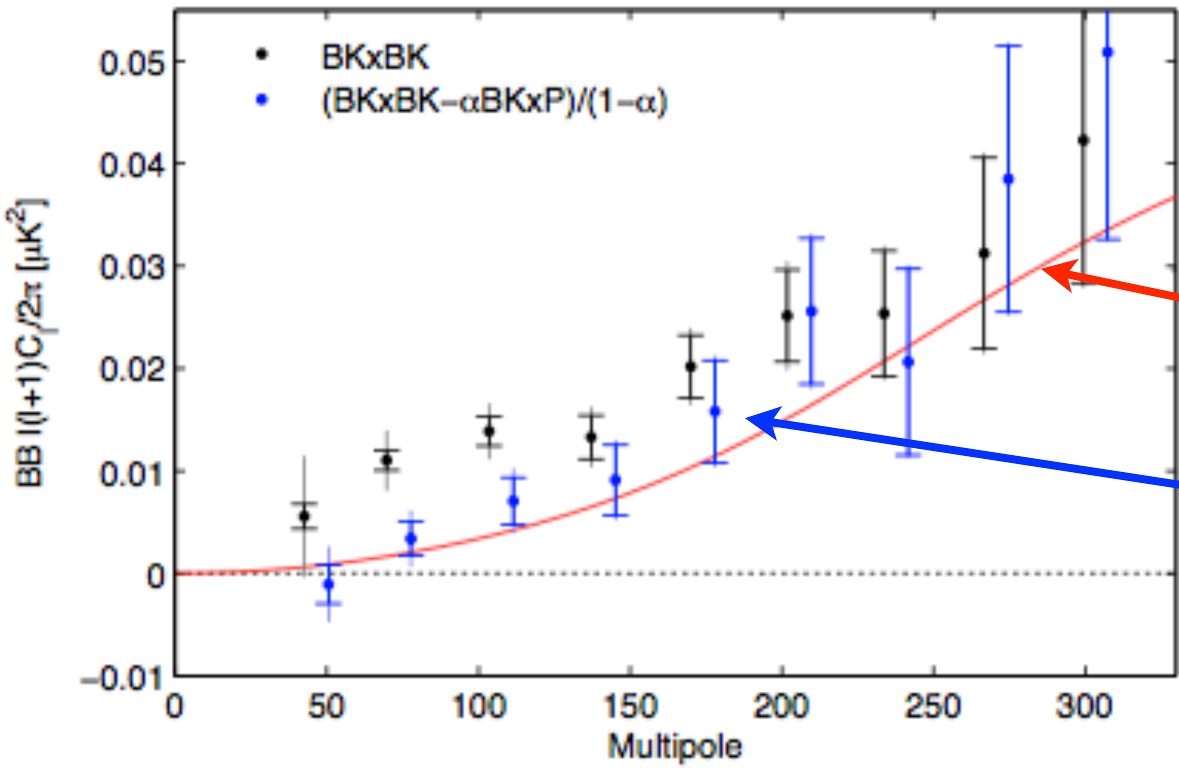

Lensed ΛCDM

After dust correction

BICEP2 + Planck joint analysis (2015)

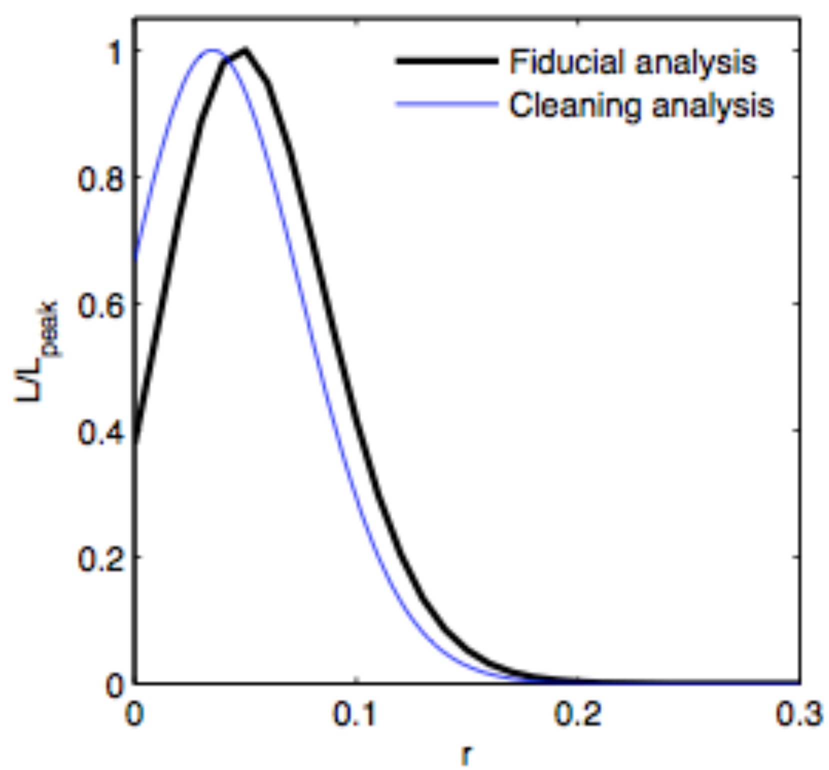

Current 95% upper limit: r < 0.08

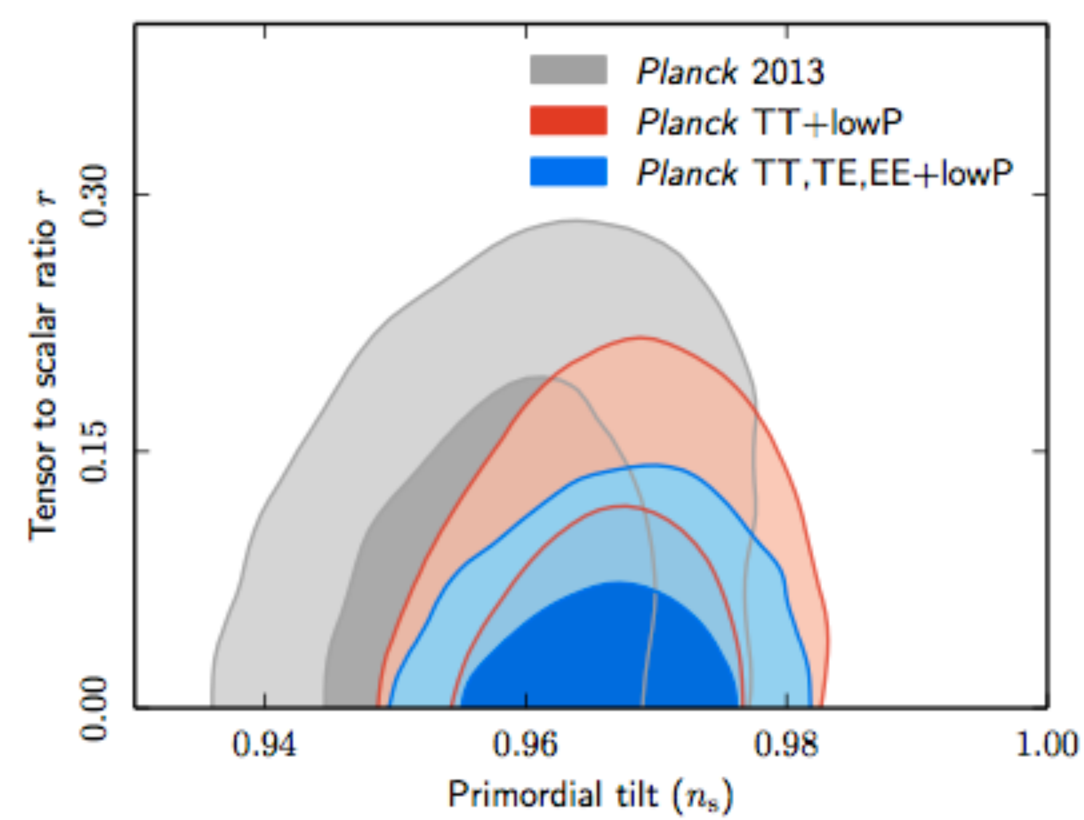

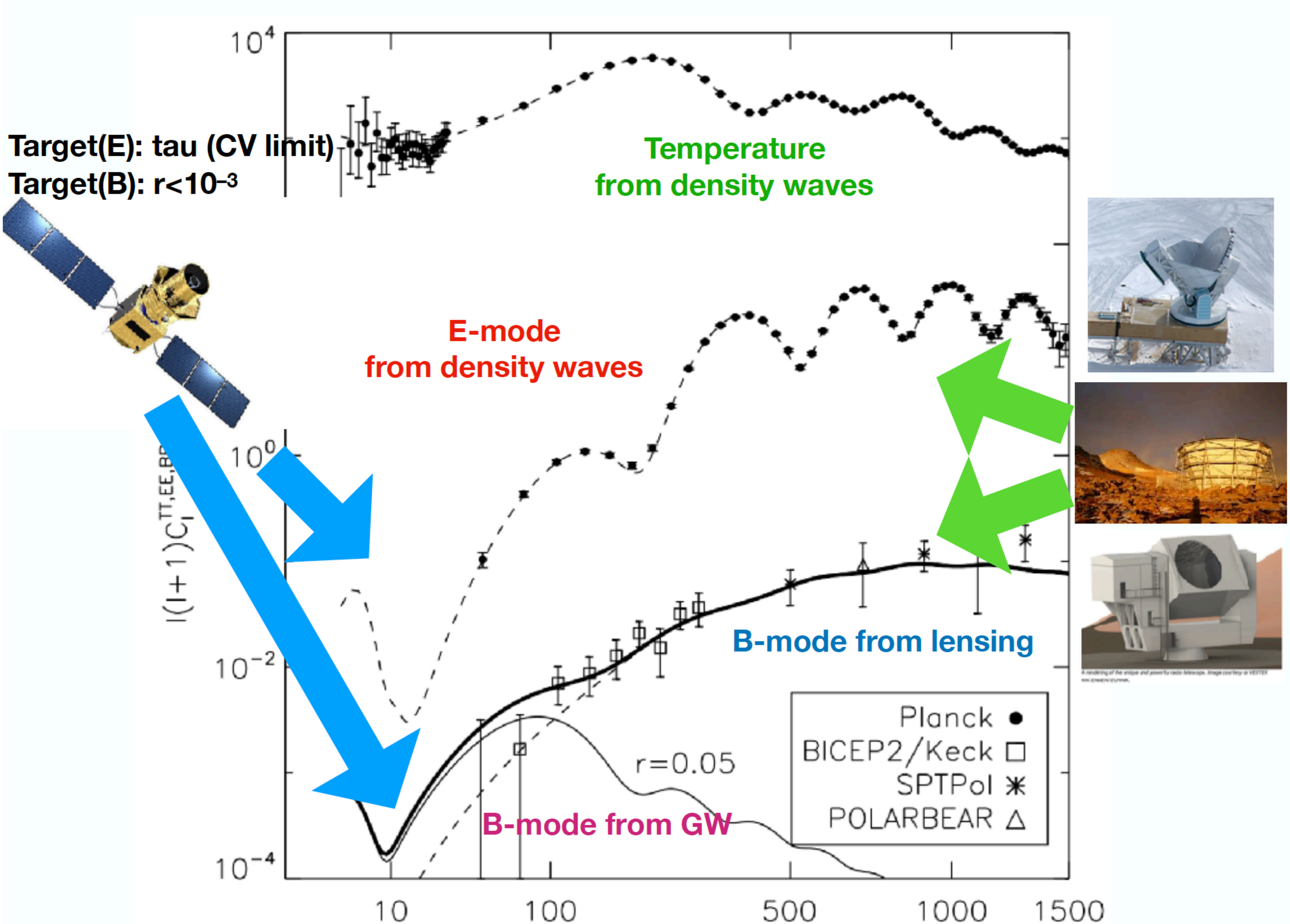

Slide courtesy: E. Komatsu

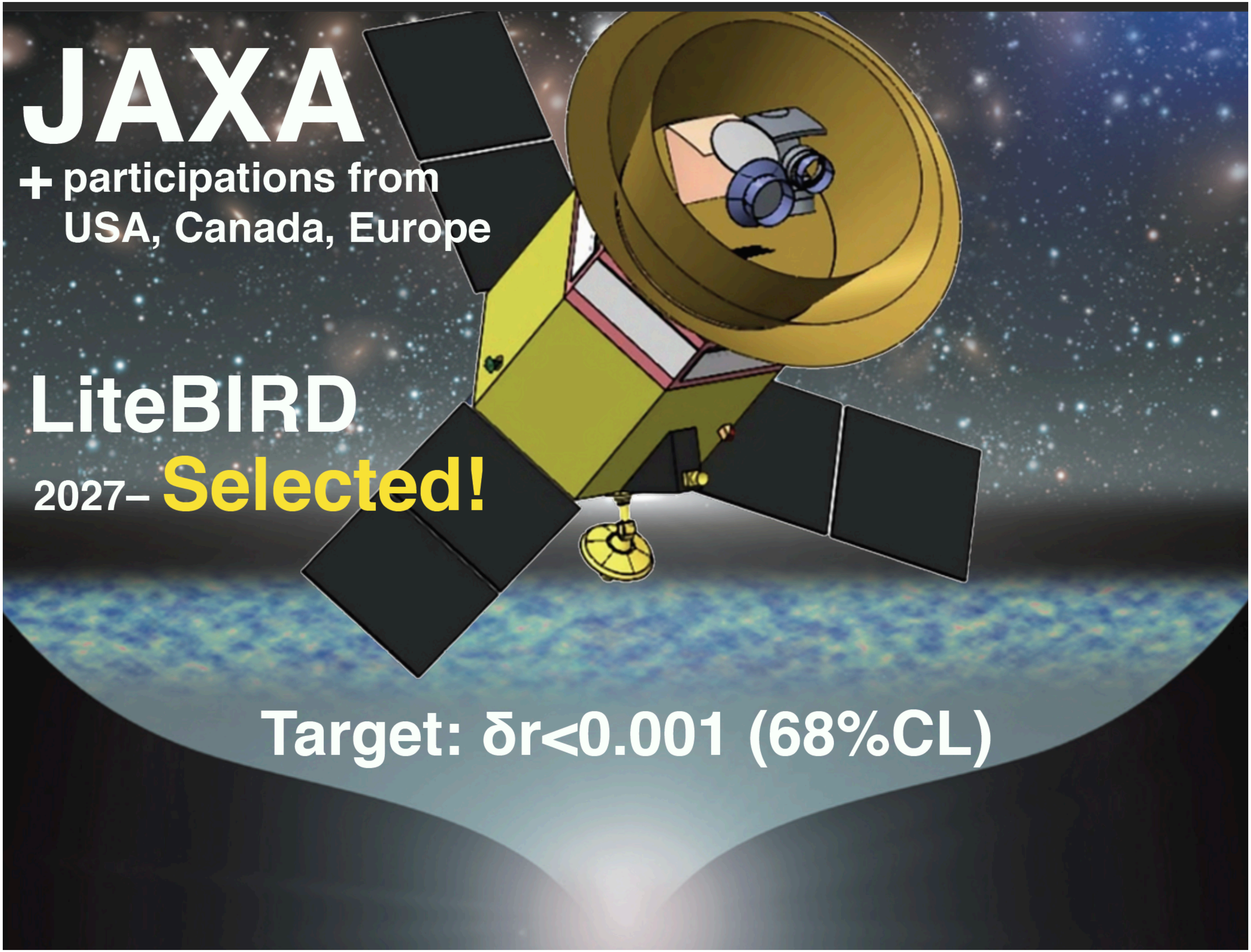
JAXA
+ participations from
USA, Canada, Europe
LiteBIRD
2027– Selected!
Target: δr<0.001 (68%CL)

SIMONS OBSERVATORY

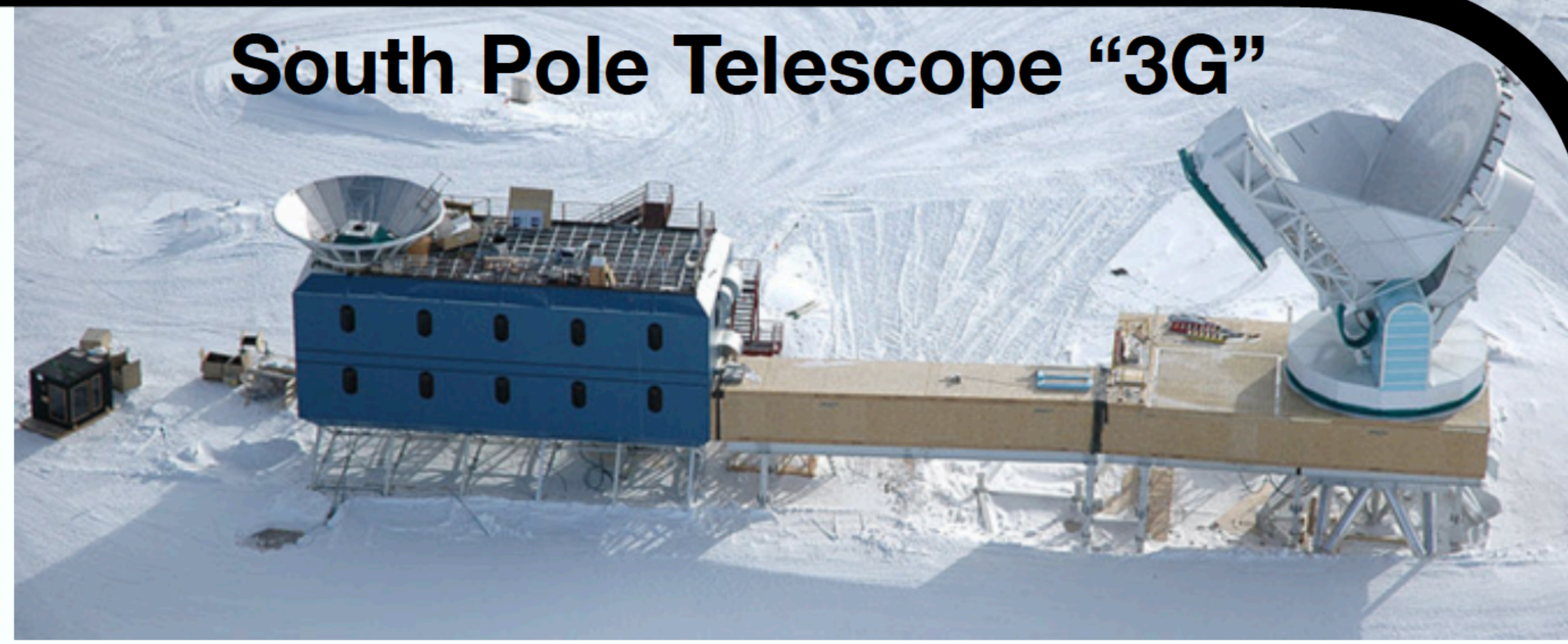

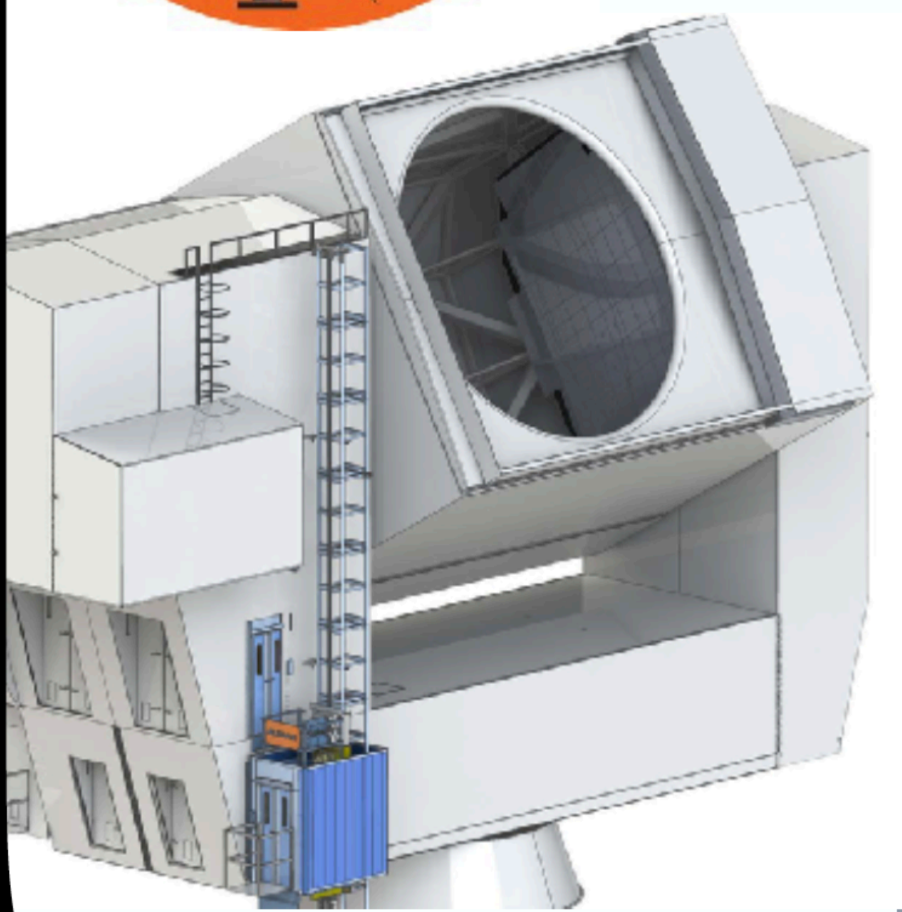

CMB-S4
Next Generation CMB Experiment

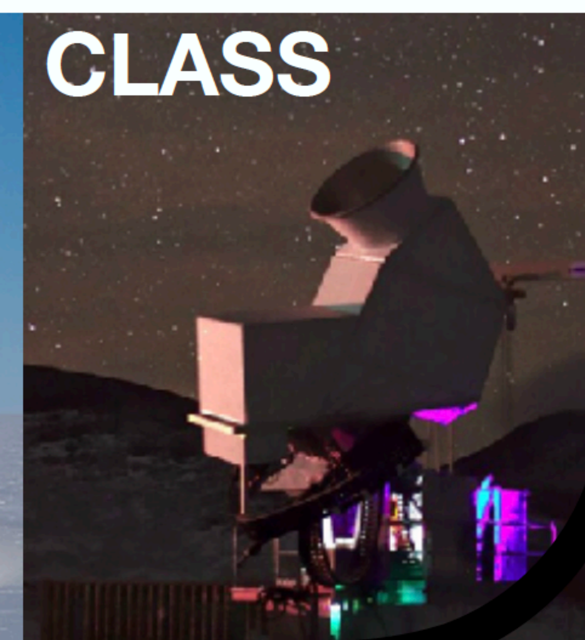

CMB Data Analysis

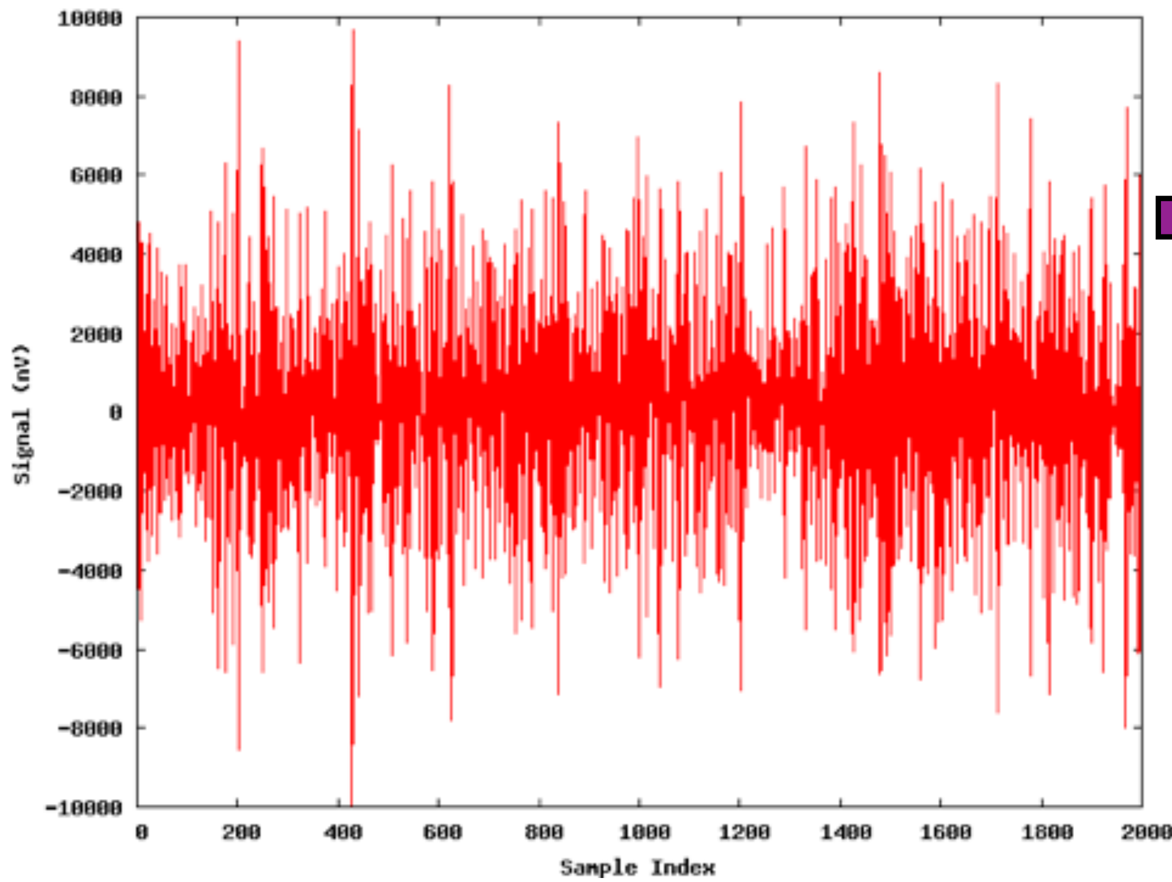

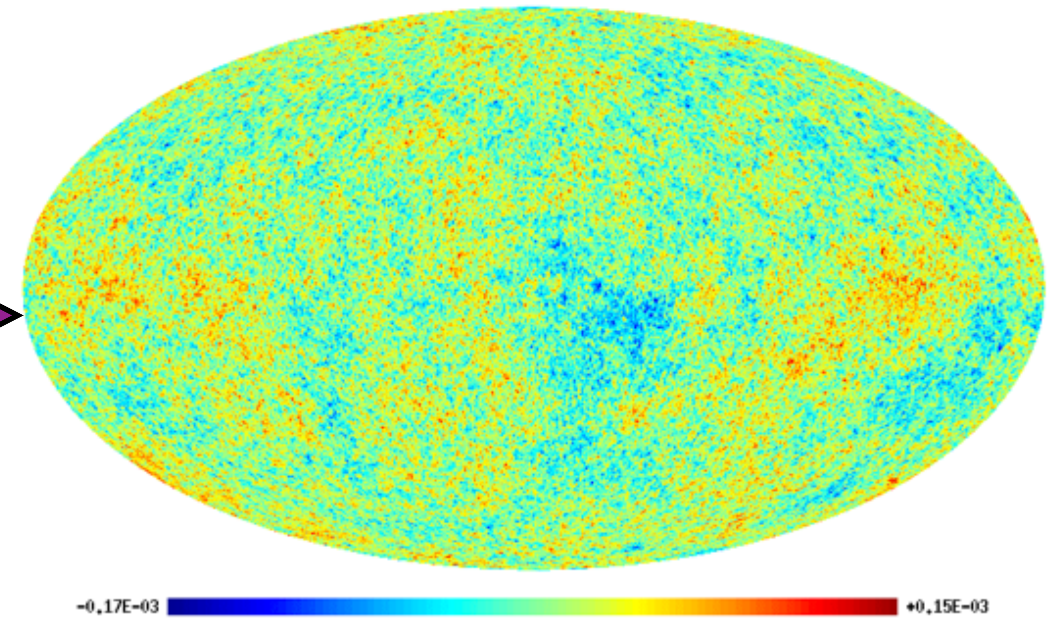

Data time-stream

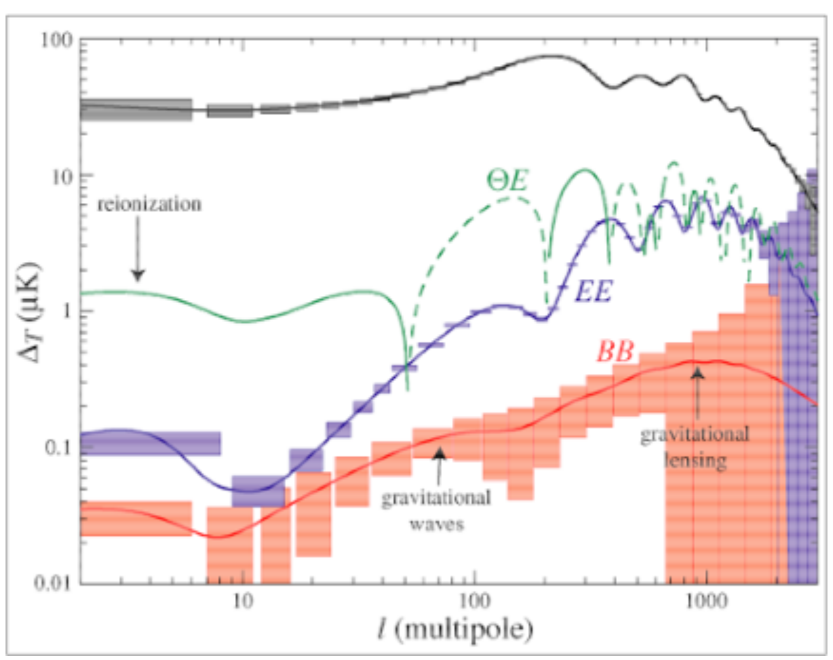

Striping

Common to get stripes in the scan direction.

Removal easy in Fourier space.

Fourier transformation also helps to separate signal and noise better (different temporal signal).

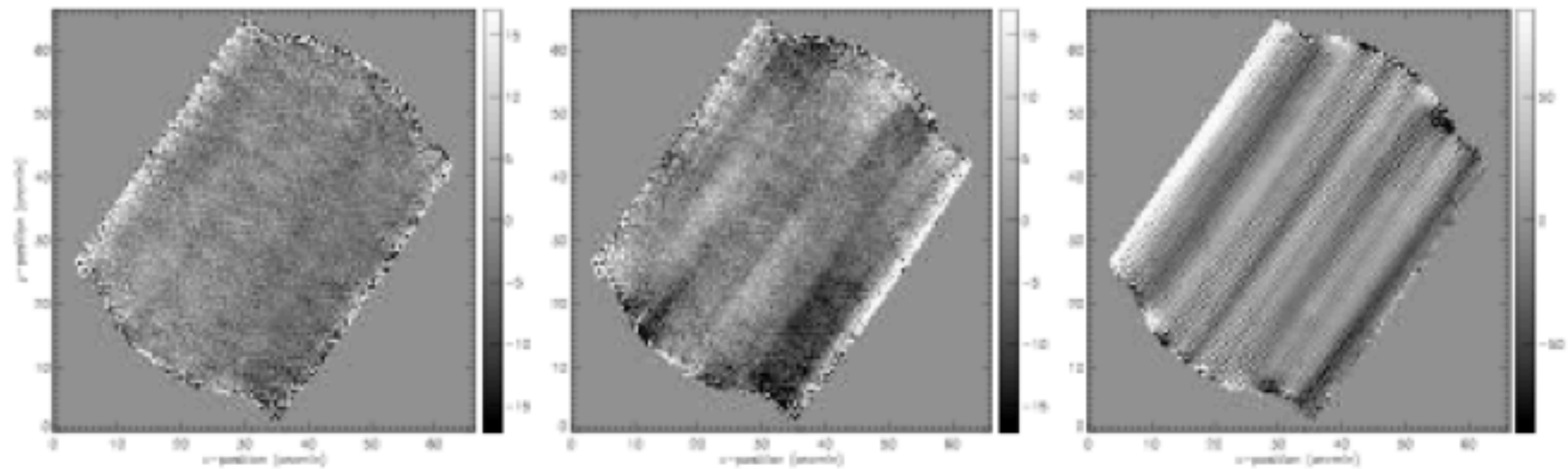

map space

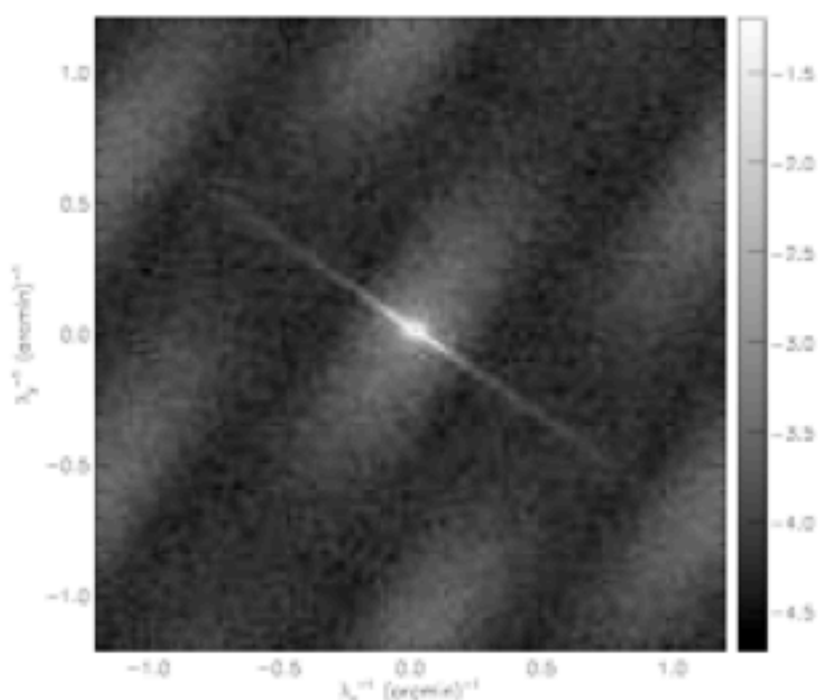

Fourier space

Patanchon et al ; BLAST data

Deglitching

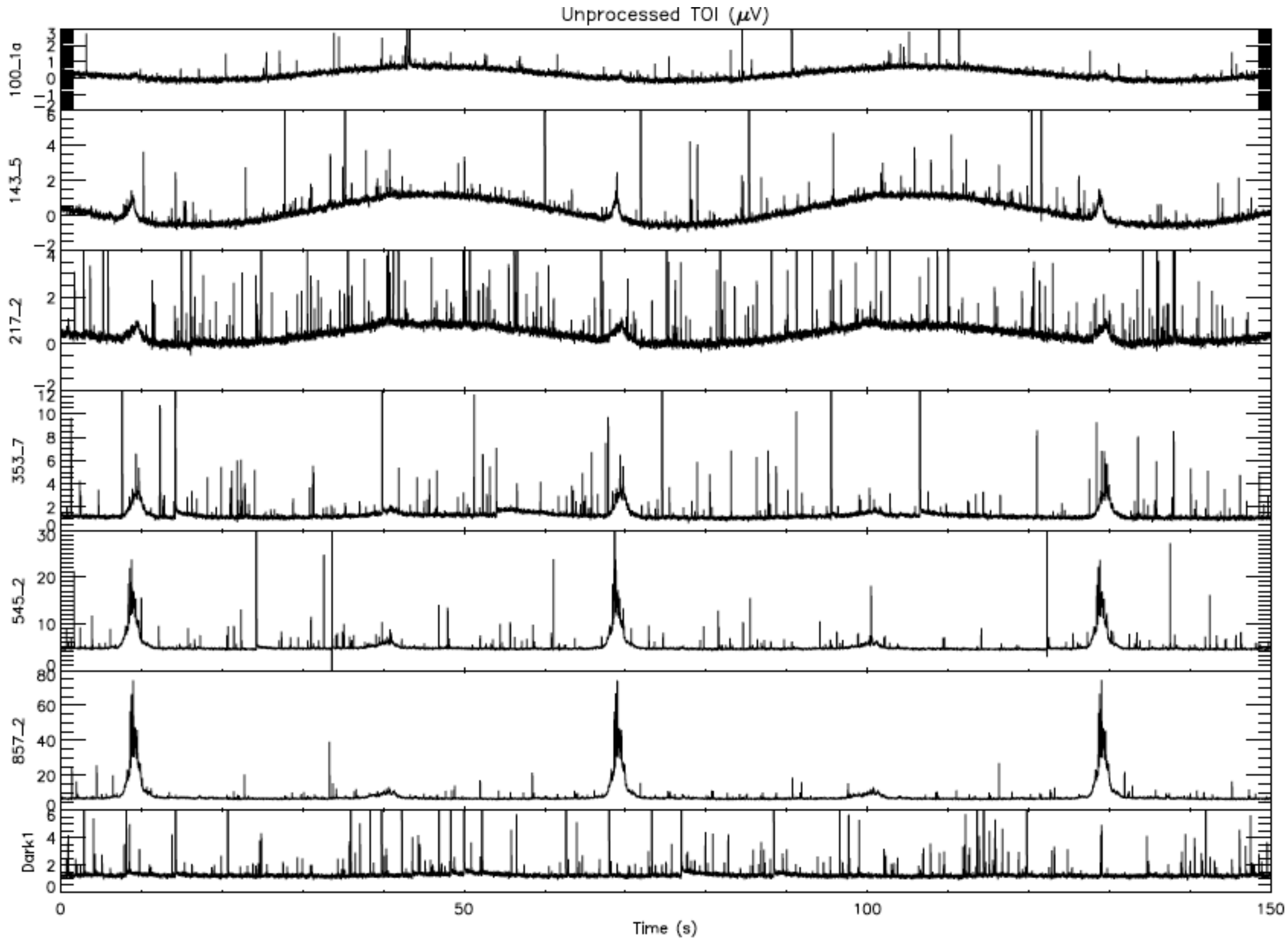

Figure 13. Examples of raw (unprocessed) TOI for one bolometer at each of six HFI frequencies and one dark bolometer. Slightly more than two scan circles are shown. The TOI is dominated by the CMB dipole, the Galactic dust emission, point sources, and glitches. The relative part of glitches is over represented on these plots due to the thickness of the lines that is larger than the real glitch duration.

Map making

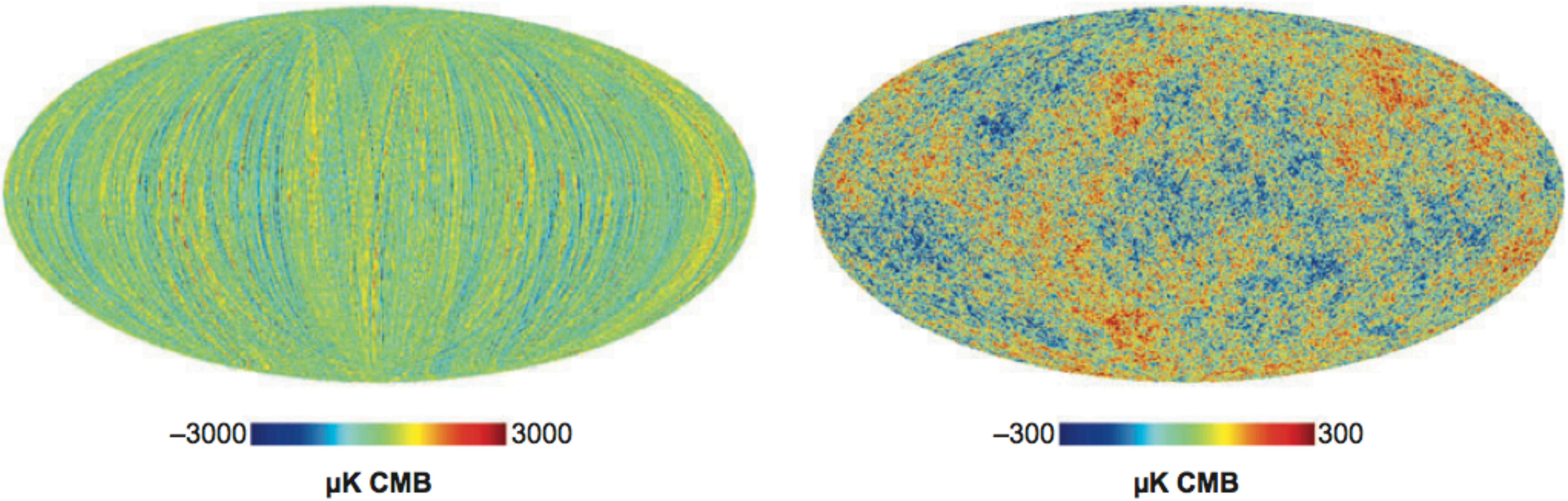

Figure 10

Effect of destriping on simulated sky maps. (*Left*) Map from a raw time stream. (*Right*) Map after applying a destriping algorithm (note the different scales). This simulation was done for the Planck High Frequency Instrument (38).

Figure taken from Samtleben et al. 2007.

Planck scanning strategy

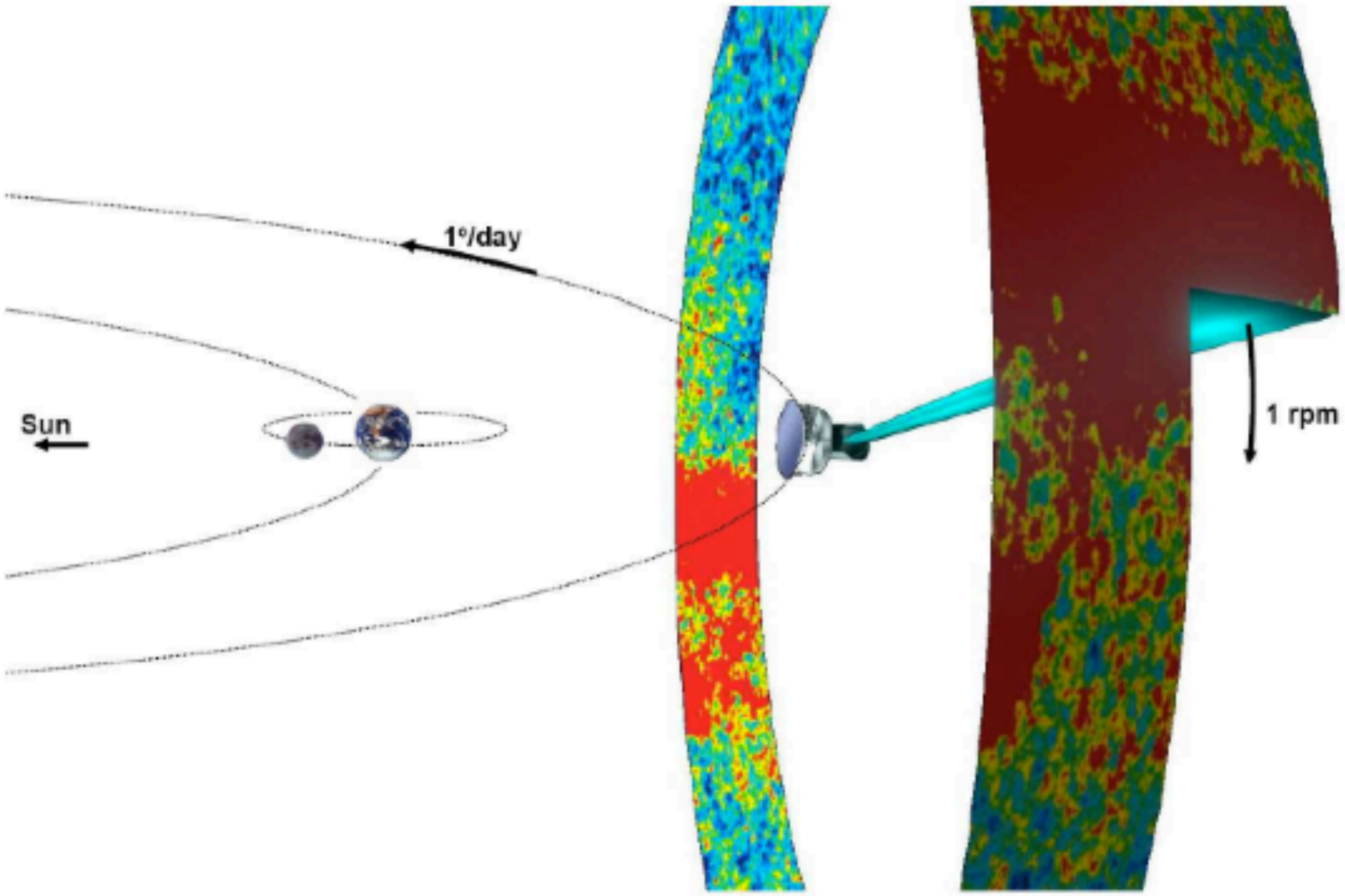

Simplified way to show the Planck scanning strategy, without additional motion of the spin axis

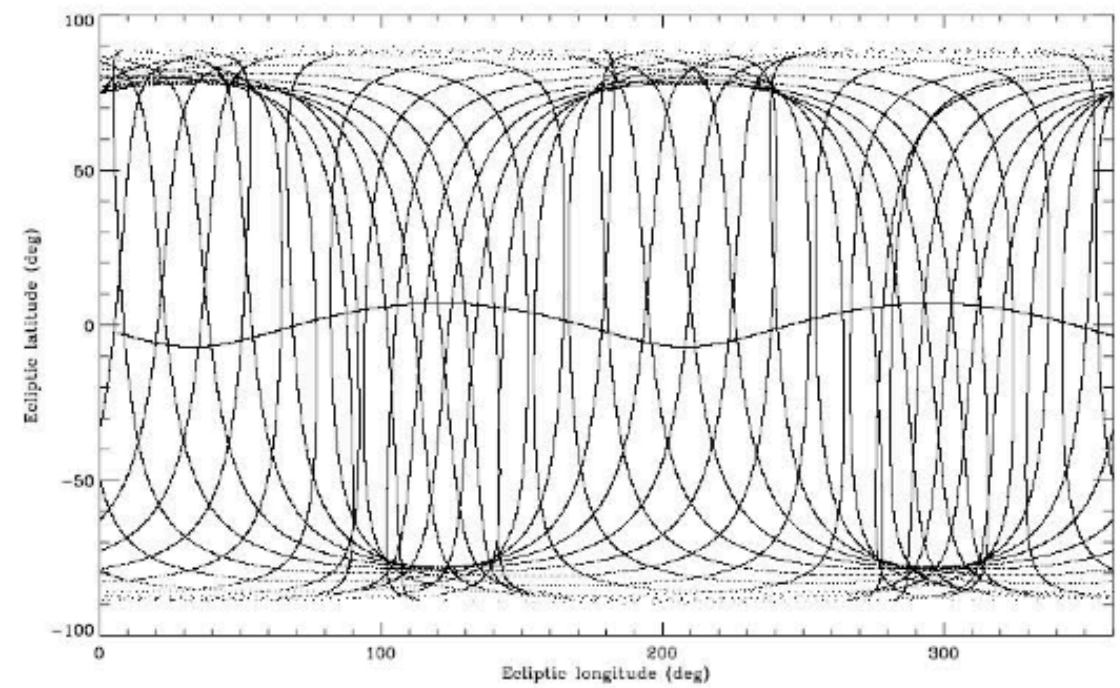

Spin axis path with a 7 degree amplitude cycloidal scanning, from #dupac2005

143 GHz hit count map

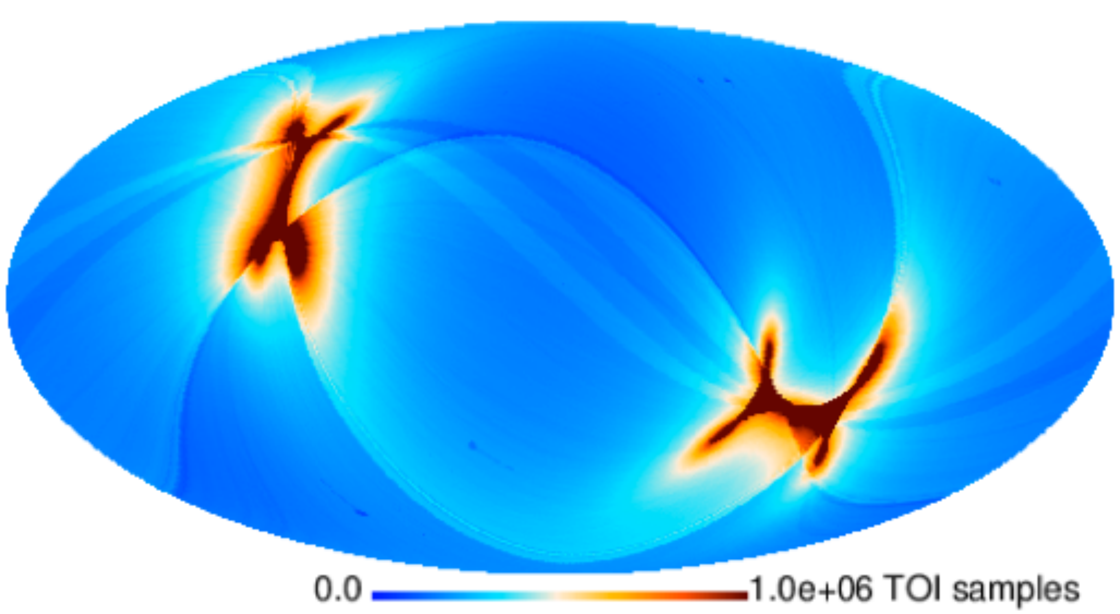

Planck TOI data & differential noise

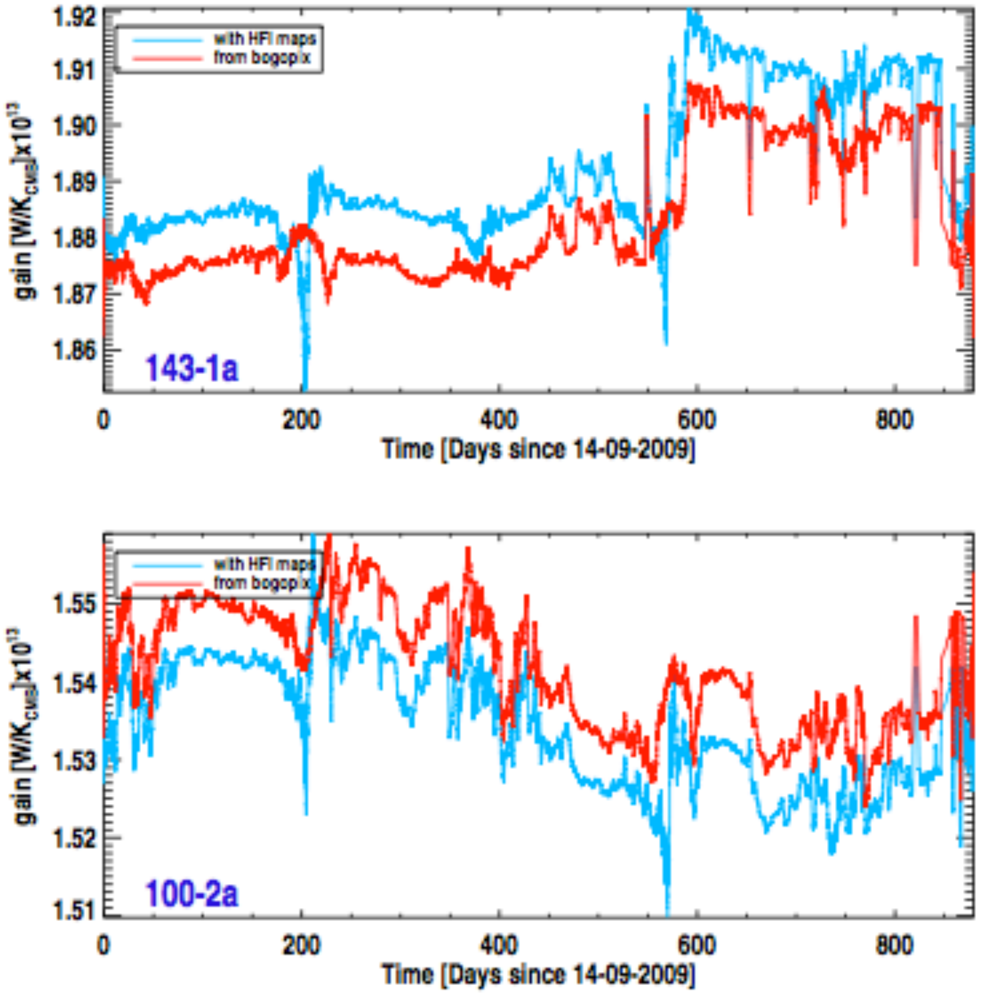

Figure 7. Example of results from `bogopix` obtained for two HFI detectors, compared with those of the Solar dipole calibration. Gain values for individual rings have been smoothed with a width of 50 rings (~ 2 days), to increase the signal-to-noise ratio of the plots. We observe a good agreement between `bogopix` results and those obtained with the HFI maps, for the relative gain variation, except for the time intervals where the Solar dipole's amplitude is low with respect to the Galactic emission. The averaged value of the gains are, however, offset by factors (different from one detector to the other) of the order of 0.5 to 1 %.

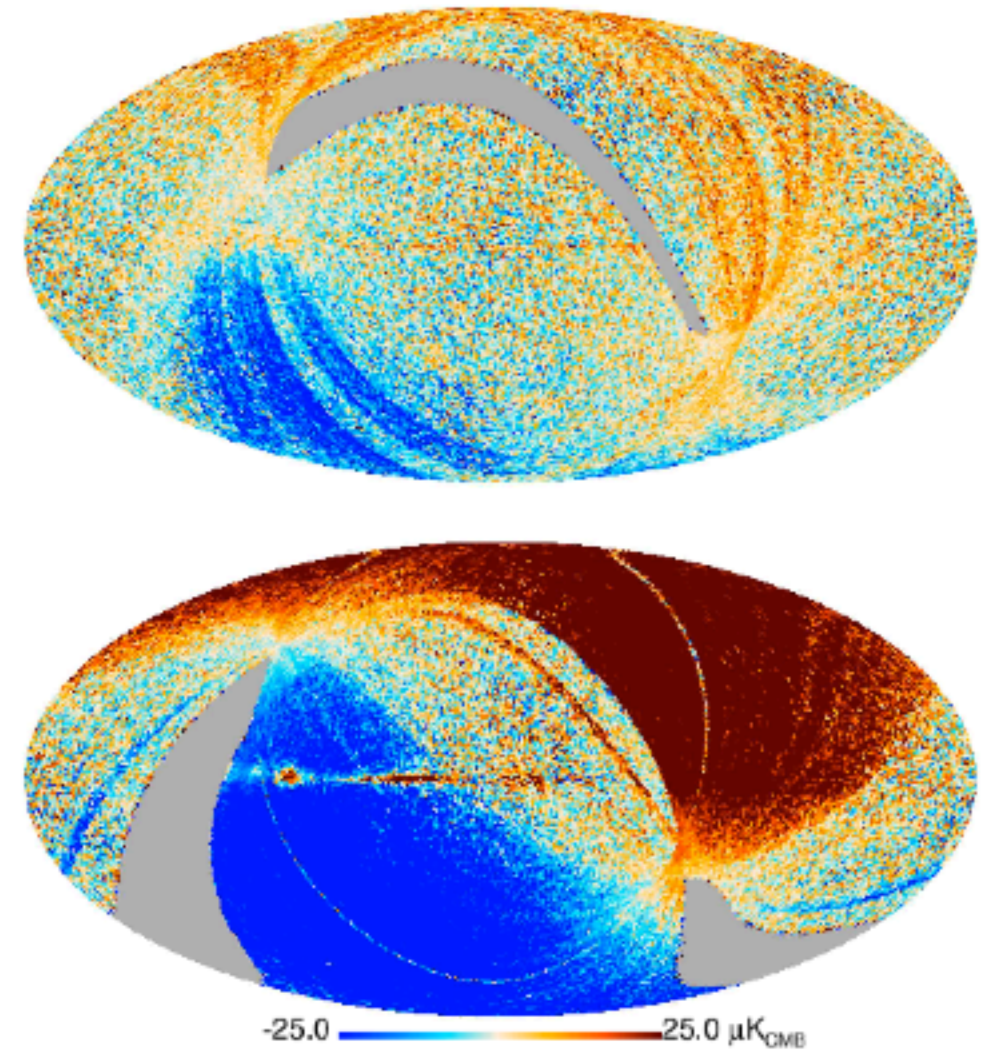

Figure 4. Differences between temperature maps built using data from detector 143-1a, for surveys 1 and 3 (top) and 2 and 4 (bottom). In both cases, large scale features appear. Their amplitude and disposition on the sky are compatible with residuals from the Solar dipole, due to time variations of the detector gain, of the order of 1 to 2 % These residuals should be compared to the amplitude of the Solar dipole, 3.353 mK_{CMB}.

Removing the Galactic & extra-galactic foregrounds

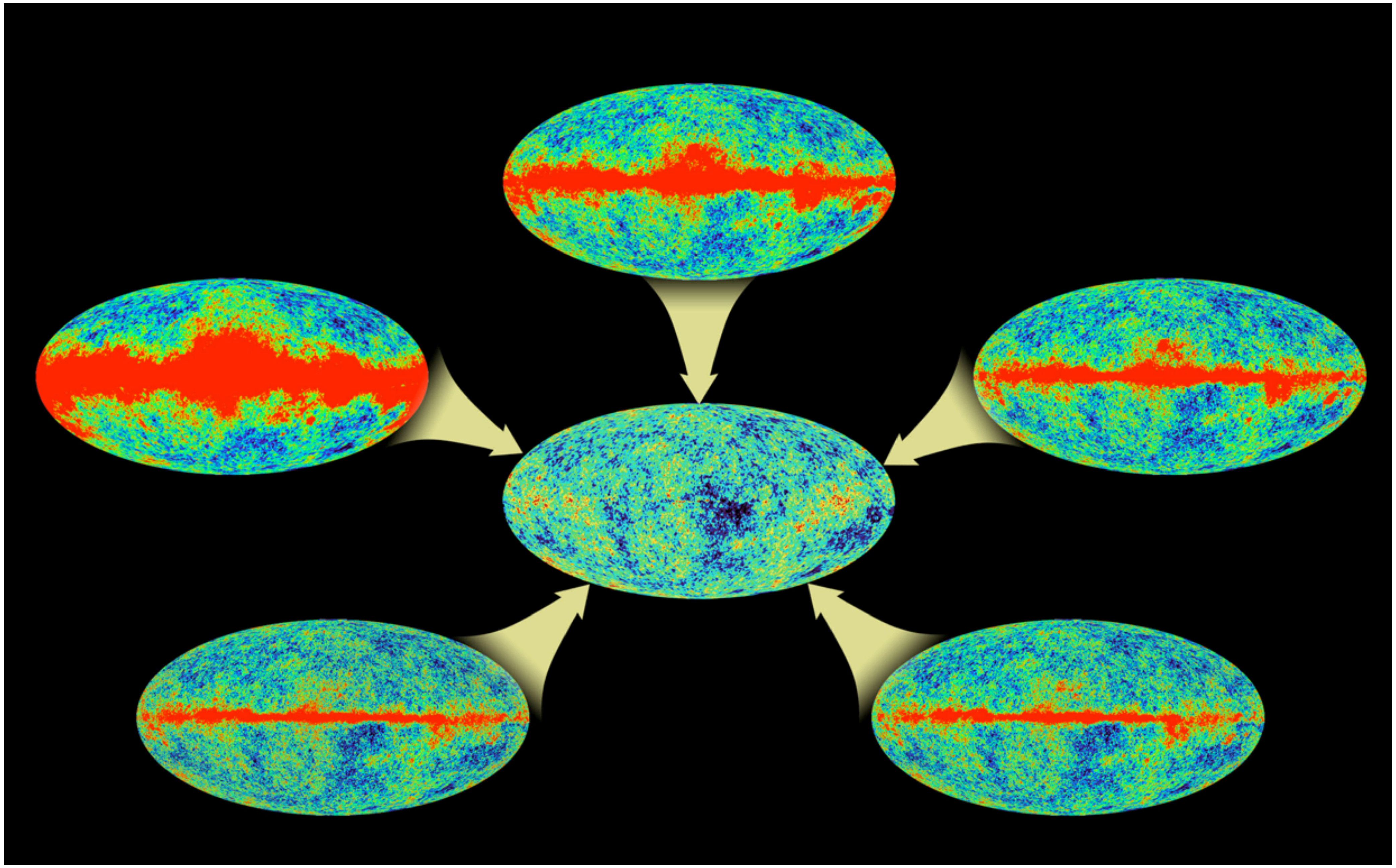

Galaxy vs. the CMB

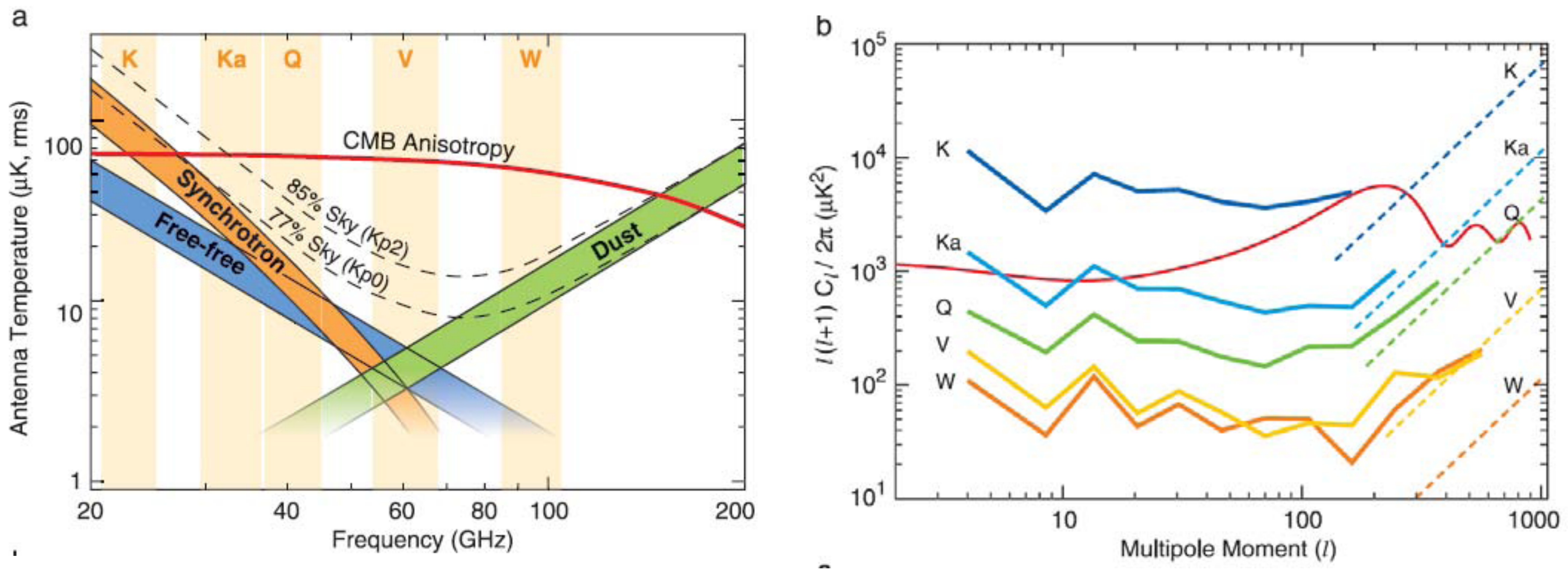

CMB vs. foreground anisotropies (Bennett et al. 2003, WMAP 1st year)

Left: Spectrum of the CMB and foreground emissions (models). WMAP frequencies were chosen such CMB mostly dominates.

Right: Foreground power spectra for each WMAP band. The dashed lines at the right are estimated point source contributions.

Polarized foregrounds

Here the signal is much lower, generally hidden under the foreground signals!

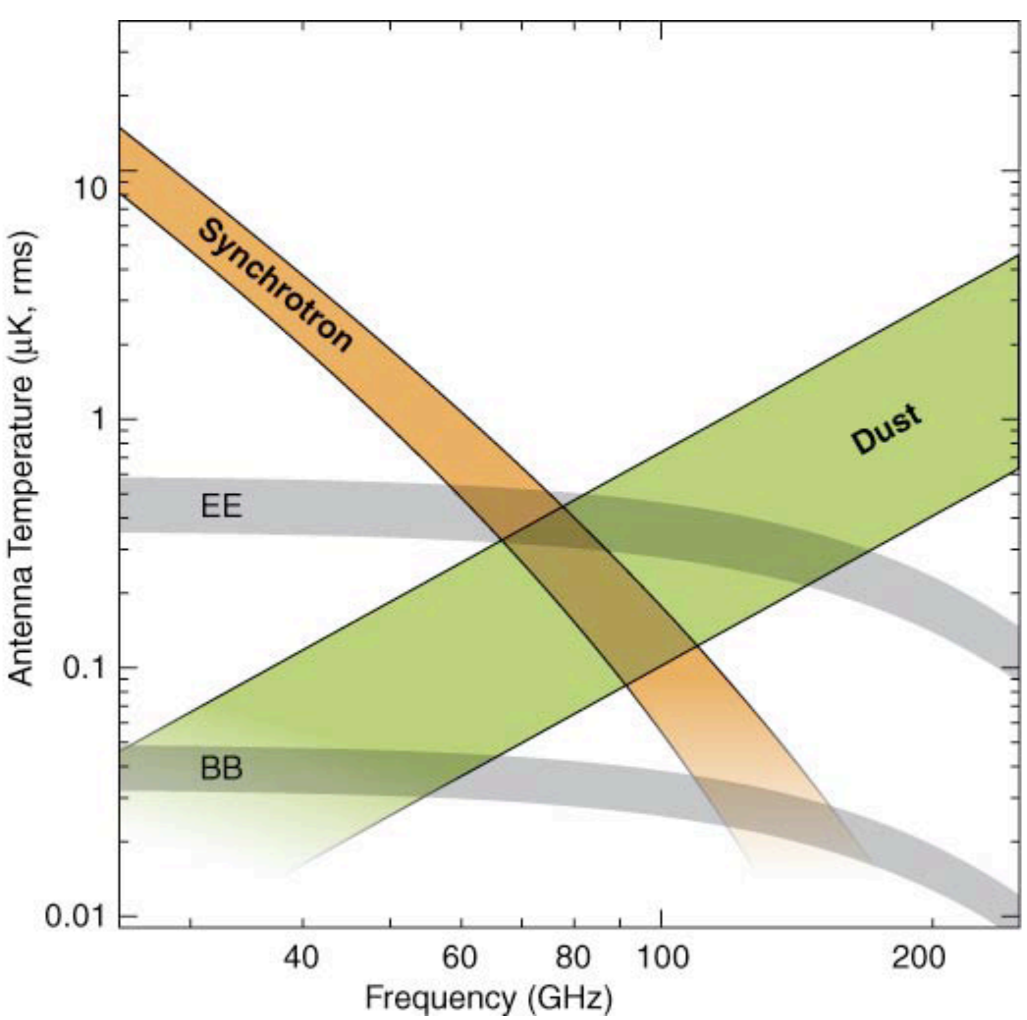

RMS fluctuations in the polarized CMB and foreground signals as function of frequency

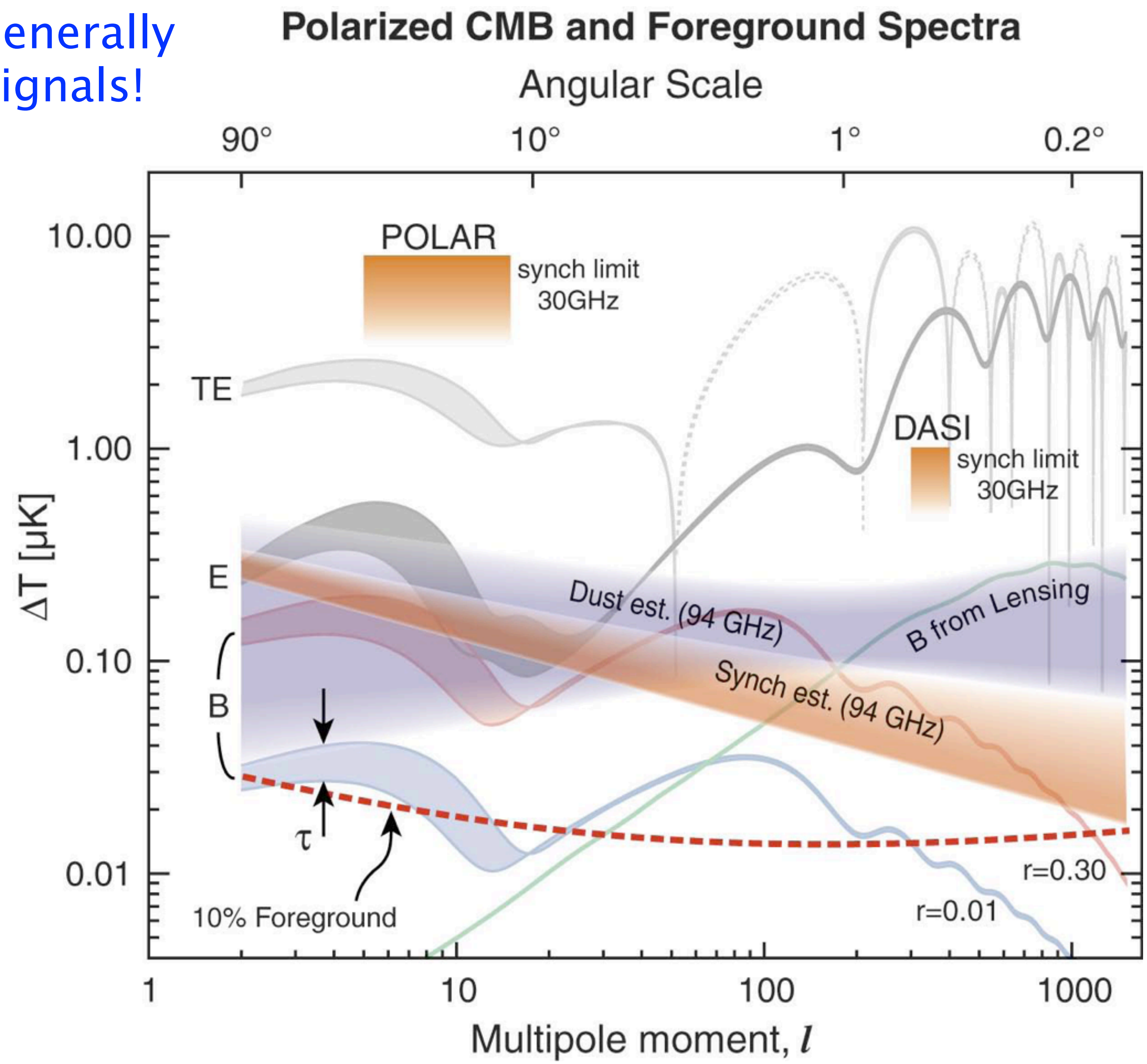

How to remove CMB foregrounds?

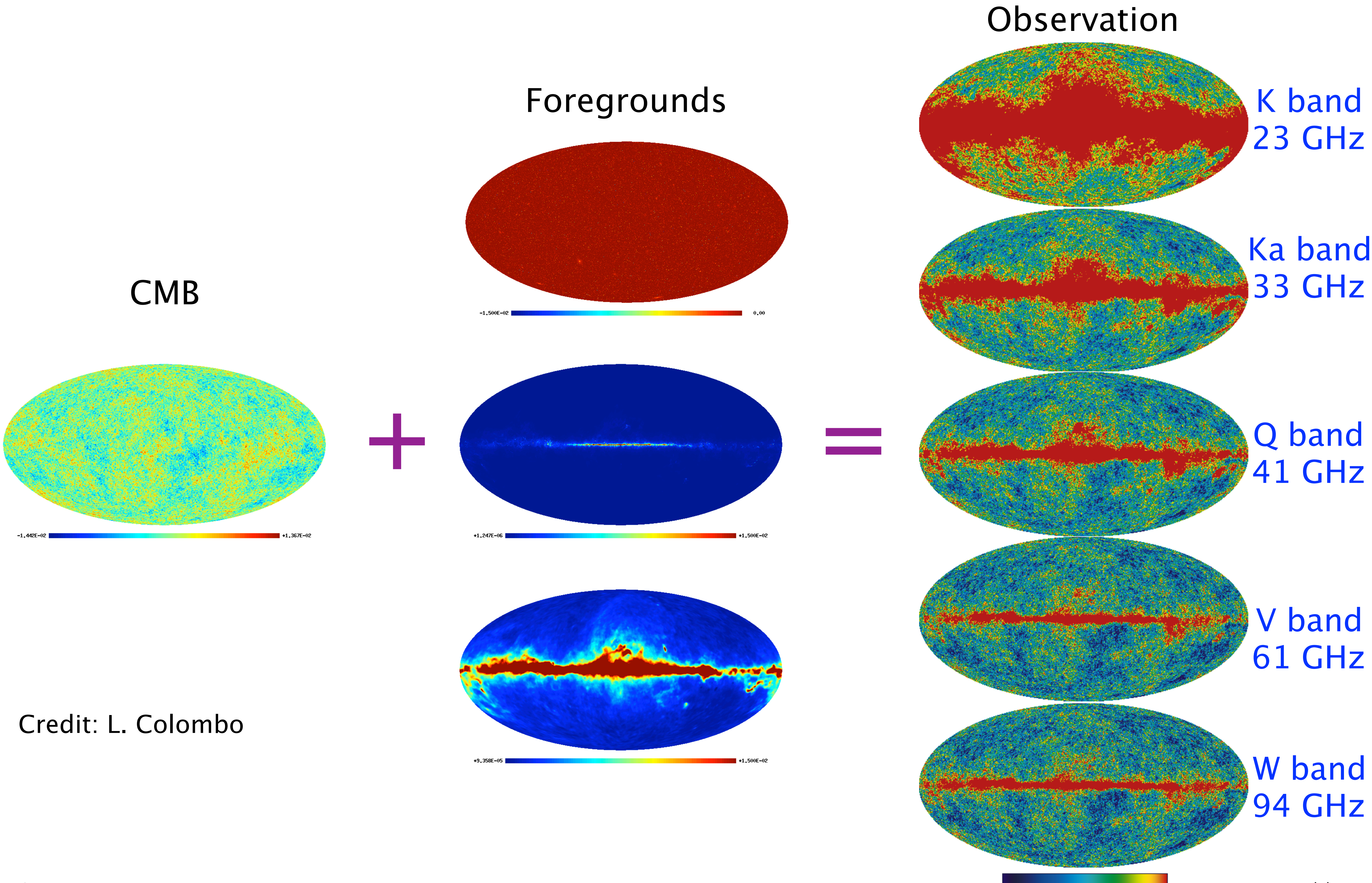

Credit: L. Colombo

Component Separation: In general it's an inversion problem

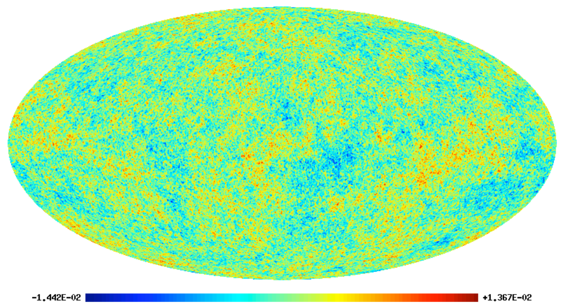

s_1

Two observing frequencies: ν_1, ν_2

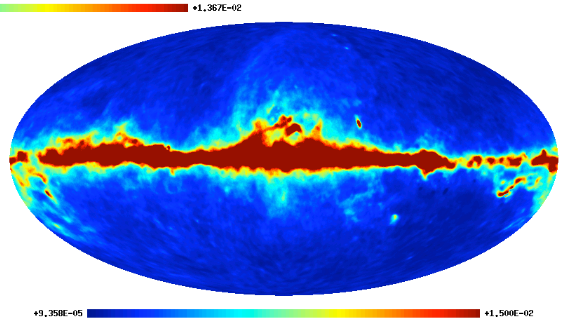

s_2

$$x_1 = a_{11}\, s_1 + a_{12}\, s_2 + n_1$$
$$x_2 = a_{21}\, s_1 + a_{22}\, s_2 + n_2$$

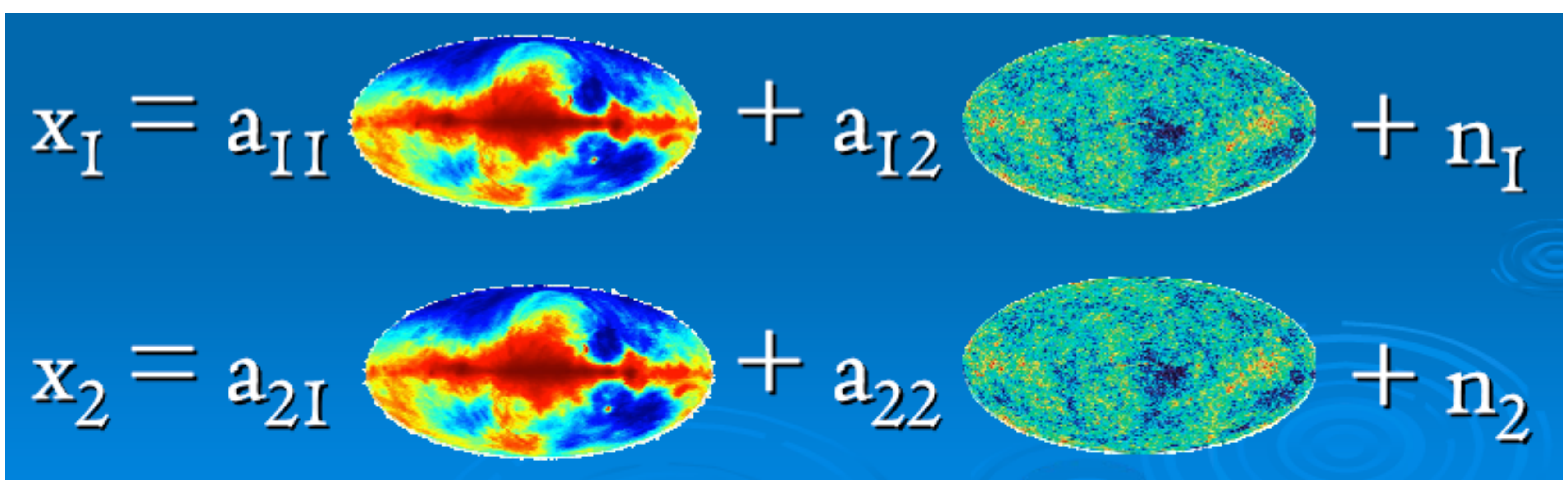

$\mathbf{x} = \mathbf{A}\mathbf{s} + \mathbf{n}$

Invert for $\mathbf{s}$

But we can make progress even without having as many channels as components (or without having detailed information on all the foregrounds)!

Component separation: ILC method

The **Internal Linear Combination (ILC)** method aims to combine different frequency maps with specific weights, such that contributions from all the contaminating signals (plus noise) are minimized.

This works especially well when we have poor knowledge of the foregrounds. But we must have a precise knowledge of the spectrum of the signal that we're interested in. Also, ILC should be used separately on different spacial scales for better results.

The term "internal" refers to the fact that no prior information or auxiliary data from other observations are needed. The ILC method is one of the most "assumption-free" map making tools available! It only requires the following two assumptions:

- The observed maps represent a linear mixture of astrophysical components and noise.
- All components are uncorrelated.

ILC method formalism (I)

From the assumption that observed maps are a linear mixture of astrophysical components and noise, we can write

$$T_i(p) = a_i s(p) + n_i(p),$$

where a_i are the components of a "mixing vector" which contains the spectrum of interest and has as many components as frequencies. $s_i(p)$ and $n_i(p)$ are the signal and noise components in each channel maps. In vector form:

$$\vec{T}(p) = \vec{a}s(p) + \vec{n}(p).$$

By forming a linear combination $s_{\rm ILC}(p) = \vec{\omega}^{\rm T}\vec{T}(p)$, the ILC method provides an estimation $s_{\rm ILC}(p)$ of the desired signal s(p). Here ω_i are the "weights", or the desired ILC coefficients.

$$s_{\rm ILC}(p) = \vec{\omega}^{\rm T}\vec{a}s(p) + \vec{\omega}^{\rm T}\vec{n}(p).$$

The goal is to find these weights ω_i which will minimize the variance in the nuisance map, n(p). From et al. Eriksen (2004) the map variance is calculated as

$$VAR(s_{\rm ILC}(p)) = VAR(s(p)) + VAR(\vec{\omega}^{\rm T}\vec{n}(p)) = \vec{\omega}^{\rm T}\hat{C}\vec{\omega},$$

where C covariance matrix of the maps (computed from data).

ILC method formalism (II)

The condition of minimization of the variance means that

$$\frac{\partial}{\partial \omega_{\mathrm{i}}}\left[\vec{\omega}^{\mathrm{T}}\hat{C}\vec{\omega}\right] = 0.$$

In addition, we have a normalization condition to preserve the sum total of the signal of interest:

$$\vec{\omega}^{\mathrm{T}}\vec{a} = \vec{a}^{\mathrm{T}}\vec{\omega} = 1.$$

It is straight-forward to solve for the weights in terms of the mixing vector (usually done by emplying Langrange multipliers). The solution is

$$\vec{\omega} = \frac{\hat{C}^{-1}\vec{a}}{\vec{a}^{\mathrm{T}}\hat{C}^{-1}\vec{a}}.$$

Therefore, the estimated map $s_{\mathrm{ILC}}(p)$ of our component of interest is given by

$$s_{\mathrm{ILC}}(p) = \frac{\vec{a}^{\mathrm{T}}\hat{C}^{-1}}{\vec{a}^{\mathrm{T}}\hat{C}^{-1}\vec{a}}\vec{T}(p).$$

Dumb ILC example: signal + noise

We have two maps, with signal and noise. The covariance matrix for observations is

$$\mathbf{C} = \begin{bmatrix} S+N_1 & S \\ S & S+N_2 \end{bmatrix} \qquad \mathbf{C}^{-1} = \frac{1}{\det(\mathbf{C})} \begin{bmatrix} S+N_2 & -S \\ -S & S+N_1 \end{bmatrix}$$

The ILC weights are simply: $\omega_1 = N_2/(N_1+N_2)$ and $\omega_2 = N_1/(N_1+N_2)$.

This is same as weighting each map I proportionally to $1/N_i$.

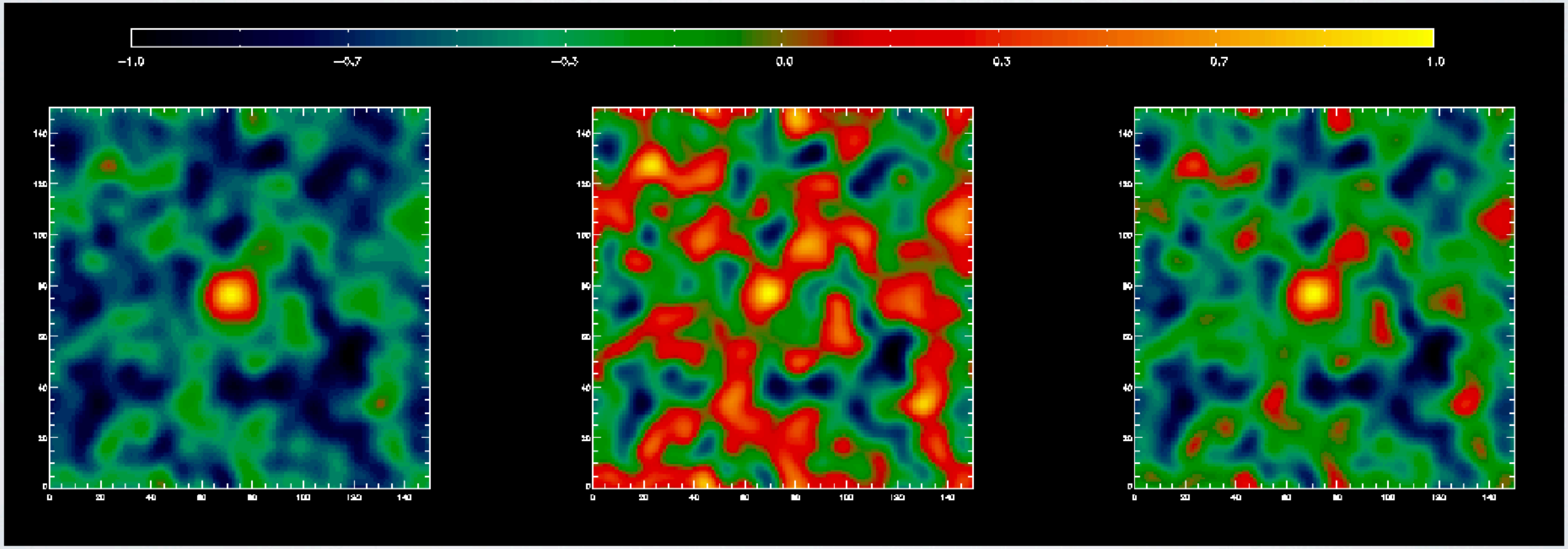

Map 1 Map 2 ILC map

Real ILC example: WMAP CMB all-sky

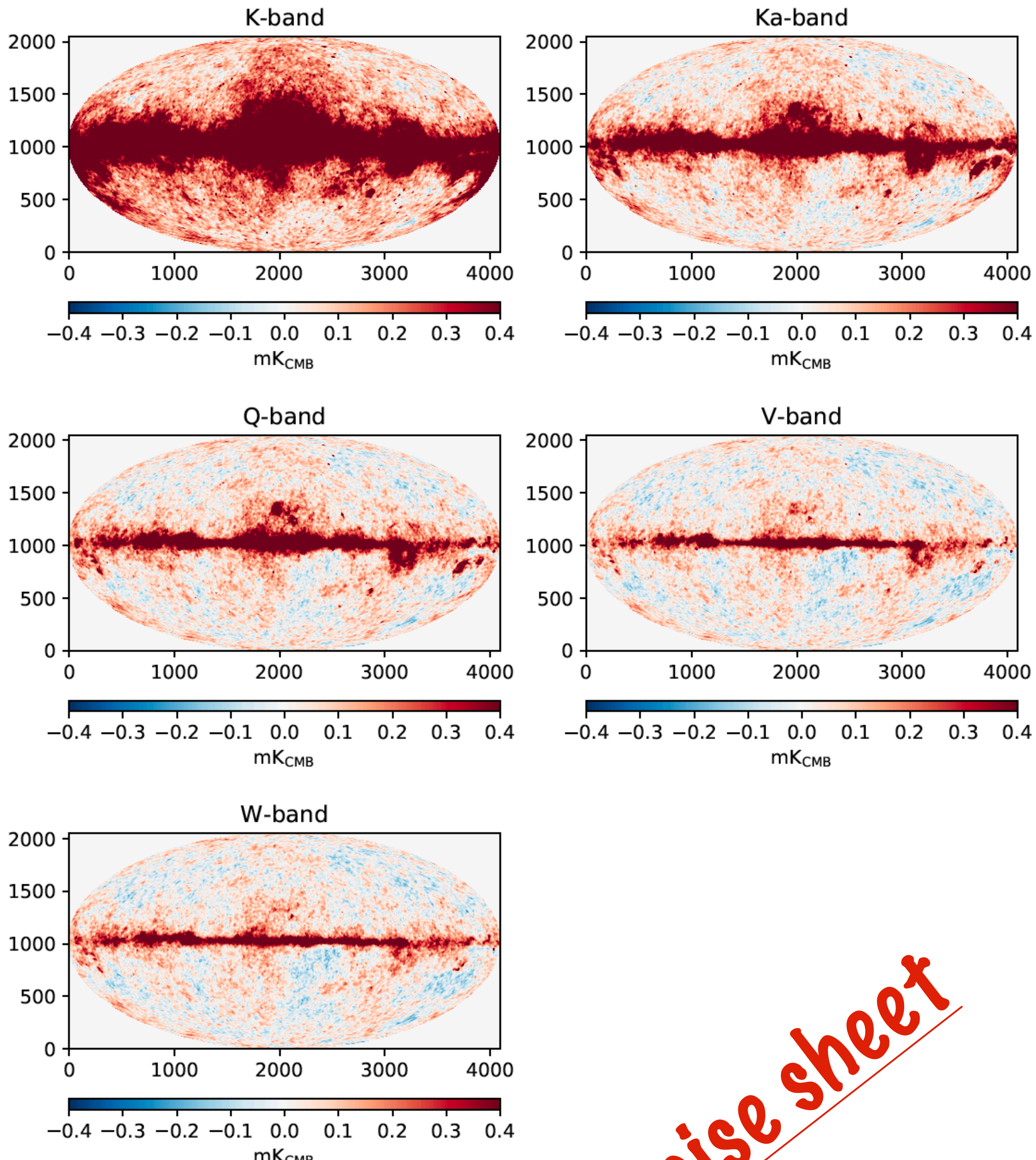

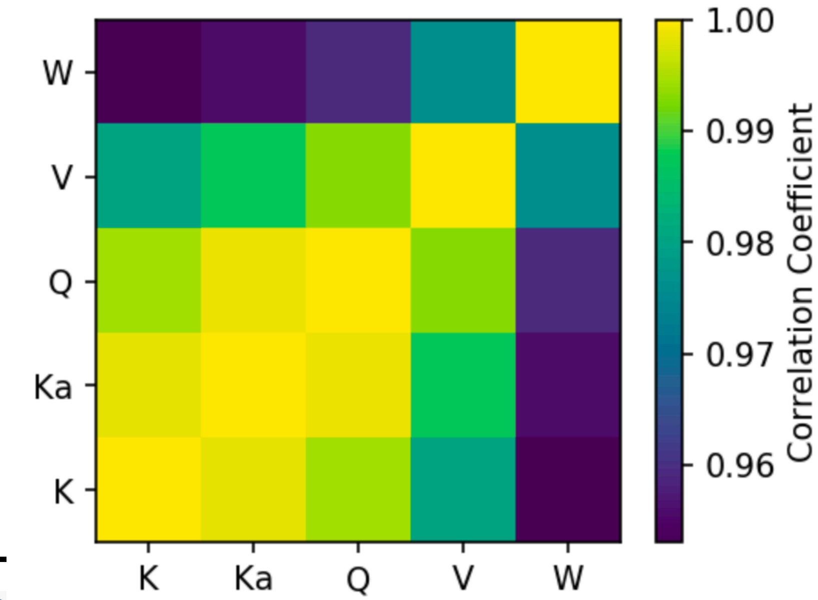


```
print(weights)
[-0.05499771 -0.03971103 -1.7916735   4.63774311 -0.02586087]
```

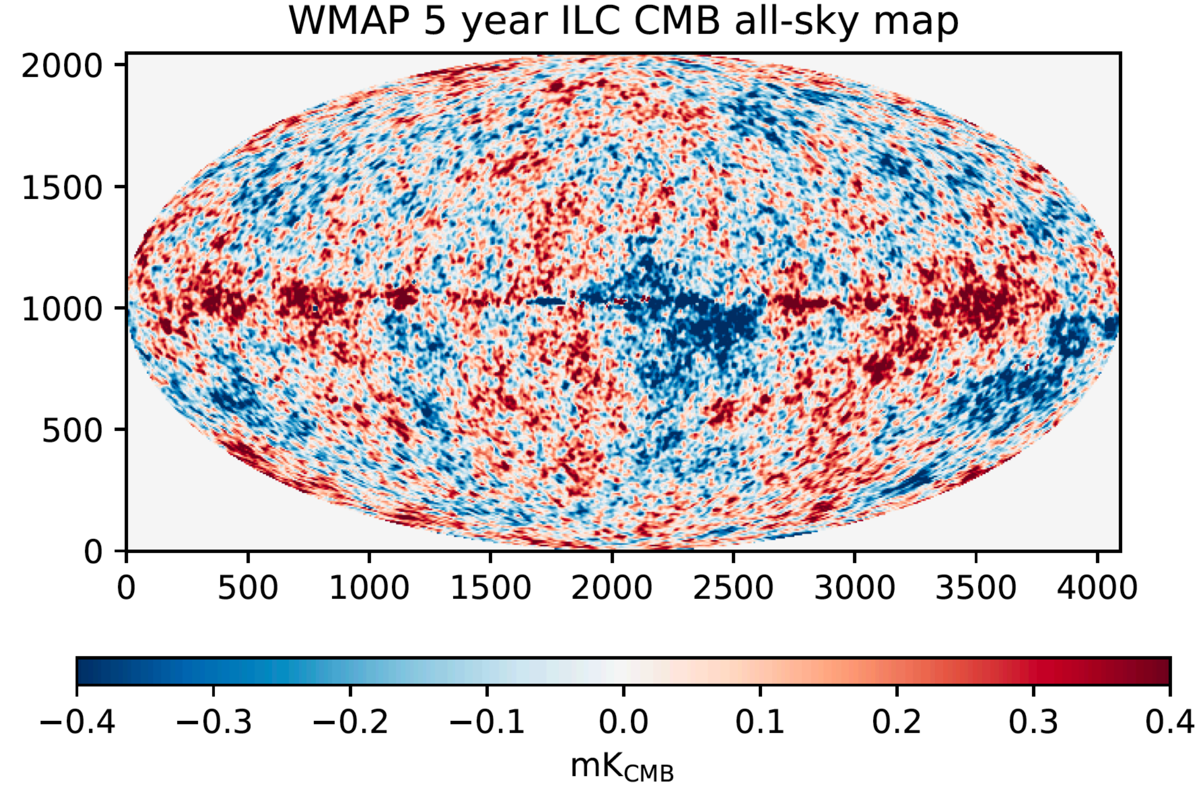

Exercise sheet

Planck CMB maps from ILC method

Planck all-sky CMB maps from several variants of the **ILC** method
(Planck 2015 results, Diffuse component separation, A&A 594, A9)

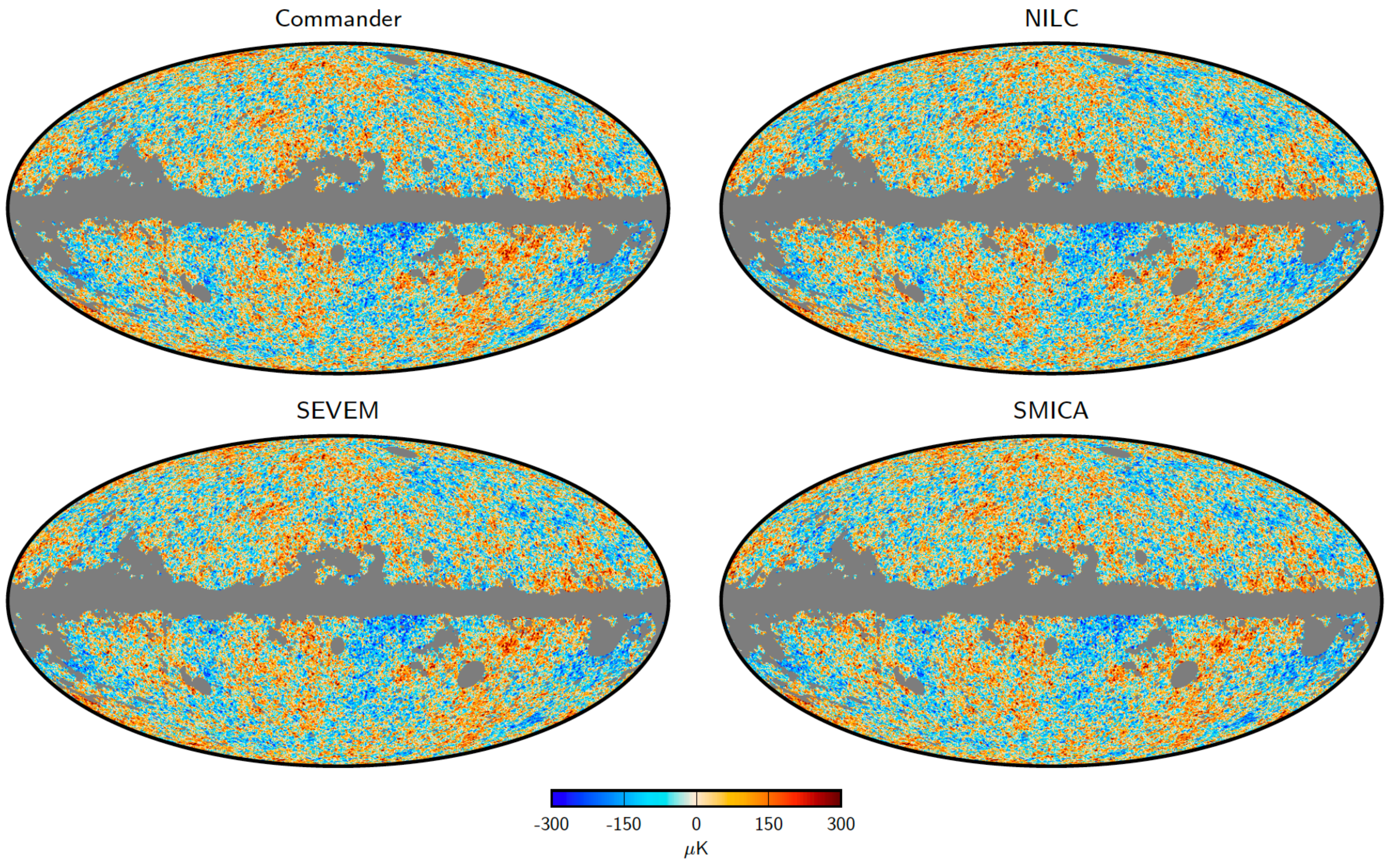

Another ILC example: SZ effect maps

Extraction of Compton-y (SZ effect) map from Planck data

(Master's thesis work by Jens Erler)

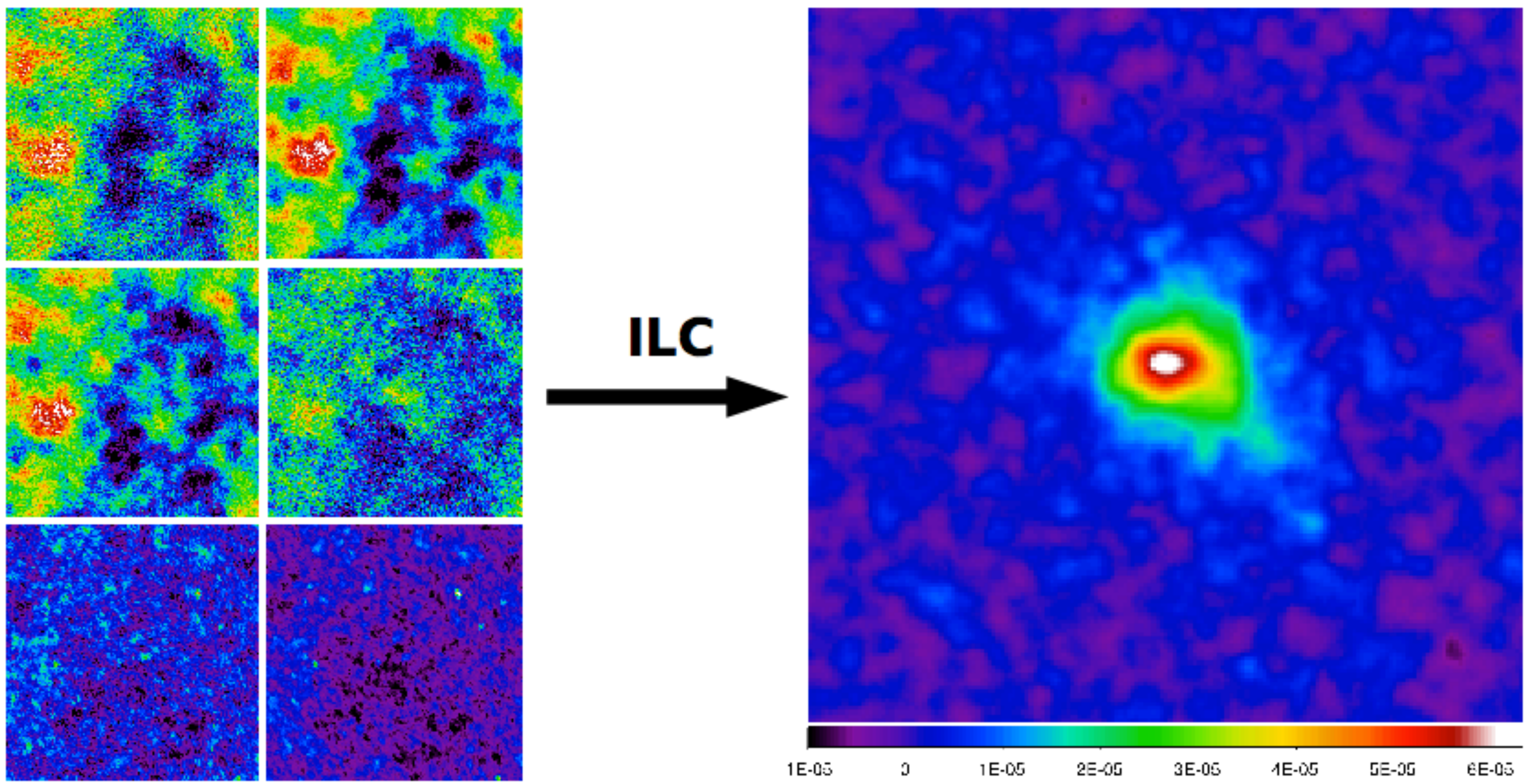

SZ effect is the topic of our next lecture!

Questions?